1991

Positron Annihilation Studies Of Defects In Silicon

Peter J. Simpson

POSITRON ANNIHILATION STUDIES OF DEFECTS IN SILICON

by

Peter J. Simpson

Department of Physics

Submitted in partial fulfilment
of the requirements for the degree of
Doctor of Philosophy

Faculty of Graduate Studies
The University of Western Ontario
London, Ontario
November 1991

ISBN 0-315-71989-3

Abstract

Measurements of Doppler-broadening of annihilation radiation from variable-energy positrons have been applied to examine the nature and distribution of defects in ion-irradiated silicon. Positron measurements were supplemented by ion backscattering/channeling to determine displaced atom distributions, and infrared absorption measurements to determine divacancy concentrations. Silicon (100) wafers were irradiated at 300K with helium ions at energies from 0.25 to 4.0 MeV and fluences from 10^{13} to 10^{16} cm^{-2}, and with silicon ions at energies from 0.5 to 5.0 MeV and fluences from 10^{11} to 10^{15} cm^{-2}. Defect annealing was observed through the divacancy annealing stage (~470 to 570K). He-irradiated silicon was restored toward single crystal quality as measured by both infrared and positron methods. For the same anneal, Si-irradiated silicon shows partial restoration of crystallinity (RBS), and removal of the optically-active divacancies, but no change in positron trapping characteristics. Annealing to between 870 and 970K restores the crystal to near pre-implant characteristics. Results are discussed in terms of existing models of damage production during ion irradiation.

Variable-energy positron methods have also been applied to study silicon layers grown by molecular beam epitaxy at low temperatures. The epilayers contain voids of ~6 nm diameter, which constitute efficient positron traps. The densities and sizes of voids in the epilayers were determined by transmission electron microscopy. Extremely narrow positron annihilation lineshapes were measured, and attributed to the formation of

positronium within the voids. Measurements of the fraction of positrons trapped by voids are compared with the predictions of diffusion-limited trapping theory.

The scope and limitations of defect profiling with variable-energy positrons and suggestions for further development of the technique are discussed.

Acknowledgments

It is a pleasure to acknowledge the gratitude I owe to my supervisor Peter Schultz. His guidance, enthusiasm and positive outlook have been indispensable. Thanks are also due to Ian Mitchell for his supervision during Peter Schultz's sabbatical leave, and for all sorts of useful discussions. I am happy to thank many people I have enjoyed working with, particularly Maarten Vos, who performed most of the ion beam work discussed herein, and Tom Jackman and Geof Aers who hosted a visit to the National Research Council and provided advice throughout this work. Also at NRC, thanks are owed to J.-P. Noël, Derek Houghton and John McCaffrey. Informative discussions with Jeff McCallum are acknowledged. I must thank H.J. Stein of Sandia National Laboratories, who provided the infrared absorption measurements. The technical support of Phin Perquin is gratefully acknowledged. Finally I thank all of the technical and secretarial staff of the Department of Physics.

Table of Contents

List of Tables

List of Figures

List of Appendices

Chapter 1

Introduction

The work described in this thesis is intended as a step forward in the development of an experimental technique for characterizing semiconductor materials. The observation that the radiation from positron annihilation in a solid carries information about the annihilation environment is not a new one: DeBenedetti *et al.* reported in 1949 that the two γ-rays produced in the annihilation event were not exactly collinear, and attributed this to the effect of the electron momentum. Since measuring the angle between the two annihilation photons provides a measure of the electron momentum distribution, considerable use was made of this technique for determining, for example, the shape of the Fermi surface in solids. In 1967 MacKenzie *et al.* reported measurements on thermally-generated vacancies in metals, utilizing the fact that positrons can be trapped by defects in a solid, and that the electron momentum distribution in such traps differs from that in the undefected solid. Studies of defects, particularly in metals, flourished, but the difficulties associated with using positrons from high energy radioactive sources, with their continuous energy spectra, were apparent.

It was not until the late 1970's (Mills, 1978; Lynn, 1979) that positron moderators with useful efficiencies were developed, permitting the formation of relatively intense beams of positrons of low, controllable energy. This development made accessible a new field of surface and near-surface positron physics. The application of variable-energy positron

beams that has attracted the most interest has been defect profiling. By measuring the Doppler broadening of annihilation radiation as a function of the energy of positrons incident on a defected crystal it is possible to extract a profile of defects in the first few micrometers of the solid. Although this is the case ideally, in practice it has taken considerable effort to advance the technique to the point where true profiling might be achieved. An obvious goal of the present study has been to develop our understanding of this spectroscopy by correlating results of positron beam experiments with information from other, longer-established techniques, specifically ion channeling/backscattering, infrared absorption, and electron microscopy. Silicon was chosen as the test material since it is readily available in high purity and with low bulk defect concentrations. Further, there is an extensive literature on point and extended defects, including radiation-induced defects. The large cross-section for capture of thermalized positrons by lattice vacancies confers a high sensitivity to vacancy-type defect distributions in the solid.

Defects in silicon are reviewed briefly, with emphasis on techniques of defect characterization. The positron technique is described in detail, particularly regarding interpretation of data, and its limitations. A systematic study of ion irradiation damage in silicon is discussed. Ion-irradiated silicon provides a useful case study for positron annihilation because defect distributions can be produced in a relatively well-controlled way. By varying the ion fluence and energy, we vary the defect concentration and the extent of the defect distribution. Annealing stages provide further insight into the nature of the defects studied.

Silicon epilayers grown at low temperatures were investigated, and

shown to contain microvoids (of size equivalent to $\sim 10^4$ vacancies), which trap positrons efficiently. This provides an interesting study of an unusual phenomenon involved in the breakdown of epitaxy, and of the physics of positron trapping in voids.

Appendix 1 consists of a paper submitted for publication, on the subject of defect profiling in indium phosphide. There is considerable industrial interest in this material, which to date has not been studied in any detail using positron methods. This work is not included in the main body of the text because of the focus on silicon, but is included as an appendix because of its relevance to the discussion of defects in ion-irradiated semiconductors.

Appendix 2 consists of another paper submitted for publication, pertaining to the formation of voids during annealing of GaAs, and positron trapping in them. Again, this was felt to be outside the focus of the main text, but is included particularly for its relevance to the chapter on positron trapping in voids in silicon.

Chapter 2

A brief review of defects in silicon

Introduction

Silicon is by far the most extensively studied of all materials. It is sufficiently well understood to form the basic material for nearly all of the solid state electronics industry, however the changing (and increasing) demands of that industry continue to motivate study of silicon by uncovering areas in which our knowledge is insufficient. The drive to smaller device dimensions, and to a greater number of devices in a single integrated circuit, places ever tighter restrictions on material properties. Despite advances in the use of group III-V semiconductors for specialized applications (particularly optoelectronics), it is not unlikely that silicon will continue to dominate the electronics field, for reasons both economic- silicon is the second most abundant element, making up 26% of the earth's crust, and is much cheaper than more exotic semiconducting materials- and technological- silicon is more mechanically robust, easier to process, and can (at least for the present) be produced with higher purity and crystal quality than the alternatives.

The electrical behaviour of silicon is dominated by the influence of defects. Intrinsic conductivity at room temperature is low since only $\sim 10^{15}$ cm^{-3} electrons have sufficient thermal energy to be excited from the valence band to the conduction band (across a bandgap of 1.1 eV) and become mobile. Carrier densities in device grade silicon are orders of magnitude higher than this, due to the effect of both intentionally-introduced dopants, and

unintentional impurities and structural defects. Dopants are often introduced by ion implantation, and this process causes structural damage which usually requires thermal treatment to remove. For these reasons much of the extensive effort dedicated to silicon has been in the specific area of defect studies.

Terminology

We can divide crystalline defects into two broad categories: extended defects and point defects. Extended defects, such as dislocations and stacking faults, will not be discussed here. To discuss point defects some terminology will first be given: defects can be *extrinsic* (i.e. impurity-related) or *intrinsic* (involving only atoms of the host-lattice species). Extrinsic or impurity-type defects can be *interstitial* (i.e. occupying a space between lattice sites in the crystal) or *substitutional* (replacing an atom of the host species on its lattice site). Intrinsic defects consist of (self-) interstitials and vacancies (empty lattice sites), and for the case of alloys (e.g. GaAs), *antisite* defects, in which one atomic species occupies a lattice site that should be occupied by a different species (e.g. Ga occupying an As lattice site).

It is often the case that the simple defects described above will interact with each other to form defect complexes such as multivacancies and various impurity-vacancy combinations. The stability of any defect configuration (simple or complex) is temperature dependent. For example, the monovacancy in silicon becomes mobile at ~70K (Corbett *et al.*, 1981a), and so at room temperature the divacancy (which anneals at ~460 to 560K (Watkins and Corbett, 1965)) is the simplest stable vacancy-type defect.

These temperatures can vary to some extent depending on the defect's charge state. Much attention has been given to the role of the divacancy in processes such as ion beam-induced transitions between amorphous and crystalline phases at the crystalline-amorphous boundary in silicon (Linnros *et al.*, 1988) There are also defect types that require a characteristic activation energy to form. For example, the non-planar tetravacancy in silicon exists only in the temperature range from ~400 to 600K (Lee and Corbett, 1974).

A further complication is introduced by the fact that a particular atomic configuration can occur with a variety of electronic configurations, so that a variety of charge states are possible for most defect types. For example, the divacancy has been observed to occur in five different charge states: V_2^{++} ,V_2^{+} ,V_2^{0} ,V_2^{-} and V_2^{--} (Corbett *et al.*, 1981a). The charge state in which a given defect type predominantly occurs often depends on the location of the Fermi level, and therefore the doping, in the material.

The crystal quality of commercial silicon is quite high, with very low concentrations of extended and vacancy-type defects. Carbon and oxygen impurity concentrations can be significant however. For material grown by the float-zone process, carbon and oxygen concentrations are typically of the order of $\sim 10^{16}$ cm^{-3} and $\sim 10^{15}$ cm^{-3} respectively. For material grown by the much more common Czochralski process carbon and oxygen concentrations are typically $\sim 10^{17}$ cm^{-3} and $\sim 10^{18}$ cm^{-3} respectively (Sze, 1985).

Techniques for defect characterization

For device technology, the aspect of defects which is of immediate interest is their effect on the macroscopic properties of the material, such

as the resistivity. To properly understand and control such macroscopic properties, and for purely scientific purposes, an understanding of the relationship between microscopic and macroscopic properties, and therefore of the microscopic configurations of defects, is desirable. To fully understand a defect, the information required falls into six categories (Corbett *et al.*, 1981a):

1. atomic and electronic configuration
2. electronic energy levels, particularly in the bandgap
3. carrier interaction mechanisms
4. formation mechanism
5. diffusion characteristics and temperature dependence
6. interactions with other defects.

A small number of silicon defects are almost completely understood, such as for example substitutional phosphorus, a common dopant. For the majority the picture is incomplete. A number of experimental techniques exist both for determining microscopic properties of defects, and for characterizing materials with regard to the defects they contain. Some of these techniques are discussed below.

Electron paramagnetic resonance

Much of what is known about the microscopic configuration of defects has been determined by electron paramagnetic resonance (EPR), also called electron spin resonance (ESR).

EPR involves the measurement of resonant absorption of microwaves by unpaired electrons in a magnetic field. In defect-free silicon, all electrons are paired and therefore have no net magnetic dipole moment. Many

defects introduce an unpaired spin, and thus a non-zero magnetic moment. In the presence of an externally-applied magnetic field such dipoles are aligned by the field, and there is a splitting of the degenerate ground state energy levels, which is the well-known Zeeman effect. Electrons can be excited from one energy level to another by absorption of microwave radiation of an appropriate frequency. In the simplest case, the electrons with unpaired spins only have a spin angular momentum, and will be separated by the applied magnetic field into two groups: those with a spin component parallel to the field, and those with a spin component antiparallel to the field. The magnetic moment of an unpaired electron is given by $\mu = 1/2\ g\ \mu_B$, where g is the gyromagnetic ratio (=2.00229) and μ_B is the Bohr magneton. The energies of the two groups of electrons in a magnetic field H are then given by $E = \pm 1/2\ g\ \mu_B H$, so the energy splitting is of magnitude $g\ \mu_B H$, and resonant transitions can be excited by microwaves of energy $h\nu = g\ \mu_B H$. In the case that an impurity of nuclear spin 1/2 is present there is a further, hyperfine splitting which introduces additional energy levels (Wertheim *et al.*, 1971).

The usual experimental arrangement is to use microwaves of a fixed energy $h\nu$ and measure microwave absorption in a sample as a function of magnetic field H. Measurements are often made at low temperature to minimize thermal broadening of spectral lines. Often the orientation of the crystal with respect to the field is rotated and absorption determined as a function of angle. It is also possible to apply uniaxial stress to samples as a means of obtaining additional information regarding defect symmetry.

EPR spectra are usually complex, due to the array of defect types which may be present in a sample, and to complicating effects such as spin-orbit

coupling. It is possible however, to determine the symmetry of a defect site, the nuclear spin of a central atom, and the nuclear spins of neighbouring host lattice atoms (Newman, 1990). By careful interpretation, and correlation with other experimental methods, EPR has been used to determine the structure (and other characteristics such as annealing behaviour) of many defect types such as the monovacancy (Watkins, 1965), divacancy (Watkins and Corbett, 1965), and numerous vacancy-impurity complexes (Corbett *et al.*, 1981b).

Although EPR is a powerful technique and has contributed much of what is known about the structure of silicon defects, it is not without drawbacks. Sensitivity can be excellent ($\sim 10^{12}$ cm^{-3}), but the defects must be paramagnetic. It is usually necessary to cool the sample to cryogenic temperatures. The sample must have a low concentration of free carriers, so heavily doped samples cannot be studied. In addition there is no depth resolution, so applicability to thin epilayers, or ion implanted materials, is limited (Newman, 1990).

Infrared absorption spectroscopy

Another technique which has been used extensively to characterize silicon is infrared absorption, or localized vibrational mode spectroscopy. Pure silicon is transparent in the infrared, however many defects introduce absorption bands in the IR region of the spectrum and can be detected in this way (Newman, 1990). The method is outlined below.

The allowed vibrational modes in a crystal fall into two bands, the acoustic and the optical, corresponding to the vibrations of unit cells in the crystal, and vibrations of atoms within the unit cell, respectively.

Outside these two bands of allowed vibrational modes lie frequencies at which the crystal cannot vibrate. For absorption of incident radiation to occur, momentum must be conserved, requiring the emission of a phonon of an appropriate frequency. If that frequency is not an allowed one, there is (to first order) no absorption; this is the reason pure silicon is transparent to infrared radiation. The addition of impurity atoms, or any other change in the structure of a perfect crystal, introduces new vibrational modes, and therefore changes the absorption spectrum of the crystal. These new modes may occur within the optic or acoustic band, in the gap between these bands, or above the optic band. In the case that the modes due to defects lie within the optic or acoustic band, little information can be obtained. However, if the new modes lie outside those bands, peaks will be introduced in the absorption spectrum characteristic of the particular defect.

The experimental method requires samples usually in the form of a slab (of thickness a few mm or less) polished on both sides, often with an angle of a few degrees between the sides to prevent multiple internal reflections. Transmission of infrared radiation through the sample is directly compared with transmission through a reference sample of the same thickness, using either a dispersive or a Fourier transform spectrometer. The Fourier transform spectrometer provides both higher speed and higher resolution, but dispersive spectrometers may give higher photometric accuracy.

Infrared absorption spectra of many silicon defects have been catalogued, often by comparison with EPR measurements. Correlations are made for example on the basis of annealing temperature. By measuring absorption spectra of samples with known defect densities it is possible to

calibrate the technique to give an absolute measure of the areal density of defects. An example of particular interest here (discussed in chapter 4) is the divacancy, which introduces a broad absorption band centred at ~1.8 μm wavelength and can be interpreted in terms of an absolute divacancy concentration (Cheng and Lori, 1968).

Infrared absorption has been extensively applied for materials characterization. Its application is somewhat limited by the need for sample preparation, lack of depth resolution, and sensitivity that varies strongly with defect type. Defect concentrations around 10^{15} cm^{-3} can be determined in some situations, and thin layers of defects (formed during ion implantation or growth by molecular beam epitaxy, for example) can be measured but with greatly reduced sensitivity due to the small active thickness of the sample.

Photoluminescence

Photoluminescence (PL) involves applying photoexcitation (usually with a laser) to a crystal, and measuring the photons emitted in de-excitation. The luminescence spectrum contains information regarding energy levels due to defects in the crystal (Lightowlers, 1990).

The laser is selected to have an energy slightly larger than the bandgap of the material to be studied (1.1 eV for silicon), so that incident photons excite electrons across the bandgap into the conduction band, producing electron-hole pairs. These pairs can then recombine by a variety of mechanisms, some of which involve photon emission. Electrons in high energy levels also lose energy by phonon emission, with the result that many energy levels *below* that to which electrons are initially excited are also

populated by the laser excitation. The resulting luminescence spectra are complicated by the fact that emission from a single energy level (for example a level in the bandgap introduced by an impurity atom) can result in numerous lines in the spectrum. This is partly because silicon has an indirect bandgap: to conserve momentum, the de-excitation is accompanied by phonon emission, so there are spectral features associated with the emission of transverse optical, longitudinal optical and transverse acoustic phonons. The binding energy of excitons (bound electron-hole pairs) must also be taken into account. The result is that for any sample containing a variety of defect types, interpretation of PL spectra can be difficult. Spectral features due to many common defects have been identified however. The technique is not directly quantitative (although it can be made quantitative by calibration using samples with known defect concentrations) because the luminescent intensity due to a particular defect type depends on capture cross-sections and branching ratios for radiative and non-radiative decay, which cannot readily be predicted. Also, the sensitivity to a particular defect type depends on the concentrations of other defects present in the sample.

Apparatus required for PL includes a laser of energy greater than the bandgap energy (two common choices are the argon 515 nm line (2.4 eV) and the krypton 647 nm line (1.9 eV)) and a spectrometer. A dispersive monochromator can be used, but as for infrared absorption measurements, a Fourier transform spectrometer is preferable. In addition a cryostat is usually required since performing the experiment at ~4K minimizes thermal broadening of spectral features.

The great strength of PL characterization lies in its high sensitivity:

impurities can be detected at concentrations as low as 10^{12} cm^{-3}. It is also possible to characterize thin layers produced by ion implantation or MBE growth, since the depth within the sample from which emitted photons can escape is limited. Scanning PL instruments have been constructed so that, for example, variations in characteristics across a large wafer can be profiled rapidly (Vetter and Winnaker, 1991). There is however, no depth resolution, and the depth which is being sampled can be uncertain since it varies with the material characteristics.

Electrical measurements

Electrical techniques such as Hall effect measurements, capacitance-voltage profiling (CV) and deep level transient spectroscopy (DLTS) will not be discussed in detail here, but their scope and limitations will be addressed. Such techniques are the industry standards for routine characterization of materials. From an engineering viewpoint, they are highly appropriate, since the properties measured (resistivity, carrier concentrations and mobilities, and energy levels in the bandgap) are those of immediate relevance to the manufacturer of devices. However all of these techniques suffer from the need to make electrical contact to the material under study, and in the case of CV and DLTS, to fabricate either a p-n or a Schottky rectifying junction, since it is the properties of a depletion region which are measured. The making of suitable electrical contacts can be a source of irreproducibility and misinterpretation in such experiments.

Summary

It will be apparent from the above discussion that no single technique

can cover all the requirements for characterization of semiconductors. EPR, infrared absorption, and photoluminescence have been used primarily for fundamental research, while electrical techniques have become routine tools of the manufacturer of electronic materials and devices. With these, and supplementary techniques which are not defect-specific, such as Rutherford backscattering/ion channeling, electron microscopy and secondary ion mass spectroscopy, the researcher has an array of tools at his disposal. What then, is the motivation to develop the use of positron annihilation for semiconductor defect characterization? The technique is sensitive to *structural* properties, while most of the techniques discussed above measure electronic properties. Sensitivity to vacancy-type defects is high compared with other methods, depth resolution is provided, and the technique is non-destructive. No sample preparation (polishing, making electrical contacts etc) is required. In addition we might expect that the re-examination of familiar phenomena using a new technique could yield new insights or perspectives on those phenomena.

Chapter 3

Defect profiling with variable-energy positrons

The University of Western Ontario positron beam facility has been described in the literature (Schultz, 1988), so only a brief description will be given here. The apparatus provides a magnetically-guided beam of $\sim 10^4$ positrons s^{-1} at energies from 0.3 to 60 keV, with facilities for the introduction of samples without breaking vacuum, and *in-situ* sample heating to 600° C.

The source of positrons used is ~30 mCi of the radioisotope ^{22}Na, which decays to ^{22}Ne with a half-life of 2.62 years, emitting a positron and a 1.275 MeV γ-ray. Positrons from the source have a continuous energy spectrum up to ~0.5 MeV. Energetic positrons from the source are incident on a tungsten single crystal foil transmission moderator of 1 μm thickness. Positrons in the moderator are slowed to thermal energies, and can then diffuse for some thousands of angstroms. Since the workfunction for positrons in tungsten is negative, those positrons which diffuse to the surface of the moderator may be re-emitted from the solid with an energy of a few eV (i.e. the workfunction potential). The energy spread in the extracted "slow" beam is typically <1 eV. The moderation process is critically dependent on both the crystal quality of the moderator foil, and the cleanliness of its surface; sub-monolayer contamination can significantly suppress re-emission of positrons from the surface. The process is not an efficient one: from a source emitting $\sim 10^9$ positrons s^{-1} we extract a beam of intensity $\sim 10^4$ positrons s^{-1}, giving a moderator

efficiency of 10^{-5}. This poor efficiency is in part due to the design of the present apparatus, which does not permit *in-situ* heating of the moderator to an adequate temperature (2000° C) for cleaning. Efficiencies of at least 10^{-4} should be readily achievable using similar foils. The best efficiencies achieved with W moderators are about 3×10^{-3} in reflection geometry and 1×10^{-3} in transmission (original references are reviewed in Schultz and Lynn, 1988). The "slow" positrons emitted from the moderator surface are accelerated by a potential of 250 volts, and pass through a region of perpendicular electric and magnetic fields (E×B plates) which deflects the beam by ~1 cm to pass between two tungsten blocks. γ-rays and fast positrons from the radioactive source are not deflected by the E×B field and are thus separated from the "slow" beam and stopped by the tungsten blocks. The monoenergetic beam is then accelerated to the desired energy (in the range 0.3 to 60 keV) electrostatically. The beam is confined by an axial magnetic field of ~100 gauss. Although in principle the beam spot size should be energy-independent, in practice the applied electric and magnetic fields are not ideal, and it is necessary to vary the axial magnetic field strength with beam energy to maintain the beam at a constant spot size of ~3 mm. Similarly, the beam spot position is not constant with energy, so the position is adjusted (as a function of beam energy) by two small magnet coils with their axes perpendicular to each other and to the beam axis.

Positrons annihilate with electrons in the target, producing two 511 keV γ-rays. The γ-rays can vary in energy from 511 keV by up to about 2 keV, and can be slightly non-collinear, in order for the momentum of the annihilating pair to be conserved. γ-rays are detected by a Canberra

intrinsic Ge detector of volume 210 cm^3 and resolution 1.3 keV (at 511 keV). In Doppler broadening experiments we measure the *width* of the 511 keV spectral line, which places an unusual demand on the detector: we require not only good energy resolution, but that the energy resolution is stable and does not change due to mechanical vibration or variations in count rate or temperature. Good gain stability of the detector and the associated pulse-processing electronics is also required. The detector must be large to obtain a useable count rate from the weak positron beam, and larger detectors are more prone to vibration-induced variations in energy resolution than smaller ones, so the choice of detector requires a compromise.

Beam operation is computer controlled. The user provides a list of beam energies in a computer file; the computer sets the beam energy, then sets the appropriate currents in the guiding and steering magnets, and acquires a 511 keV γ-ray peak of typically 2.5×10^5 counts, then sets the next beam energy from the list provided. The full list of beam energies is usually repeated six times, giving a total of 1.5×10^6 counts per data point. Thus a typical experiment with 35 data points and a count rate of 600 s^{-1} requires 24 hours to complete.

Monoenergetic positrons (in the energy range 0.3 to 60 keV) are implanted into the sample to be studied. In penetrating the solid the positrons lose energy rapidly, thermalizing in ~10 picoseconds. The mean depth $\bar{z}$ (Å) of implantation into the sample may be varied by changing the incident beam energy E (keV):

$$\bar{z} = (400/\rho)\, E^n \qquad (3\text{-}1)$$

where ρ is the density of the solid (g cm^{-3}) and n is a constant deduced empirically to be $n = 1.6 \pm 0.1$ (Valkealahti and Nieminen, 1984). Recent results reported by Baker *et al.* (1991) indicate that equation (3-1) is not accurate for all materials; it is in good agreement with experimental data for Al (Mills and Wilson, 1982) and should be applicable to silicon since the density and atomic number are similar. This point is discussed further in chapter 5. The depth distribution of thermalized positrons is broad and asymmetric. It can be described by a Makhovian distribution:

$$P(E,z) = (mz^{m-1}/z_0^m)\, \exp[-(z/z_0)^m] \qquad (3\text{-}2)$$

$$\text{with } z_0 = \frac{\bar{z}}{\Gamma(1/m + 1)} \qquad (3\text{-}3)$$

where m = 2.0 (Valkealahti and Nieminen, 1984). Positron implantation depth as a function of energy is shown in figure 3-1. The Makhov implantation profile is illustrated in figure 3-2.

The depth at which the positrons annihilate is not only determined by this broad implantation profile but also by the diffusion that occurs after the positron has thermalized. The diffused positron distribution n(z) can be described by a one-dimensional diffusion equation (Mills and Murray, 1980):

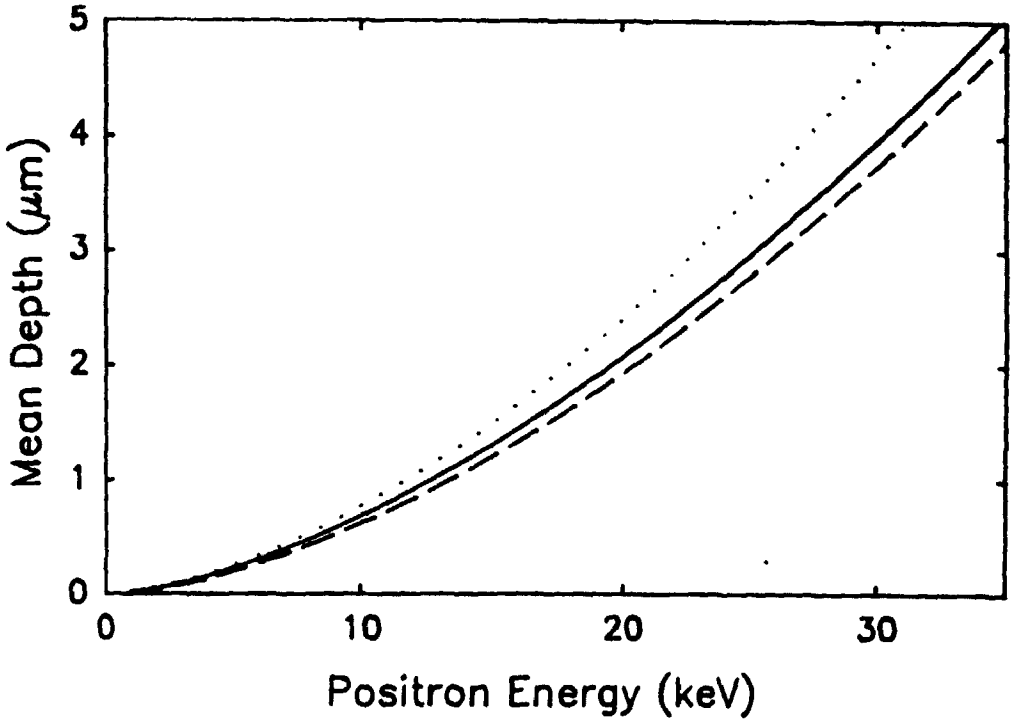

Figure 3-1: Mean positron implantation depth in silicon vs. energy. The solid line shows the mean depth given by equation 3-1, with the parameter n=1.6. The upper (dotted) line shows the mean depth given by equation 3-1 with n=1.65, discussed in chapter 5. The lower (dashed) curve shows mean depths scaled from recent measurements on Al by Baker *et al.* (1991).

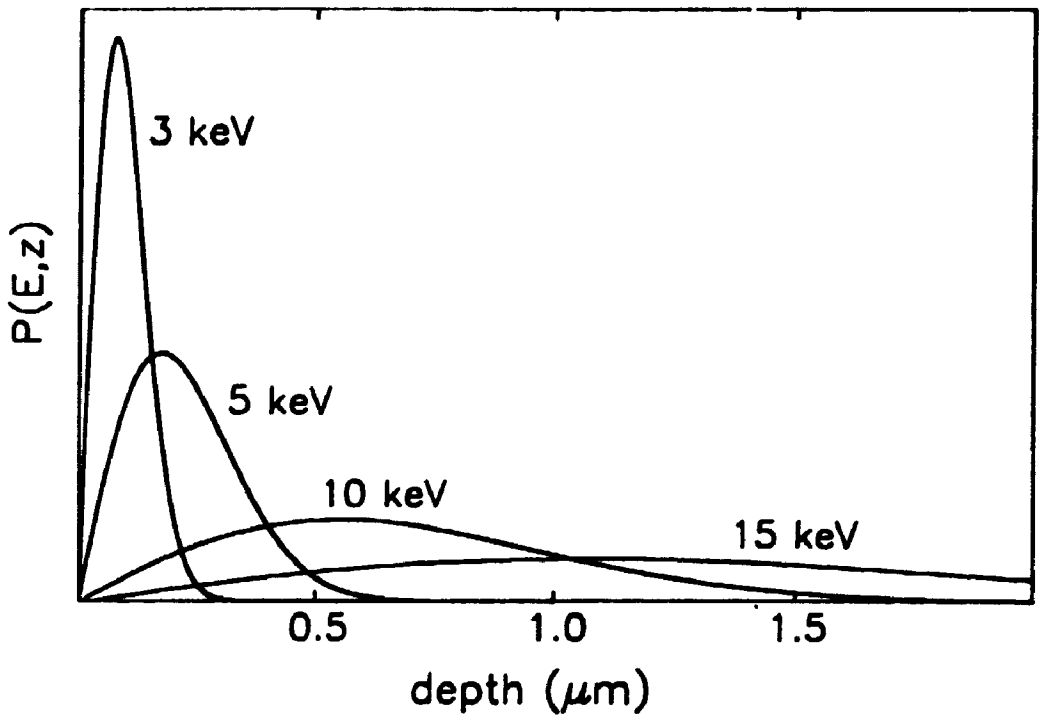

Figure 3-2: The Makhov implantation profile described by equations 3-2 and 3-3 is illustrated for several different positron energies.

$$\left[D_+ \, n''(z)\right] - \left[n'(z)\nu_d(z) + n(z)\nu_d'(z)\right] - \left[n(z)\lambda_{eff}(z)\right] + \left[P(E,z)\right] = 0. \quad (3\text{-}4)$$

Primes denote differentiation with respect to z. Thus we have a diffusion term $D_+ n''(z)$ where D_+ is the positron diffusion coefficient ($cm^2 \cdot s^{-1}$), and a field-induced mobility term $n'(z)\nu_d(z) + n(z)\nu_d'(z)$ where $\nu_d(z) = \mu \, \varepsilon(z)$, with μ the positron mobility ($cm^2 \cdot V^{-1} \cdot s^{-1}$) and $\varepsilon(z)$ the electric field ($V \cdot cm^{-1}$). A "sink" term due to annihilation is given by $n(z) \, \lambda_{eff}(z)$ and a source term is given by the implantation profile P(E,z). The effective annihilation rate is

$$\lambda_{eff}(z) = \lambda_f + \nu C(z) \quad (3\text{-}5)$$

where λ_f is the "free" annihilation rate in the undefected solid ($=4.55\times10^9$ s^{-1} for Si (Dannefaer, 1987)), ν is the specific defect trapping rate (s^{-1}) and C(z) the defect concentration (per atom). Thermal positrons diffuse through a defect-free solid for ~200 picoseconds before annihilating. In the presence of a uniform concentration of defects the fraction F of positrons trapped by defects is given by

$$F = \frac{\nu C}{\nu C + \lambda_f} . \quad (3\text{-}6)$$

Assuming a trapping rate ν of 3×10^{14} s^{-1} per defect (the trapping rate for monovacancies in silicon, reported by Dannefaer (1987)), 5% of the positrons will be trapped by defects at a homogeneous defect concentration of 8×10^{-7} per atom ($\sim10^{16}$ cm^{-3}) and 95% at a defect concentration of 3×10^{-4} per atom

($\sim 10^{19}$ cm^{-3}). These values roughly indicate the range over which one can measure defect concentrations: defect concentrations smaller than 8×10^{-7} will not trap a measurable fraction of positrons, while an increase of the defect concentration above 3×10^{-4} will not lead to a noticeable increase in the fraction of positrons trapped. In practice larger defect concentrations that extend over limited regions of the solid can still be measured (at least approximately) because of their effect on positron diffusion.

The surface of the solid is also an efficient trap for positrons. The positron can be reemitted from a clean surface, either free, or bound with an electron as positronium, but the probability of this is negligible for the (oxide covered) surface of samples discussed here (Schultz and Lynn, 1988).

Annihilation may thus occur from one of three possible states: freely diffusing, trapped at the surface of the solid, or trapped by a point defect. This is illustrated schematically in figure 3-3. In the annihilation event, the momentum of the electron creates a Doppler shift in the energy of the γ radiation emitted. Thus the width of the 511 keV line is sensitive to the electronic environment in the solid, and will differ between positrons trapped by defects and those annihilating in the perfect crystal. This effect is due to both a change in the electron momentum distribution in the region of a defect, and the reduced overlap of the positron wavefunction with high-momentum core electrons permitted by an open volume defect in the crystal lattice.

In the present work, γ-ray spectra are analyzed using the W parameter, defined as the number of counts in the wings of the 511 keV peak (507.3 to 509.7 and 512.3 to 514.7 keV) divided by the total counts in the peak (506.2

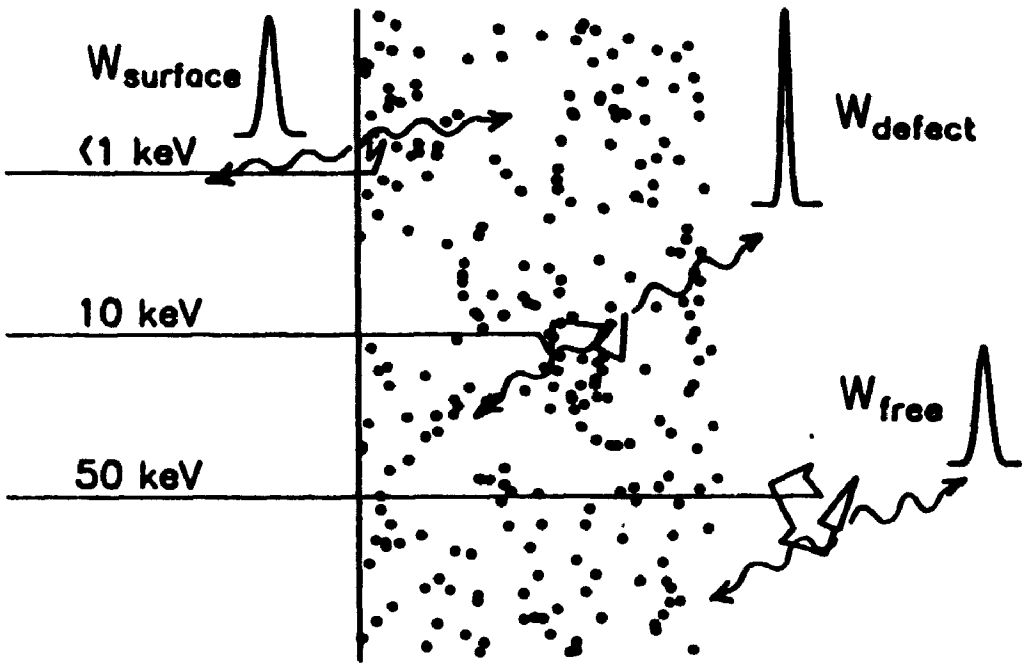

Figure 3-3: Defect profiling is illustrated schematically, for a sample consisting of a defected layer on a defect-free substrate. At low energies most positrons diffuse to the sample surface and annihilate there, resulting in the γ-ray lineshape parameter W_s. At higher energies the positrons can be trapped by defects, resulting in a change in the Doppler-broadened lineshape. At the highest implantation energies, the positrons are implanted past the defected layer, and we obtain a measurement of the W parameter for freely diffusing positrons, W_f.

to 515.8 keV). Historically, greater use has been made of the S parameter, defined as the number of counts in the central region of the 511 keV peak divided by the total counts in the peak. In our case, the central region is defined as that from 510.2 to 511.8 keV; the total is as defined above. Statistical precision of either parameter is given by:

$$\frac{\Delta W}{W} = \frac{1}{\sqrt{W\,N}} \quad \text{or} \quad \frac{\Delta S}{S} = \frac{1}{\sqrt{S\,N}} \qquad (3\text{-}7)$$

where N is the total number of counts in the spectrum, typically about 1.5×10^6. The energy windows are chosen in such a way that the S parameter has a value of about 0.5, and the W parameter about 0.25. For the specific case of ion-implanted silicon we observe that the W parameter is slightly superior to S. In this case, changes in W are typically ~1.9 times larger than changes in S, while S is statistically better by a factor of $\sqrt{2}$ (since it involves twice as many counts in the spectrum), thus the greater sensitivity of W marginally outweighs its lesser statistical precision. More important is the fact that the W parameter is in practice less susceptible to spectrometer instabilities, i.e. it is more resistant to changes caused by shifts in the centroid of the peak due to gain drift. Due to variations in detector resolution and the exact choice of energy "windows", the absolute values of lineshape parameters will vary among laboratories, but the ratio of measured values to the parameter obtained for defect-free bulk silicon should be intercomparable. Efforts have been made to extract more information from Doppler broadening experiments, either by more sophisticated parameterization of the lineshapes (see e.g. Mantl and

Triftshäuser, 1978) or by applying statistical techniques to reduce the scatter in values of S or W parameters (Leffler *et al.*, 1990). It is not apparent however, that any of these methods constitute an improvement over the simple parameterization currently in use.

The W parameter vs. energy data are analyzed using the program POSTRAP4 (Aers, 1990), which solves equation (3-4) above, the diffusion equation for positrons in a semiconductor, including the effect of defects and electric fields. POSTRAP4 calculates, for each incident positron beam energy E, the fractions of positrons which annihilate in defects $F_d(E)$, which annihilate while freely diffusing in the bulk crystal $F_f(E)$, and which annihilate at the surface $F_s(E)$, for each model of defects and electric fields in the sample. The experimental lineshape parameter W(E) can then be fitted using the equation

$$W(E) = W_s F_s(E) + W_f F_f(E) + W_d F_d(E) \quad (3\text{-}8)$$

where W_s, W_f and W_d are the characteristic lineshape parameters for annihilation at the surface, freely diffusing in the bulk, and trapped in a defect, respectively. The parameter W_s is obtained from the data for low energy implantation, in which nearly all positrons diffuse to and become trapped at the sample surface. W_s depends on the condition of the surface, and usually varies slightly from sample to sample. W_f is usually obtained from positron implantation at high energy, in which case nearly all positrons annihilate in the defect-free bulk crystal beyond the depth of the defected layer being analyzed.

The fitting procedure is illustrated in figure 3-4. A model defect

Figure 3-4: The positron fitting procedure is illustrated, for the case of Si implanted with 10^{15} 3 MeV Si ions cm^{-2}. A defect distribution must first be assumed (top panel), in this case derived from TRIM (see chapter 4). The profile can be simulated with a few blocks of defects without loss of accuracy due to the smearing effects of the positron implantation profile and diffusion. The diffusion equation for positrons in the solid is then applied to determine the fraction of positrons annihilating in each of three states (bottom panel). The W parameter at each beam energy is then just a linear combination of these 3 states, producing the fit shown (solid line) in the middle panel.

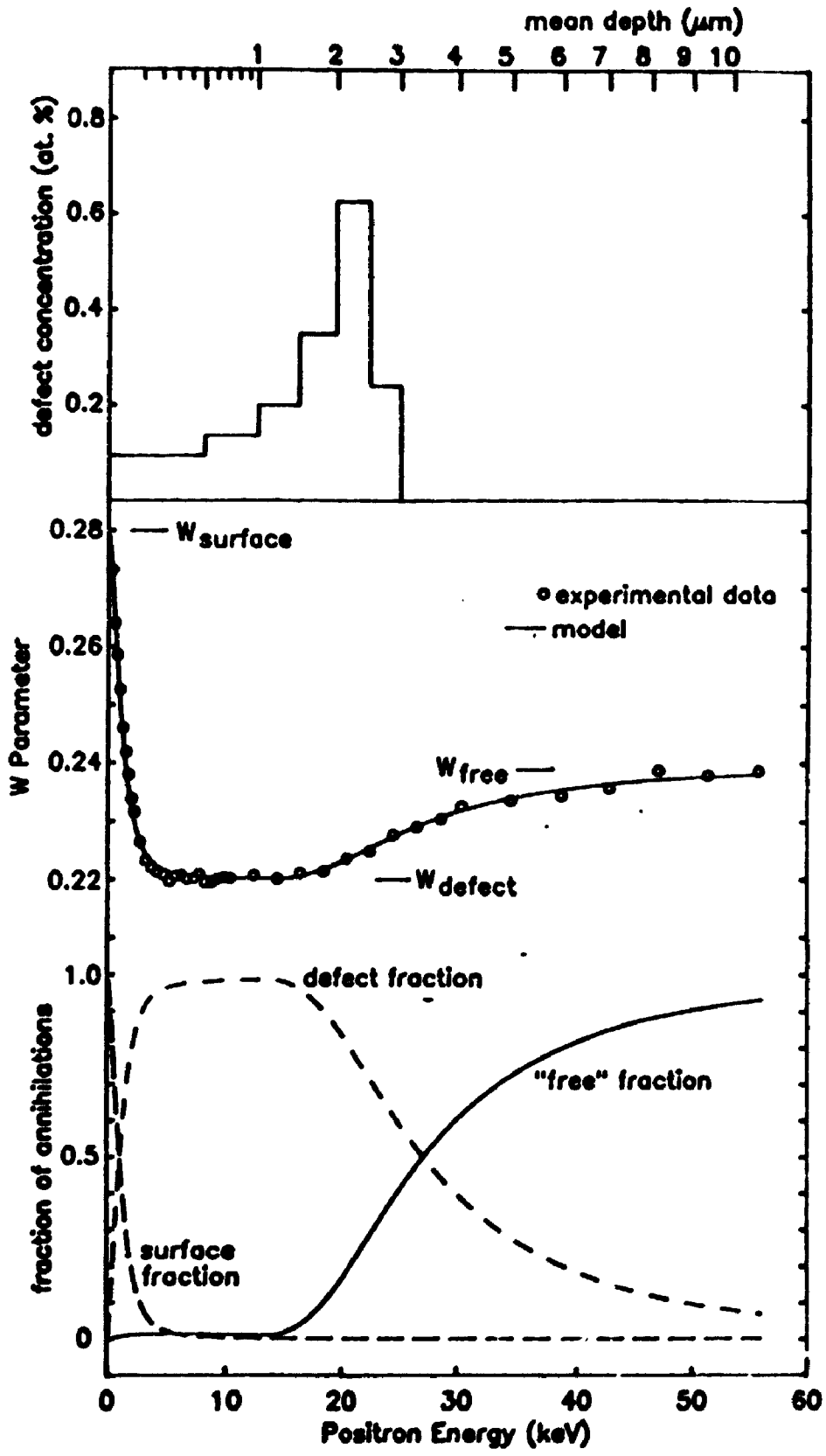
mean depth (μm)
1
2
3
4
5
6
7
8
9
10
defect concentration (at. %)
0.8
0.6
0.4
0.2
W Parameter
0.28
0.26
0.24
0.22
W surface
experimental data
model
W free
W defect
fraction of annihilations
1.0
0.5
0
defect fraction
"free" fraction
surface fraction
0
10
20
30
40
50
60
Positron Energy (keV)

distribution (in this case based on TRIM, see chapter 4) is assumed (top panel). The fraction of positrons trapped in defects and at the surface is calculated for each positron energy, using POSTRAP4, (bottom panel). Then using equation 3-8 above a W parameter is obtained for each positron energy and compared with the experimental results (middle panel).

In principle we can determine the defect parameter W_d, defect concentrations and distributions, and the magnitude of electric fields using this fitting procedure, although only a single "average" type of defect can be characterized in any single sample, i.e. information regarding more than one kind of defect co-existing in a sample cannot be separated. In practice there is considerable interdependence among the fitting parameters, so that for instance it may be difficult to distinguish between a large concentration of defects with W_d similar to W_f, and a smaller concentration of defects with W_d much different from W_f. It can also be difficult to distinguish among the effects of a change in diffusion coefficient, an electric field, and a small concentration of defects. Near-surface electric fields are common in silicon and have been measured using positrons (Schultz *et al.*, 1988). Diffusion constants have been measured ranging from ~2.1 to 2.7 $cm^2\ s^{-1}$ for Si wafers, to 2.9 $cm^2\ s^{-1}$ for layers grown by molecular beam epitaxy (Schultz *et al.*, 1988). Corresponding diffusion lengths are ~2000 to 2500 Å. In the modelling procedure described, it is assumed that the diffusion coefficient D_+ is unchanged by the addition of defects to a crystal. The effect of defects in reducing the positron diffusion is however accounted for in the modelling procedure by the trapping of positrons by defects, i.e. diffusing positrons are described by a constant D_+, but defect trapping removes some fraction of the positrons from the

freely diffusing state. Thus the positron diffusion length L_+ is reduced with increasing defect trapping:

$$L_+ = \left[\frac{D_+}{\nu C + \lambda_f}\right]^{1/2} \qquad (3\text{-}9)$$

A detailed discussion of this is given by Tandberg *et al.* (1989). The effect on the measurements of introducing (during ion irradiation for example) scattering centres which reduce the diffusion length but do not trap positrons is unclear. The present modelling procedure does not account for this and it is not apparent that such a refinement could readily be made.

To reduce the ambiguities in the modelling procedure caused by the interdependence of parameters the approach usually adopted is to perform a series of experiments on samples with some known relationship between them, for example, ion irradiation with varying fluence, or varying ion energy. Another useful technique is to chemically etch a known quantity of material from the sample surface, and then look for consistency between results before and after etching. A third approach is to correlate positron measurements with results obtained by other experimental techniques, such as electron microscopy (Simpson *et al.*, 1990), secondary ion mass spectroscopy (Simpson *et al.*, 1989), infrared absorption or ion channeling (Simpson *et al.*, 1991).

There are now a dozen or so groups world-wide working on defect profiling with positron beams. What has been achieved in the 10 years or so of development of the technique? Triftshäuser and Kögel (1982) reported the first determinations of sub-surface defect profiles, for the case of He

ion-irradiated Ni and Cu, but the defect profile was not modelled in detail. Developments since then have involved solving the diffusion equation (equation 3-4) by a variety of numerical and analytical techniques. The culmination of this decade of development is represented by two computer routines: POSTRAP4, discussed above, and VEPFIT (van Veen, 1990). VEPFIT solves equation (3-4) for a variety of cases, including heterogeneous multilayer samples, that make it very general and broadly applicable. It remains the case that an initial model of the defect profile is required: there are no routines available to analyze defect profiling data directly. Part of the reason for this is that the solutions to this mathematical problem are not unique: there are in general a range of possible models that can reproduce any given set of data to within the experimental uncertainties.

The fundamental weakness in positron defect profiling remains however, not in the mathematics of the analysis, but in the uncertainty of the underlying physical constants and the precision of the experimental data. The fundamental data required as input to the fitting routines, such as defect trapping rates and lineshape parameters, are in most cases not known. Using positron lifetime measurements (which permit defect-specific interpretation, rather than the measurement of a single, "average" defect type as in Doppler-broadening studies) and samples of known characteristics produced by electron irradiation, Mascher *et al.* (1989a) have determined the positron trapping rate for divacancies in Si, with a stated factor-of-two uncertainty. A Doppler-broadening lineshape parameter value has also been reported for this defect (Keinonen *et al.*, 1988). Similar results have been obtained for vacancy-type defects in GaAs (Saarinen *et al.*, 1991). An

approximate lineshape parameter has been assigned for oxygen impurities in Si (Chilton *et al.*, 1990). For the majority of cases however, the technique remains somewhat qualitative, awaiting further systematic, fundamental studies to establish the required background. That this is so has not prevented application of the technique to a variety of materials-processing problems in which even limited, qualitative information has proven to be useful.

Chapter 4

Ion beam induced damage in silicon

Introduction

The most important materials issues in silicon device manufacturing pertain to the introduction of dopants in a controlled way. The predominant method of dopant introduction for many years was diffusion. This method is being supplanted by ion implantation, which affords greater control over the location of dopant species, and offers the possibility to make structures not feasible using diffusion methods, such as buried thin insulating layers. While the control over dopant profiles is not as good as that provided by direct incorporation *during* growth (by molecular beam epitaxy or chemical vapour deposition), ion irradiation provides a versatile technique for post-growth modification. The ion bombardment process introduces defects, and thermal processing is required to anneal these. Thermal processing is also often required to electrically activate the doping species, i.e. to induce dopant atoms to occupy substitutional sites in the crystal lattice, rather than interstitial ones. Since the earliest reports of experiments on ion implantation into silicon (Mayer *et al.*, 1968) a continuing interest has been shown in microscopic descriptions of the associated radiation damage.

Ion irradiation induced defects

In coming to rest in a solid, an energetic (~MeV) ion must give up its kinetic energy to the solid, where most of that energy is eventually dissipated in the form of heat. The energy loss mechanisms are of two

kinds- electronic stopping and nuclear stopping. The incident ion interacts with electrons and nuclei in the solid through the Coulomb force. Interactions with electrons cause most of the energy loss of the incident ion, but do not contribute significantly to the damage introduced to the crystal lattice. That damage is produced by direct nuclear collisions: the energetic ion collides with an atom of the lattice, imparting some fraction of its energy to that atom. If the energy imparted to the lattice atom is greater than some threshold energy of ~15 to 20 eV, that atom will be displaced from its lattice site. If the displaced atom has sufficient energy, it can go on to displace further atoms from the lattice by "secondary" collisions. The immediate result is that vacancy-interstitial pairs (Frenkel pairs) are produced. Both vacancies and interstitials in silicon are mobile at room temperature. A large fraction of these pairs can recombine, and those that remain can interact with each other and with impurity atoms to form a variety of defect types: multi-vacancies, vacancy-impurity complexes etc.

The cross-sections for nuclear and electronic stopping processes vary with energy. The nuclear and electronic stopping powers (or energy loss per unit of distance travelled) for the case of silicon ions in silicon are shown in figure 4-1. The nuclear stopping power peaks at ~15 keV and decreases above that energy, with the result that the majority of the damage introduced by an ion is in the end-of-range region. The density of the damage produced depends on the ion mass, energy, flux and fluence, and on the substrate temperature during irradiation. For heavy incident ions, the density of damage in the end-of-range region can be sufficient that an amorphous zone is created. In general the ion track in the solid will

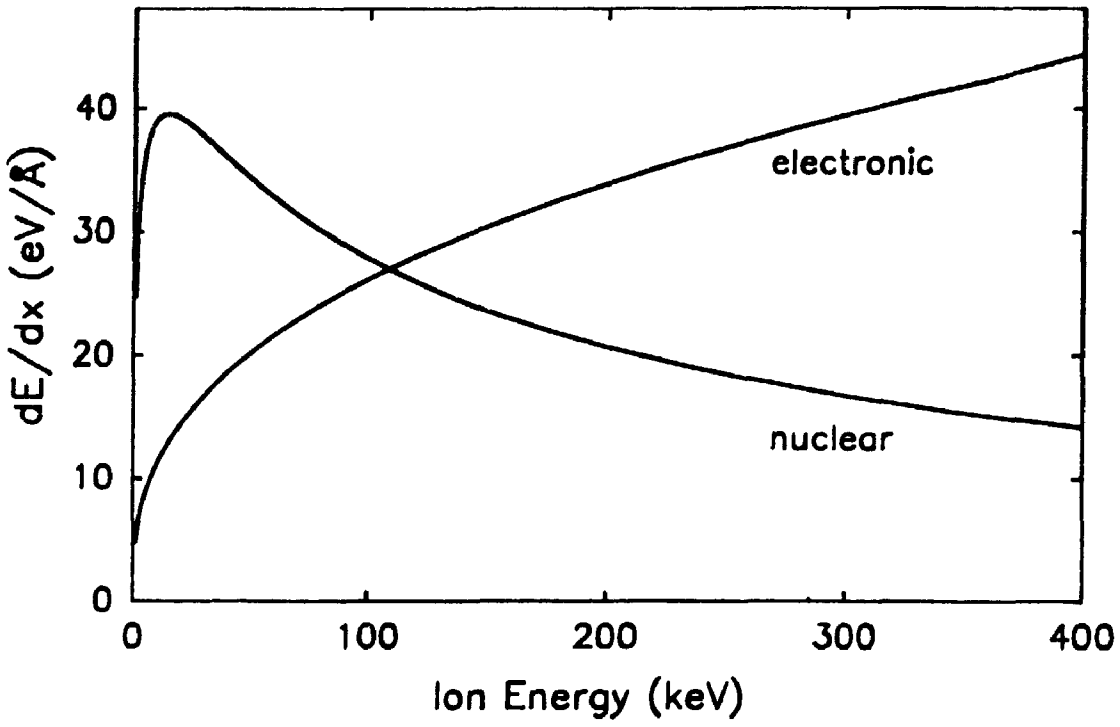

Figure 4-1: Nuclear and electronic stopping powers as a function of energy for the case of silicon ions in silicon. Note that the electronic stopping is dominant at high energies.

consist of a vacancy-rich core, surrounded by a region rich in interstitials.

The processes of ion stopping are sufficiently well understood to be simulated by a Monte Carlo routine. A well-known example of this, called TRIM (Biersack and Haggmark, 1980), was used in the present study. These calculations give a good estimate of the number of atoms initially displaced by each incoming ion, and thus the depth distribution of vacancies. However many of the defects initially formed will recombine or cluster and such condensation processes are not included in the calculation. Also the calculations assume an amorphous solid and thus do not simulate channeling effects of the implanted ions. Provided that the ion beam direction is not along a major crystallographic axis this is an acceptable approximation. TRIM profiles of vacancy production in silicon due to irradiation by silicon ions at 0.54, 3 and 5 MeV, and by helium ions at 0.25 and 0.7 MeV are shown in figure 4-2. It will be noted that the damage is peaked in the end-of-range region and that the density of damage is more than an order of magnitude higher for Si ion irradiation than for He.

Of the many point defects identified in ion-implanted silicon (Corbett *et al.*, 1981a) the divacancy has been singled out for particular attention. In an infrared absorption study of 400 keV ^{11}B, ^{64}Zn and ^{121}Sb implanted silicon, Stein *et al.* (1970) were able to relate divacancy formation to the energy deposited in collisional processes up to a critical energy density at which amorphous zones are believed to form. In their study of ion beam-induced transitions between amorphous and crystalline phases at the crystalline-amorphous boundary in silicon, Linnros *et al.* (1988) identified the divacancy as the defect responsible for crystal growth or amorphization

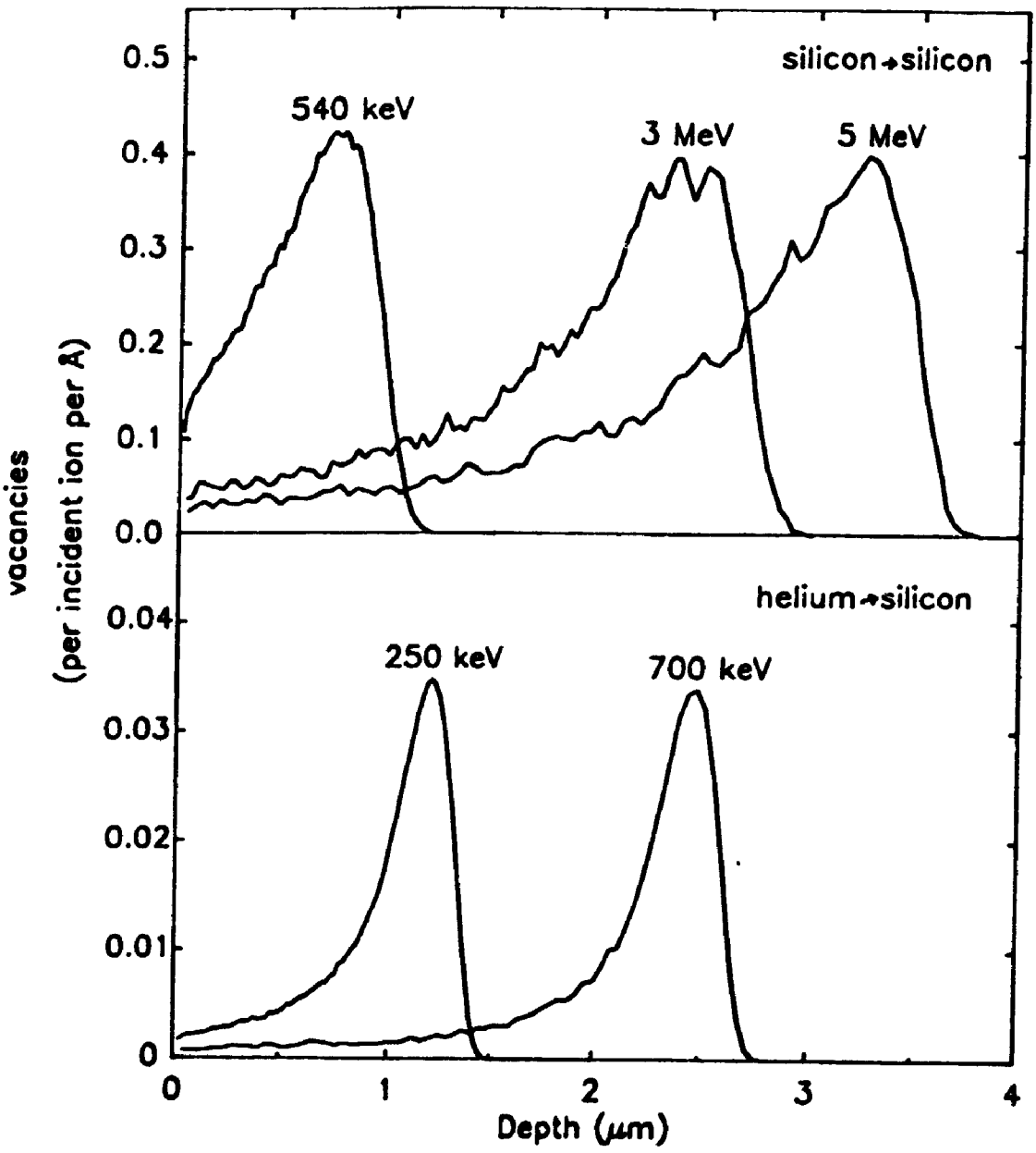

Figure 4-2: Vacancy production as calculated using the TRIM code. The top panel shows the result for silicon implantation, and the lower one for helium. Note the difference in the vertical scales. The vacancy profiles for He^+ implantation, and to a lesser extent for Si^+ implantation are peaked near the end of range of the implanted ions.

in the temperature range 200 to 400° C, the outcome being controlled by sample temperature and ion flux. Likewise, divacancy production was identified as the central process in two discrete modes of damage accumulation during silicon self-ion irradiation (Holland *et al.*, 1989).

The intent of this study was to re-examine the nature and growth of ion beam damage in silicon using the positron beam technique, supplemented by ion backscattering and optical absorption data. Beams of ~MeV energy He and Si have been used for the irradiations to produce an abundance of relatively simple defects.

Ion channeling/backscattering

Channeling/backscattering using light ions (typically 3 MeV He^+) is a well-established technique for measuring the depth distribution of defects created by ion implantation (Feldman *et al.*, 1982). The channeling technique measures the number of atoms that are displaced from their lattice sites (interstitial atoms, atoms in amorphous or disordered zones etc) by directing a beam of ions onto a crystal in a channeling direction (i.e. along a major crystallographic axis) and measuring the energy spectrum of backscattered ions. In a simplified picture, channeled ions can not backscatter from atoms at lattice sites, but may backscatter from displaced atoms. Non-channeled (or dechanneled) ions will have a "random" backscattering probability from both lattice atoms and displaced atoms. Thus the normalized backscatter yield $\chi(z)$ (aligned yield divided by random yield) from depth z is given by:

$$\chi(z) = [1-\chi_d(z)] \frac{N_d(z)}{N} + \chi_d(z) \qquad (4\text{-}1)$$

where $\chi_d(z)$ is the dechanneled component at depth z. $N_d(z)/N$ is the fraction of atoms displaced from their lattice sites. Some channeled ions will dechannel due to small angle deflections by displaced atoms and thus the dechanneled fraction will increase as:

$$\frac{d\chi_d}{dz} = \sigma_d \frac{N_d}{N} (1-\chi_d) \qquad (4\text{-}2)$$

The dechanneling cross section σ_d is chosen in such a way that the defect concentration at a depth much larger than the range of the ions is equal to zero. At the surface no dechanneling has taken place, so the number of displaced atoms is given by :

$$N_d(0) = N - \frac{\chi(0) - \chi_v(0)}{1 - \chi_v(0)} \qquad (4\text{-}3)$$

where χ_v is the normalized yield from an unimplanted crystal. From the number $N_d(z)$ of displaced atoms we can calculate the increase of the dechanneled fraction at depth z and use this to successively determine the number of displaced atoms at larger depth.

This, together with an energy-to-depth conversion using the (known) stopping power of the incident ions, will provide us with a defect depth profile.

Infrared absorption

Positron annihilation and channeling each provide information about a category of defects: open volume defects, and displaced atoms, respectively. In ion implanted silicon an infrared absorption band centered at 1.8 μm

wavelength is attributed to the divacancy (Stein *et al.* 1969; Stein and Beezold, 1970). Because the monovacancy becomes mobile in Si well below room temperature (Corbett *et al.* 1981a), the divacancy is the simplest vacancy-type defect present. Moreover it has been shown that the infrared absorption technique can be calibrated so that an absolute areal density of divacancies can be determined (Cheng and Lori, 1968). A comparison between the number of vacancy-type defects observed by positron annihilation spectroscopy and the number of divacancies is then possible.

Samples for infrared absorption measurements were polished on both sides, and subsequently implanted from both sides in order to increase the signal strength. Optical transmission measurements were made at room temperature using a Nicolet Model 605X FTIR spectrometer.

Implantation

Wafers of (100) p-type float zone silicon 0.5 mm thick were implanted at an off-normal orientation, using the University of Western Ontario 1.7 MV Tandetron accelerator. ^{4}He ions were implanted at energies of 0.25, 0.5, 0.7 and 4 MeV, in doses from 10^{13} to 10^{16} ions cm^{-2}, and ^{28}Si ions were implanted at energies of 0.54, 3 and 5 MeV in doses from 10^{11} to 10^{15} ions cm^{-2}. The beam was rastered to give uniform irradiation over an area ~75 mm in diameter. Beam current was maintained at 0.3 μA or less to minimize beam heating of the samples, although some beam heating (a few tens of degrees) did occur. Recent ion channeling measurements of the disorder produced by 1 MeV self-ion irradiation of silicon indicate that changes in temperature of this magnitude may be sufficient to alter significantly the type of damage remaining after annealing (Schultz *et al.*, 1991). The samples were

characterized by positron annihilation, RBS/channeling and infrared absorption both as-implanted and after annealing stages.

Silicon implantation in silicon

Room temperature results

Figure 4-3 shows the W parameter versus positron energy for silicon implanted with 540 keV Si^+ ions to fluences from 10^{11} to 10^{15} cm^{-2}. (Data for 10^{15} cm^{-2} are offset downward for clarity). For the unimplanted sample the measured W parameter decreases slowly with positron energy until the "free" value W_f is reached. This is a consequence of the fact that with increasing energy fewer and fewer positrons will diffuse to and annihilate at the surface. For positron energies exceeding ~12 keV the W parameter is virtually constant, i.e. $W=W_f$. Data from a sample implanted to 10^{11} ions cm^{-2} show a small but significant decrease in the W parameter over the region from ~5 to 15 keV positron energy. Increasing the irradiation dose produces further decreases in the W parameter, monotonic with ion fluence, until a saturation level is reached. The data for fluences of 10^{14} and 10^{15} ions cm^{-2} are very similar, indicating that the positron trapping is saturated, i.e. in the damaged region all positrons are trapped by defects, and adding more defects does not lead to more trapping. Some limited sensitivity to increasing defect concentrations remains however, since the region over which saturation trapping occurs becomes broader with further increasing defect concentrations. Ion channeling measurements of similar samples indicated a factor of ~2.5 increase in defect concentration in going from an ion dose of 10^{14} to 10^{15} cm^{-2}. This indicates that the damage is not saturated (although the positron trapping is) but is increasing

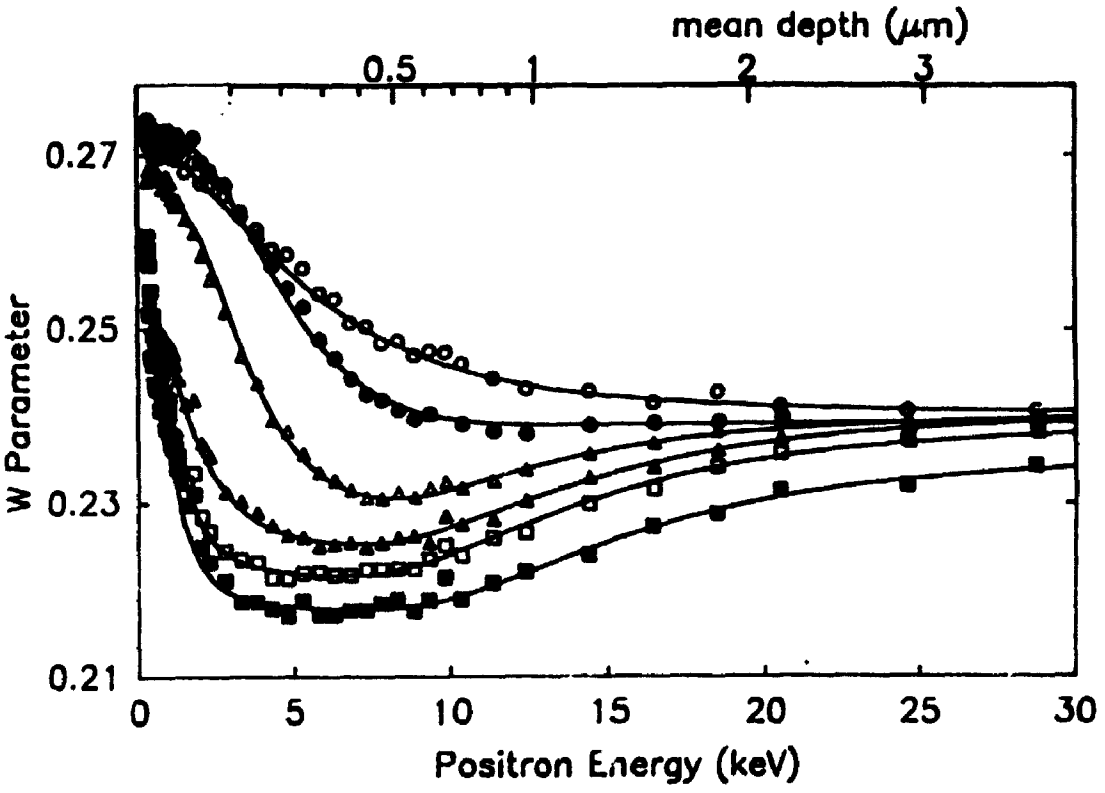

Figure 4-3: W parameter versus positron energy as a function of fluence of 540 keV Si ions implanted. Unimplanted ○ , and fluences/cm^2 of 10^{11} ●, 10^{12} △, 10^{13} ▲, 10^{14} □, and 10^{15} ■. Data for 10^{15} ions cm^{-2} are displaced downwards by 0.005 for clarity. Solid lines show fits to the data. With increasing Si dose the W parameter around 5 to 10 keV decreases due to an increase in the implantation damage.

less-than-proportionally with ion fluence. Ion channeling measurements of samples implanted to fluences less than 10^{14} Si ions cm^{-2} were not possible due to the limited sensitivity of the technique.

As was stated in chapter 3, interpretation of positron annihilation data can be ambiguous, and it is often desirable to measure a range of samples with known relationships between them to reduce these ambiguities; such a case is examined here. To fit the positron data in figure 4-3, two different models are possible, as follows:

Model 1: Assume that for the two lowest dose implantations (i.e. 10^{11} and 10^{12} ions cm^{-2}), the damage should increase (approximately) proportionately with ion dose, since the damage cascades are sufficiently few to minimize interactions between them. Thus we require for these two samples that the derived defect concentrations differ by a factor of 10, and that W_d is the same for both, since the types of defects present should be the same. Applying these constraints removes ambiguity due to the interdependence between W_d and defect concentration, and we find that the parameter W_d/W_f obtained is 0.935. This value can be associated through previous measurements with divacancies- fitting S parameters (a related measure of γ-ray linewidth, see chapter 3) extracted from the same experimental data, we find $S_d = 1.035 \pm 0.005$, in agreement with values previously identified with divacancies, for example $S_d = 1.034$ (Keinonen *et al.*, 1988). This is not intended to imply that the defects must be divacancies, nor that we have measured the divacancy W parameter. This point is further discussed below.

It is found for the higher fluence implants that the same W_d value can no longer be used, since the minimum experimental W/W_f parameter is *less*

than 0.935, so W_d must decrease with increasing ion dose. It is assumed that the fraction of vacancy-type defects *larger* than divacancies (and having lower W_d parameters) increases with increasing ion fluence to produce this effect.

Model 2: An alternative model requires the assumption that the defect type should not change with ion dose. Then the parameter W_d (for all ion fluences) is chosen to be equal to the lowest experimental W parameter, obtained for the highest implantation dose (in which case the positrons are all trapped by defects, so that $W_{experimental} \cong W_d$). However, using this lower W_d parameter to fit the low dose data (10^{11} and 10^{12} ions cm^{-2}) results in defect concentrations which differ only by a factor of ~5, which does not seem reasonable.

Results of fits to the data are summarized in table 4-1.

In fitting the positron data, it is (as discussed in chapter 3) necessary to first assume a model for the defect profile in the sample, and then calculate (using POSTRAP4) for each incident energy the fractions of positrons annihilating at the surface, freely diffusing in the bulk crystal, and trapped by defects. The resulting fractions are fit to the experimental data by assigning values to the W parameters for each of the three states. For ion-irradiated samples a suitable source of a starting model for the shape of the defect profile is the profile of vacancy production vs depth given by TRIM calculations. For the 540 keV Si ion implanted samples discussed above, the positron data were fit assuming the shape of the defect distribution to be given by TRIM, but not the absolute magnitude. The shape of the defect distribution given by TRIM is in good agreement with ion

channeling measurements. It was also possible, however, to fit the positron data assuming as a profile a "block" of defects of constant concentration, extending to the maximum depth predicted by TRIM for the incident ions, 0.8 μm. W_d parameters resulting from such a model were similar to those obtained using the TRIM profile.

To further test the depth profiles extracted from positron data, samples were implanted with Si^+ ions at energies of 3 and 5 MeV. The ranges of these ions are ~2.5 and 3.3 μm respectively. Positron data resulting from these samples are shown in figures 4-4 and 4-5. Results were similar to those described above for the case of 540 keV implantation, with the exception that the data could *not* be fit by assuming a constant "block" of defects extending from the surface to the maximum ion depth. The data were in all cases well fit by assuming the TRIM vacancy profile. Results are summarized in table 4-1.

To fit the positron data discussed in this chapter a defect trapping rate $\nu = 6\times10^{14}$ s^{-1} was assumed, twice the monovacancy trapping rate given by Dannefaer (1987). This value was chosen since it was assumed that divacancies might be the predominant positron-trapping defect. More recently, a direct determination of the divacancy trapping rate has been reported by Mascher *et al.* (1989a), and this is discussed in detail below. Errors in this parameter translate directly to errors in the derived defect concentration C because the product νC determines the fraction of positrons trapped by defects- see equation 3-6. Assuming this value for ν, a defect production rate of ~180 per incident ion was obtained for the low fluence 540 keV implants. This is much smaller than the number of vacancies per incident ion produced as calculated using the TRIM code (~2900 per ion).

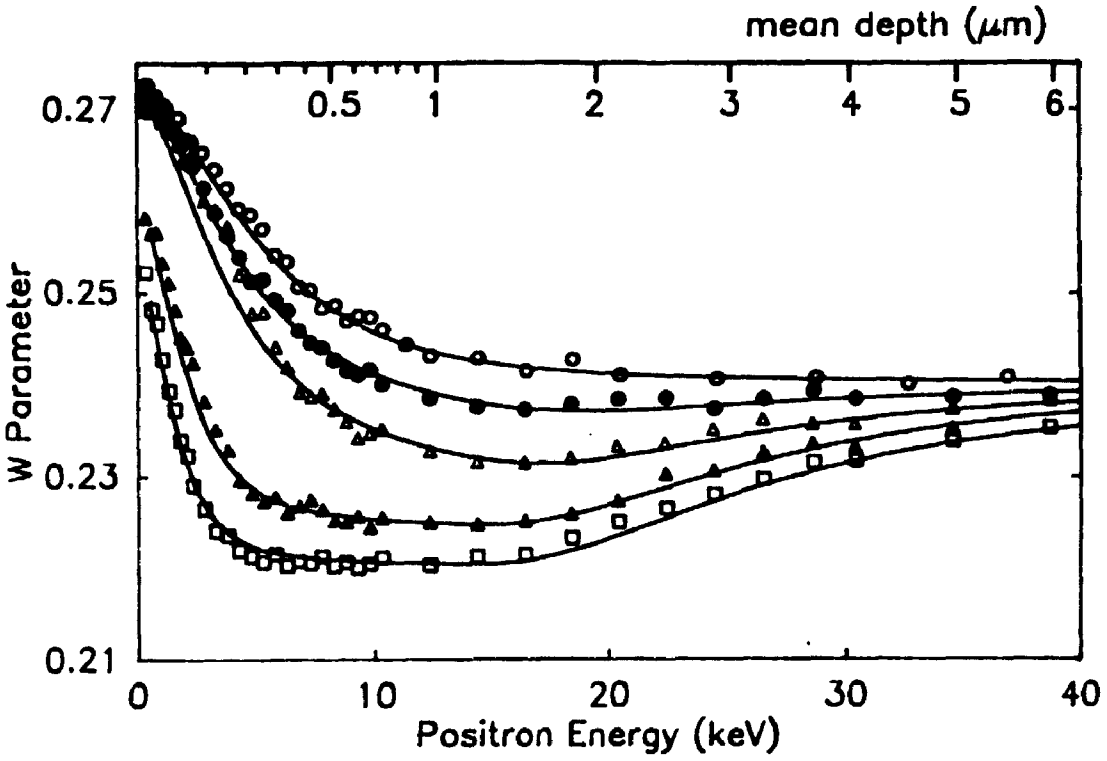

Figure 4-4: Positron data from Si implanted with 3 MeV Si ions at fluences of 10^{11} ●, 10^{12} △, 10^{13} ▲ and 10^{14} □ ions cm^{-2}. Unimplanted ○. Solid lines show fits to the data. Data for 10^{15} ions cm^{-2} are not shown due to similarity to data for 10^{14} cm^{-2}.

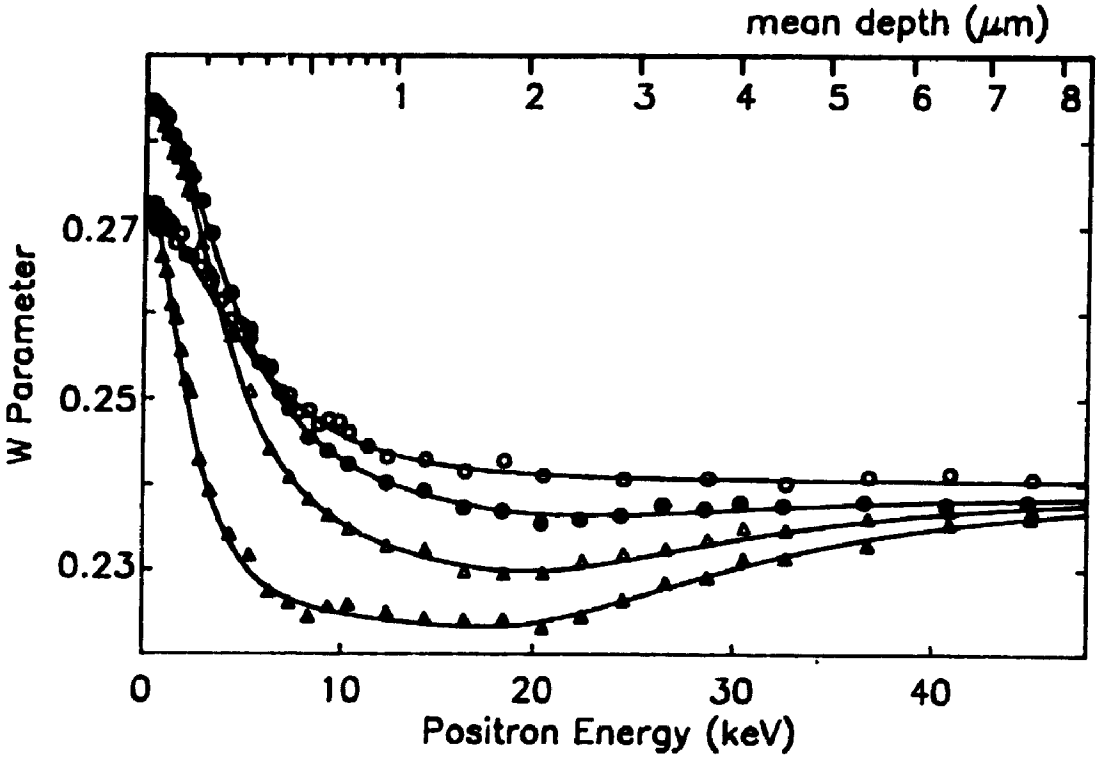

Figure 4-5: Positron results for Si implanted with 5 MeV Si ions at fluences of 10^{11} ●, 10^{12} ▲ and 10^{13} ▲ ions cm^{-2}. Unimplanted ○. Solid lines show fits to the data.

Table 4-1: Summary of data. Defect concentrations (cm^{-2}) as derived from positron annihilation, IR absorption (divacancies), RBS (number of displaced atoms), and TRIM. Numbers given for TRIM are obtained by multiplying the number of vacancies per incident ion resulting from the simulation by the ion fluence. Positron results marked by a * represent a lower limit on the defect concentration, and cannot be considered accurate due to the model of two competing defect types discussed in the text.

			defect concentration (cm^{-2})			
energy (MeV)	dose (10^x cm^{-2})	W_d/W_f	positron	I.R. (V-V)	RBS	TRIM
Si ions						
0.54	11	0.937	1.8×10^{13}			2.9×10^{14}
	12	0.937	1.8×10^{14}			2.9×10^{15}
	13	0.930	9.0×10^{14}			2.9×10^{16}
	14	0.923	3.0×10^{15}		5.5×10^{16}	2.9×10^{17}
	15	0.923	6.5×10^{15}		1.4×10^{17}	2.9×10^{18}
3.0	11	0.935	4.0×10^{13}			4.6×10^{14}
	12	0.935	2.9×10^{14}			4.6×10^{15}
	13	0.930	2.3×10^{15}			4.6×10^{16}
	14	0.920	1.1×10^{16}	6.5×10^{15}		4.6×10^{17}
	15	0.918	2.3×10^{16}		2.3×10^{17}	4.6×10^{18}
5.0	11	0.935	4.9×10^{13}			4.9×10^{14}
	12	0.935	4.9×10^{14}			4.9×10^{15}
	13	0.930	3.7×10^{15}			4.9×10^{16}
He ions						
0.25	14	0.925	6.5×10^{14}*			1.6×10^{16}
0.5	16	0.913	2.7×10^{15}		7.7×10^{16}	
0.7	13	0.935	9.0×10^{13}			1.8×10^{15}
	14	0.935	9.0×10^{14}			1.8×10^{16}
	15	0.920	1.3×10^{15}*	1.3×10^{15}		1.8×10^{17}
	16	0.913	2.7×10^{15}*	2.6×10^{15}		1.8×10^{18}
4.0	14	0.935	1.8×10^{15}			2.3×10^{16}

The number of displaced atoms measured by ion channeling is also much greater than the number of vacancies measured by the positron method (see table 4-1), but less than that predicted by TRIM.

Infrared absorption measurements performed on a sample implanted with 3 MeV energy Si ions to a fluence of 10^{14} ions cm^{-2} on back and front surfaces, showed a divacancy concentration *per side* of 6.5×10^{15} cm^{-2}, again well below the number of displaced atoms ($\sim10^{17}$ cm^{-2}) interpolated from the RBS data, and slightly less than the number of defects measured by positron annihilation: 1.1×10^{16} cm^{-2}.

Figure 4-6 summarizes the relationship between defect concentrations (derived from positron measurements) and Si ion fluence.

Annealing

RBS measurements of a sample implanted to 10^{15} cm^{-2} with 0.54 MeV Si ions, then annealed for ten minutes at 500K, showed partial recovery of lattice order with a 50% reduction in the disorder signal. No further recovery was observed through isochronal annealing at 700K. The disorder peak disappeared completely from the channeling spectrum after a ten minute anneal at 900K, a temperature sufficient to activate the amorphous-to-crystalline transition.

By contrast, a 30 minute anneal at 573K of the 10^{14} cm^{-2} 3 MeV Si ion implant was sufficient to remove the 1.8 μm absorption peak (5555 cm^{-1}) from the infrared absorption spectrum, implying that the divacancies had annealed. A featureless absorption continuum at 5000 cm^{-1} and beyond indicated that optically active scattering centres remained in the sample.

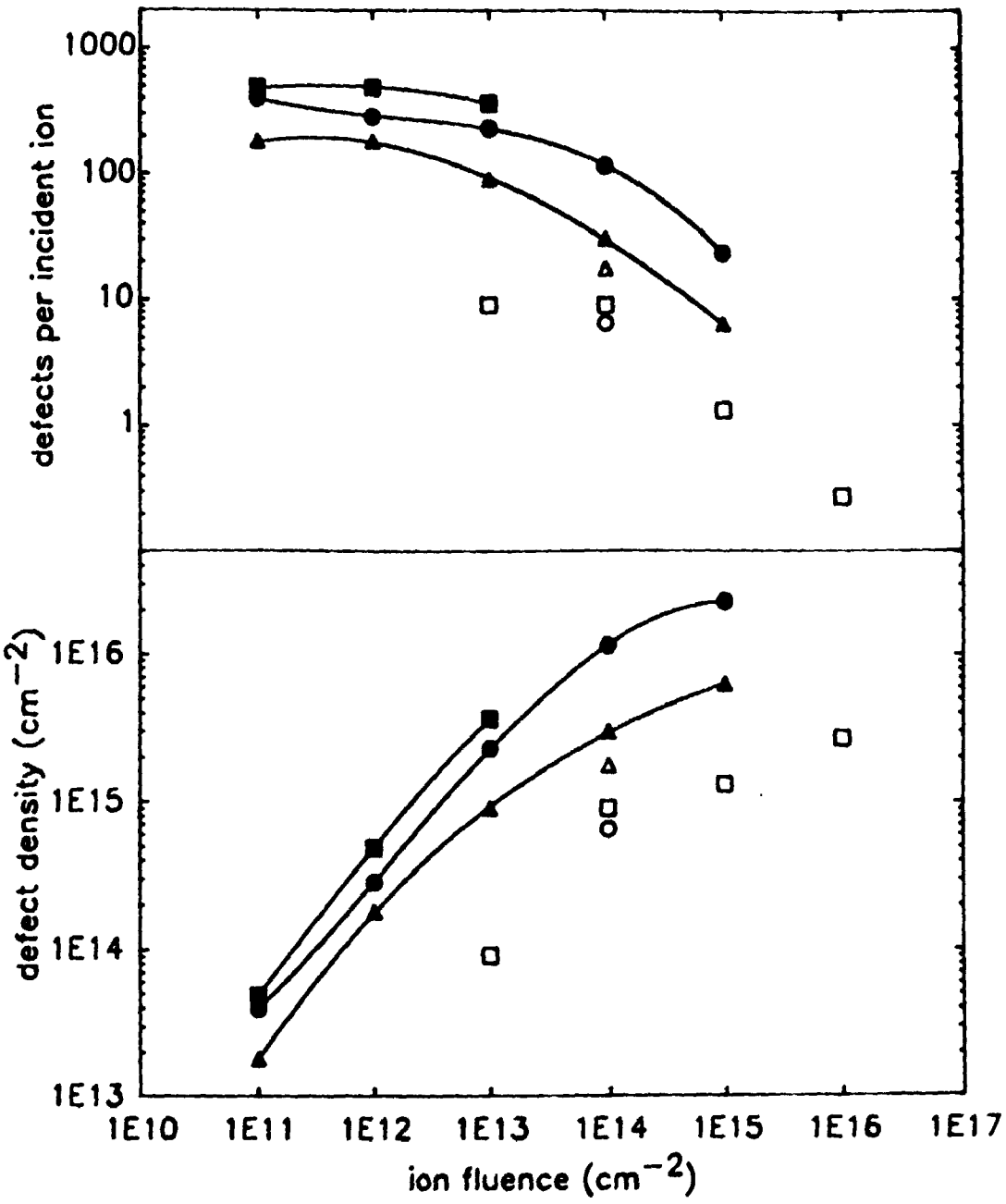

Figure 4-6: The relationship between implantation dose and the number of defects as observed by positron annihilation. Silicon at 0.54 ▲, 3.0 ● and 5.0 ■ MeV; Helium at 0.25 ○, 0.7 □ and 4.0 △ MeV. Solid lines are a guide to the eye.

The positron results for annealing of the 3 MeV Si implant, 10^{13} ions cm^{-2} are shown in figure 4-7. Annealing at 620K, well above the divacancy annealing temperature of 560K (Watkins and Corbett, 1965) had only a small effect on the positron trapping (a change in the surface condition of the sample but no change in the bulk; in some cases the W parameters decreased marginally). While the conventional interpretation would be that the defects responsible for positron trapping had not changed, this is inconsistent with the IR evidence. If the disappearance of the divacancy absorption was to be attributed to a change in the divacancy charge state (assumed neutral), for example, it would be expected that the positron trapping would also change measurably. One possible explanation for this is that the mobile vacancies clustered together into larger vacancy aggregates, i.e. multivacancy defects which are detectable by positron trapping but no longer optically active at 1.8 μm wavelength.

Annealing to 970K resulted in recovery of the crystal to near pre-implant quality, with a defect concentration $<1\%$ of that prior to annealing, as measured by positron annihilation. The nature of the remaining defects, stable to high temperatures, is not certain.

Helium implantation in silicon

Room temperature results.

Positron data for 700 keV He implantation doses of 10^{13}, 10^{14}, 10^{15} and 10^{16} ions cm^{-2} are shown in figure 4-8. Solid lines show fits to the data, the results of which are also listed in table 4-1. An energy of 700 keV was chosen since the ion range (~2.5 μm) is very similar to that of 3 MeV Si ions, discussed above. The fluences chosen were higher than those used for

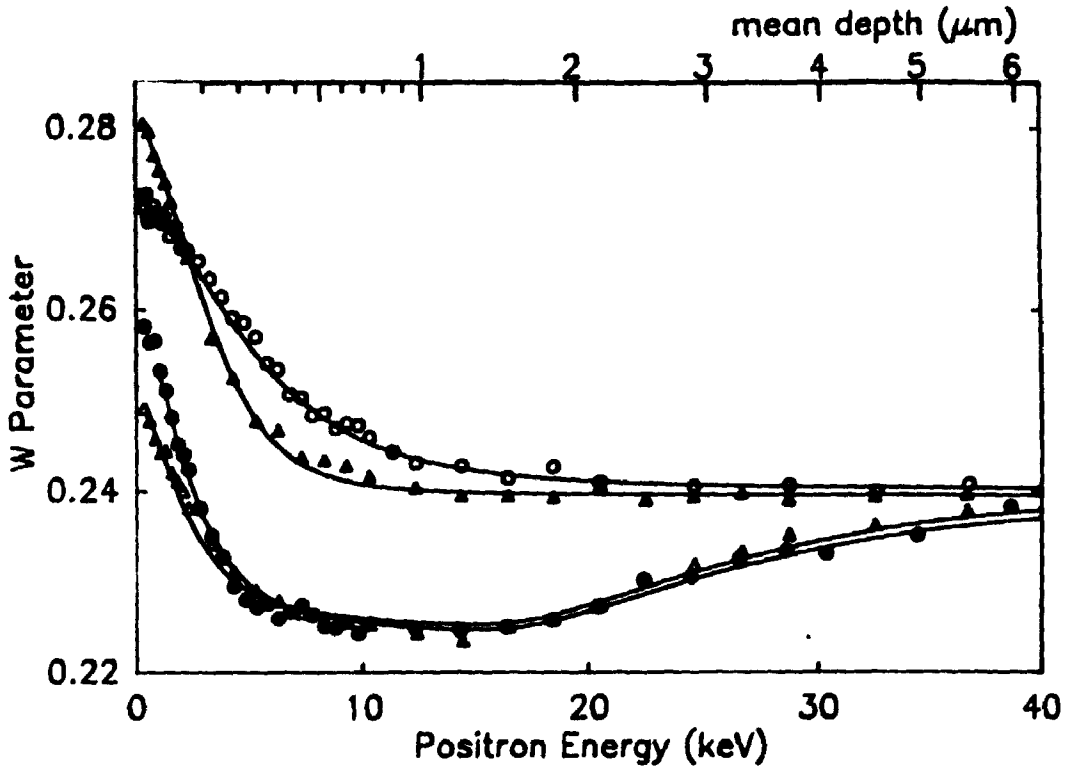

Figure 4-7: Annealing of a sample implanted with 10^{13} 3 MeV Si ions cm^{-2}. The data are unchanged (except for small changes in the surface oxide) at 620K, well above the divacancy annealing temperature. The main annealing occurs at temperatures in the 870 to 970K range. Unimplanted ○, implanted ●, annealed at 620K △ and annealed at 970K ▲.

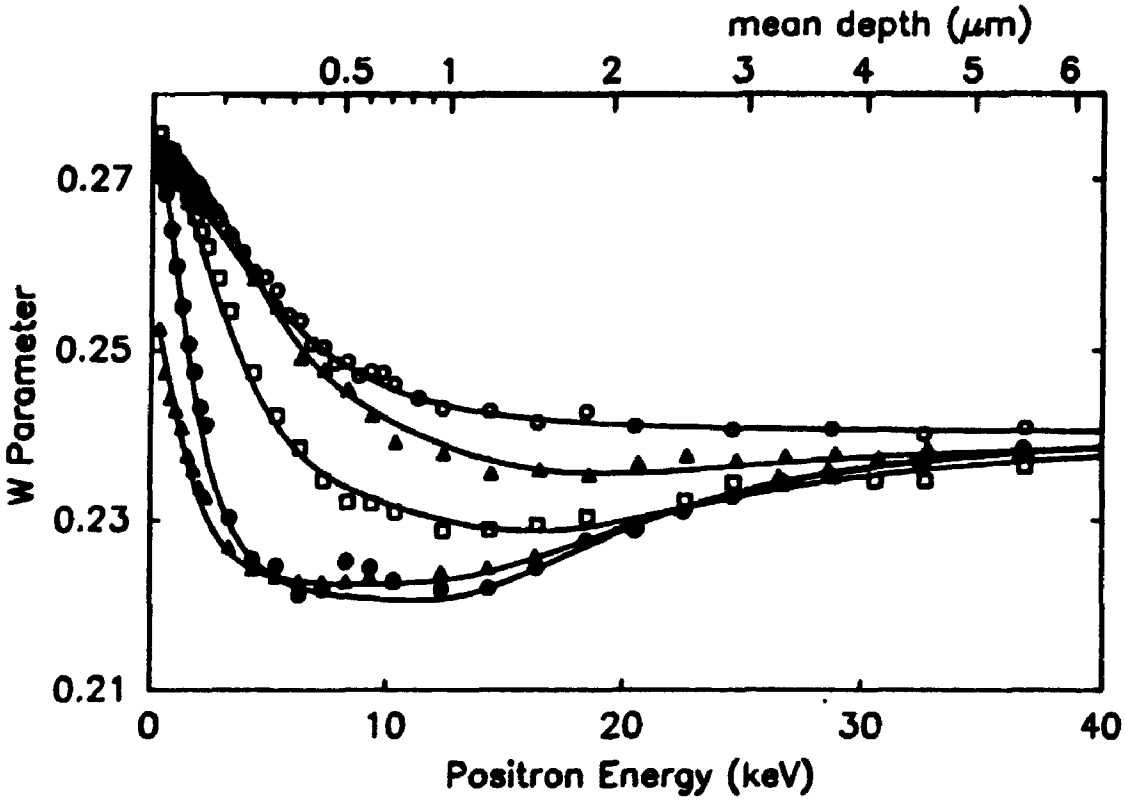

Figure 4-8: Positron data for 700 keV He ion implantation. Unimplanted ○, 10^{13} cm^{-2} ▲, 10^{14} cm^{-2} □, 10^{15} cm^{-2} △ and 10^{16} cm^{-2} ●.

Si ions, in accord with the TRIM prediction that the damage produced by He ion irradiation is an order of magnitude less than that produced by Si ions.

As was the case for the low fluence silicon irradiations (10^{11} and 10^{12} cm^{-2}), it was assumed that the defect concentration should increase in proportion to the He ion fluence for the two lowest fluences (10^{13} and 10^{14} cm^{-2}). Applying this condition resulted in a defect parameter $W_d = 0.935 \pm 0.005$, similar to the low-fluence silicon implanted samples.

It will be noted that, except for a change in the surface lineshape parameter W_s, the data for the 10^{15} and 10^{16} ions cm^{-2} doses are very similar. This is due to the same saturation effect discussed above for Si ion irradiation, i.e. in the energy range ~6 to 10 keV, nearly all positrons annihilate from a defect-trapped state, and the addition of more defects has little effect on the measured γ-ray lineshape. The saturation value for W in this case is the same as that observed for Si ion irradiation, suggesting that differences in the damage caused by high fluence light and heavy ion irradiations cannot be distinguished by positron spectroscopy alone. The defect model used to fit the data for the 10^{13} and 10^{14} ions cm^{-2} cases was based on the shape of the vacancy profile produced by the TRIM simulation program, and the absolute defect concentration was varied until a good fit was obtained. However, it was found that for the higher dose 700 keV helium implants (10^{15} and 10^{16} ions cm^{-2}), the W vs. E curve could not be fitted with a defect profile shape based on TRIM calculations, or, equivalently, on damage profiles extracted from RBS/ion channeling data. In order to fit the positron data it was necessary to assume a shallower defect profile, with the majority of the defects at a depth less than 1 μm. The range predicted for the implanted ions is ~2.5 μm, and the majority of the damage is

expected to be near the end of range.

Similar disagreement has been reported by others who have used positron methods to study damage in silicon irradiated with 100 keV P ions (Hautojärvi *et al.*, 1988), 35, 60 and 100 keV H ions (Keinonen *et al.*, 1988) and 80 keV B ions (Uedono *et al.*, 1989).

Positron data are shown in figure 4-9 for samples implanted with He ions at energies of 250 keV, 700 keV (as discussed above) and 4 MeV for a fluence of 10^{14} ions cm^{-2}. The range of the damage distribution increases with He ion energy. The positron data were fitted using the TRIM profile for the vacancy distribution. (In the 4 MeV case, the ion range, ~17 μm, is greater than the maximum attainable positron range, ~12 μm at 60 keV.) For the 250 keV case it was found that the extracted damage profile was again shallower than that predicted by TRIM, as it was for the high dose implants at 700 keV.

By increasing the energy of the incident He ions from 250 keV to 4 MeV the nuclear stopping close to the surface is changed by a factor of 10 (from 0.13 to 0.013 $eV \cdot Å^{-1}$) but the electronic stopping is changed by less than a factor of 2 (from 32 to 17 $eV \cdot Å^{-1}$). The large difference in the extracted defect density close to the surface between the 250 keV and 4 MeV implantations suggests very strongly that the damage scales with nuclear, rather than electronic stopping, in accordance with the generally accepted view of damage production in Si (Davies, 1984).

Infrared measurements of a silicon sample implanted from each side with 1.0×10^{16} He ions cm^{-2} at 700 keV energy showed the divacancy concentration to be 2.55×10^{15} cm^{-2} per side. Similar to the silicon ion implanted samples, this is much less than the number of displaced atoms deduced from

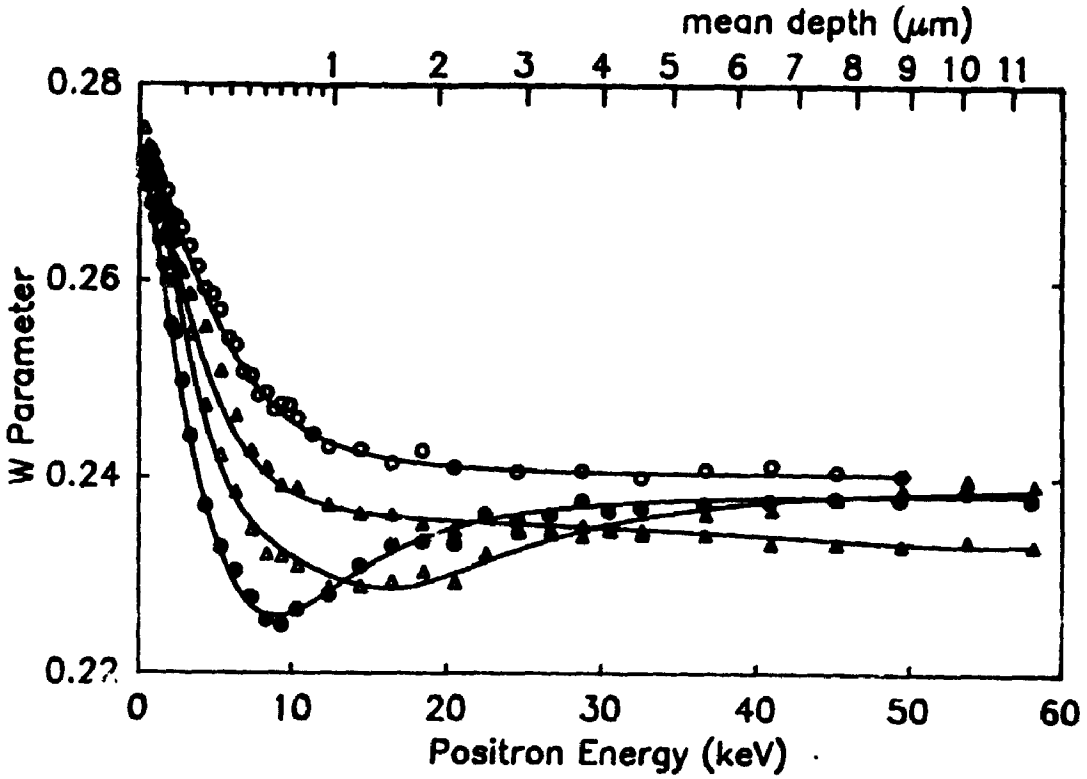

Figure 4-9: The dependence of the damage as measured by positrons on the energy of implanted He ions. With increasing implantation energy the minimum of the W parameter shifts to higher positron energy. In the case of the 4 MeV He implantation the minimum is expected at a positron energy exceeding 60 keV. From the large difference in W parameters close to the surface it is apparent that the amount of near-surface damage decreases with increasing ion energy, in accordance with the energy dependence of the nuclear stopping. Unimplanted ○, 0.25 ●, 0.7 ▲ and 4.0 ▲ MeV.

ion channeling measurements, and is comparable with the number of defects measured by positron annihilation. The comparison with positron results must be made with some caution, however, due to the disagreement in depth profile. This is discussed further below.

Annealing

Annealing of the He implanted silicon at 570K for one hour removed the majority of damage, as shown by the positron data in figure 4-10 for the case of 10^{16} cm^{-2} 500 keV He ions. This temperature is close to the reported divacancy annealing temperature of 560K (Watkins and Corbett, 1965). Annealing of the He-implanted Si sample at this temperature also removed the 1.8 μm infrared absorption. We conclude that the defect responsible for the majority of positron trapping in these samples below this temperature was the divacancy. In the case of the higher doses (10^{15} and 10^{16} He ions cm^{-2}) however, it was noted that a second type of defect, with $W_d/W_f > 1$, appeared after annealing. We speculate that this is caused by a helium related defect, since it appears to be at approximately the end of range of the implanted ions, 2.5 μm (corresponding to a positron energy of ~20 keV). The discrepancy between depths of damage obtained from the positron measurements and other techniques may be caused by a superposition of profiles for two defect types, with opposing effects on the γ-ray lineshape. Why this is not seen for all cases of He implantation is not clear, but it may be related to the concentration of He in the sample, since it was observed for the two highest doses (10^{15} and 10^{16} cm^{-2}) at 700 keV, and for the 10^{14} cm^{-2} 250 keV sample, in which the shorter ion range results in a slightly increased He ion concentration. He concentration in the

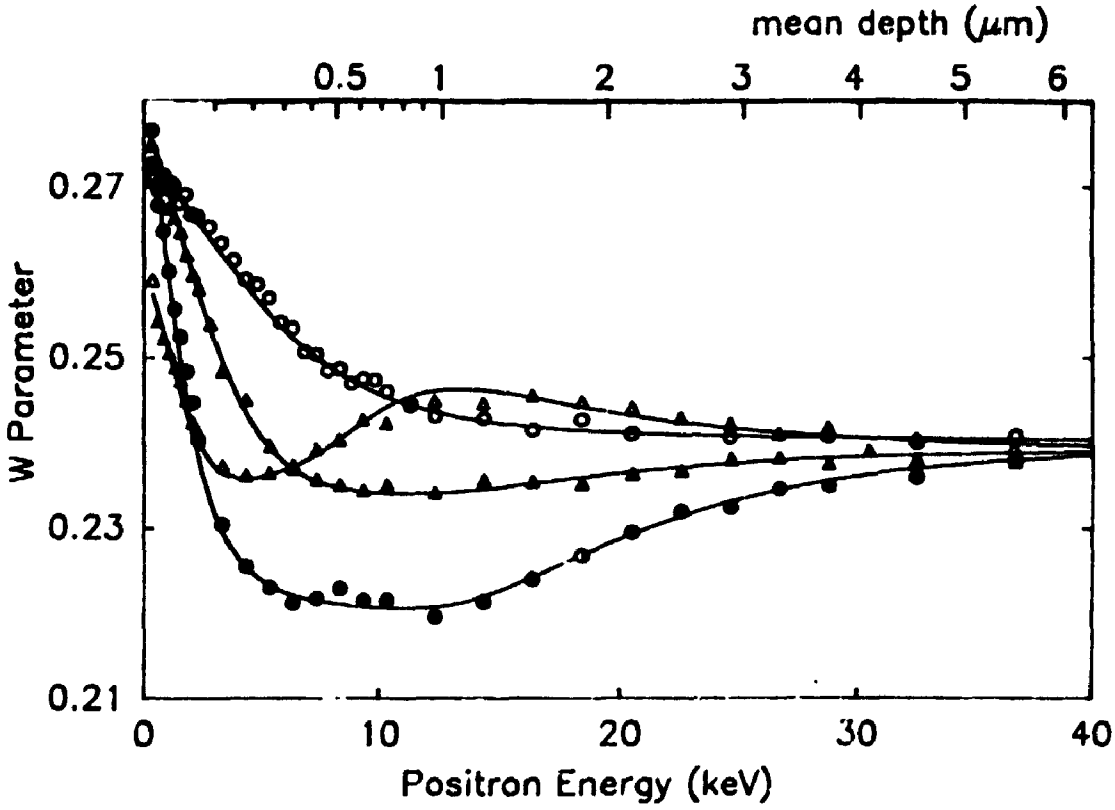

Figure 4-10: Annealing of a sample implanted with 10^{16} 500 keV He ions cm^{-2}. In contrast with the case of Si ion implantation the damage anneals near 570K, the temperature range at which the divacancy becomes mobile. Uninplanted ○, implanted ●, annealed at 570K ▲ and annealed at 970K ▲.

samples (determined by TRIM simulations) peaks at 3.4×10^{18} and 3.4×10^{19} cm^{-3} for 700 keV He ion fluences of 10^{14} and 10^{15} ions cm^{-2} respectively, and at 3.6×10^{18} cm^{-3} for 250 keV He at a fluence of 10^{14} cm^{-2}.

Discussion

Positron trapping rates

Recent positron lifetime measurements gave positron trapping rates of $\nu = 0.5$ to 1.0×10^{15} s^{-1} for neutral divacancies, 1.8 to 3.5×10^{15} s^{-1} for negative divacancies, and 3.5 to 7.0×10^{15} s^{-1} for doubly negative divacancies (Mascher *et al.*, 1989a). In the p-type wafers used for this study, and for defect concentrations high enough to drive the local material intrinsic- which is approached under most of our Si ion implant conditions- the majority of divacancies are expected to be neutral (Watkins and Corbett, 1965). For the sample implanted with 10^{14} 3 MeV Si ions cm^{-2}, we measured 1.1×10^{16} defects cm^{-2} while infrared absorption indicates there were 6.5×10^{15} divacancies cm^{-2}. We can adjust the rate ν to bring the positron result into exact agreement with the infrared absorption measurement; then $\nu = 1.0\times10^{15}$ s^{-1}, consistent with the value reported by Mascher *et al.* (1989a) to within the experimental uncertainty. This, however, does not take into consideration that defects other than the divacancy, or a mixture of divacancy charge states, may be trapping positrons. The helium implantation data cannot be used with confidence for such a comparison because of the possibility of two competing defect types as discussed above.

It is apparent from the infrared absorption data that divacancies constitute a significant fraction of the positron-trapping defects in these samples. To reconcile this with the absence of an annealing stage at the

divacancy annealing temperature for the Si implants, we speculate that upon annealing the divacancies agglomerate into larger vacancy clusters, with the product νC (positron trapping rate times concentration) remaining roughly constant. This would explain the apparent disagreement between the positron measurements and other techniques for annealed samples. Further investigation is required to identify the defect species remaining after annealing.

Defect production rates

In the limit of low fluences, the number of vacancies per incident ion measured by positrons is ~0.1 of that calculated by TRIM. This suggests that ~90% of the Frenkel pairs produced annihilate by recombination.

Dose dependence

Because of interactions between damage cascades, the defect concentration increases less than linearly with ion fluence for fluences above $\sim 10^{12}$ cm^{-2} for Si ions and $\sim 10^{14}$ cm^{-2} for He ions. It is not possible to fit the positron data if one assumes that the number of defects and ion dose increase proportionally beyond 10^{12} ions cm^{-2} for Si and 10^{14} ions cm^{-2} for He.

Temperature dependence

There is a clear difference in the annealing behavior of the He and Si implanted samples. In the case of the Si implantation the level of the damage measured by positrons remains roughly constant up to temperatures at

which amorphous Si recrystallizes (~870K). In the case of He irradiation the damage seems to anneal out at (or a little above) the temperature at which the divacancy becomes mobile. From the infrared measurements we know that in both cases a considerable number of divacancies are present. In positron lifetime spectroscopy experiments, at the temperature at which divacancies became mobile, an increase in the lifetime of the trapped positrons was observed (larger vacancy clusters grow by agglomeration of more than one divacancy) whereas the trapped fraction decreased (fewer of these larger clusters) (Mascher *et al.*, 1989b; Dannefaer, 1976). A similar phenomenon may be occurring in our samples, but it is not trivial to predict how the cluster size will influence the γ-ray lineshape in Doppler broadening measurements. Besides agglomeration, the divacancies can also be trapped at an interstitial cluster and annihilate in this way. It may be that a different ratio of the recombination and agglomeration processes in the Si and He cases causes the qualitatively different behaviour.

Energy dependence

For all our Si implantations and low dose He implantations, the defect profiles measured by positrons are consistent with the shape of the defect depth distributions as obtained from TRIM calculations and from RBS/channeling. For the high dose He ion implanted samples the positron results disagree with both TRIM and RBS/channeling results. The positron results indicate a shallower damage depth than that established by these other techniques. This may be an indication of the formation of a He related defect at larger depth, which influences the W parameter in the opposite direction. The amount of near-surface damage observed for the He

implants at energies of 0.25, 0.7 and 4.0 MeV scales with the nuclear stopping power of the implanted ion, in accord with the view that it is the nuclear, not electronic, processes which produce damage in the lattice.

Anomalous Defect Profiles

The agreement found in this study between positron data and the defect profiles predicted by TRIM for silicon self-ion irradiation shows that the modelling procedure used to fit the positron data provides an adequate approximation to the processes of positron diffusion and trapping. There have been however, several studies of ion-irradiated semiconductors in which the depth profiles derived from positron measurements disagree with those obtained by other methods. Discrepancies are larger than could be accounted for by uncertainties in the positron implantation profile (equations 3-1 to 3-3). Specific examples mentioned previously include implantation with 100 keV P ions (Hautojärvi *et al.*, 1988), 35, 60 and 100 keV H ions (Keinonen *et al.*, 1988) and 80 keV B ions (Uedono *et al.*, 1989). In all of these cases (and our own high-fluence He irradiations) the damage profile extracted from positron measurements was anomalously short- often less than half the range of the implanted ions. For our He irradiations the cause of the depth discrepancy is believed to be the introduction of an impurity-type defect (i.e. the implanted species) at the end of the ion range. This could also have been the case in other studies. It is also possible that for some of these the discrepancy was due to the effect of the implanted impurity ions on the charge states of the residual defect distribution. Since the positron trapping rate of defects is strongly dependent on their charge states (see e.g. Mascher *et al.*, 1989a), the shape of the derived defect profiles will

be affected by any non-homogenous distribution of defect charge states within the damaged region. Such a distribution of defect charge states could be introduced by the Fermi level shifts and band bending associated with implanted dopants. It would be of interest to study systematically the effect of the starting material on these results, examining p- and n- type materials with both high and low doping levels.

More difficult to understand are the results of studies of silicon self-ion irradiation which resulted in positron defect profiles in disagreement with other techniques. Mäkinen *et al.* (1989) reported damage profiles peaked in the near-surface region (a peak would be expected near the end-of-range where the nuclear stopping power is at a maximum) for 12 MeV silicon implantation in silicon. Unfortunately the maximum positron beam energy available was only 25 keV so the deepest probing depth (~3 μm) was less than the range of the implanted ions (5.6 μm). Uedono *et al.* (1991) reported defect profiles much deeper than predicted by TRIM for 200 keV silicon self-ion irradiation, at fluences of 5×10^{14} and 1×10^{15} cm^{-2}. For lower fluences (5×10^{12} and 5×10^{13} cm^{-2}) the agreement they found between TRIM and positron-derived defect profiles was reasonable. It was also reported however, that the S parameters (a measure of γ-ray lineshape, see chapter 3) observed for the implanted region *decreased* (corresponding to an *increasing* W parameter) with increasing ion fluence above 5×10^{13} cm^{-2}. It was suggested that this was due to amorphization at high ion fluences, because they suggested that the S parameter value for amorphous silicon is lower (thus W is higher) than that for positrons trapped by vacancy-type defects in silicon. This could affect the shape of the measured profiles since the region of crystal beyond the peak of the ion-induced damage would

contain vacancy-type defects introduced by the small fraction of incident ions which penetrate well beyond the mean ion range. The defect profile might appear artificially deep because the S parameter for these defects is higher (W lower) than that assumed for the bulk of the damage. Why such an effect was not also seen in our studies (at higher energies than the 200 keV implantations studied by Uedono) is not clear.

Preliminary investigations at UWO of silicon amorphization by successive implantations at liquid nitrogen temperature (78K) of 2×10^{15} cm^{-2} silicon ions at energies of 2.0, 1.0, and 0.5 MeV also resulted in damage profiles deduced from positron measurements that were inconsistent with TRIM predictions. It is possible however, that a more complete understanding of the non-monotonic change of lineshape parameters with ion fluence at the crystalline-amorphous transition (like that reported by Uedono *et al.* (1991)) would resolve this conflict. We have also made preliminary measurements of silicon implanted with 1 MeV silicon ions to fluences from 10^{11} to 10^{14} cm^{-2} at temperatures from 115 to 620K, using both p- and n-type substrates. The shape of the extracted defect profiles (measured at room temperature) was found to vary with implantation temperature. Finally, our preliminary study of Si implantation damage in InP is discussed in detail in appendix 1. In this case defect profiles were again inconsistent with TRIM, and furthermore, they varied little with the energy of the implanted ions. All of these anomalous profiles are at this point not well understood, and are a topic for future investigation.

Summary

Positron beam measurements put a slightly altered perspective on the

character of defects produced by ion irradiation of silicon and on post-irradiation annealing. We have resolved a difference in the annealing behaviour of damage due to implantation of light and medium mass ions: Si irradiation damage does not show an annealing stage at the divacacny annealing temperature, possibly because the high density of damage causes vacancy clustering to occur when the vacancies become mobile. The inhomogeneous defect distributions which can be produced by ion irradiation can complicate the interpretation of positron annihilation data, particularly with regard to the depth distribution of damage. The relationship between positron annihilation data and that provided by longer-established techniques such as electron paramagnetic resonance needs to be examined. Methodical investigation of the effect of dose rate and implantation temperature (i.e. dynamics), impurity type and substrate doping would clearly be helpful.

Chapter 5

Microvoids in MBE-grown silicon

Introduction

Molecular beam epitaxy is a technique for growing semiconductor layers of high crystal quality and controlled composition. In an ultra-high-vacuum chamber, material is evaporated from a source onto a substrate wafer mounted on a temperature-controlled stage. Dopants can be evaporated simultaneously. The evaporation rates can be controlled by adjusting the evaporant temperature, and evaporation can be started and stopped abruptly using mechanical shutters, so the composition of the layers (and therefore their electronic properties) can be controlled with close to monolayer precision, giving great potential for device engineering (Bean and Kasper, 1988). A significant difficulty arising particularly in MBE growth of silicon has been the surface segregation of co-evaporated dopants. Some improvement is obtained by using a low-energy ion beam, rather than evaporation, to introduce dopants, but segregation remains a problem. Dopant incorporation is improved by growing at reduced temperatures ($<700^\circ$ C), however as the temperature is reduced significant concentrations of extended defects are formed, the electrical quality of the layers is diminished (Jackman *et al.*, 1989) and the concentration of vacancy-type defects increases (Simpson *et al.*, 1989).

Much effort has been brought to bear on the problem of low temperature growth. Jorke *et al.* (1989a and b) have studied the effect of growth rate and temperature on epitaxial breakdown, and observed a transition from

epitaxial to polycrystalline to amorphous growth. Eaglesham *et al.* (1990) reported a limiting epitaxial thickness dependent on growth temperature, so that room temperature growth of a defect-free layer of limited thickness was possible. These studies used transmission electron microscopy (TEM) to assess the crystal quality of the epilayers. TEM is not sensitive to point defects, so the quality of the layers described as "defect-free" remains in question.

In a study of low temperature epitaxy at the National Research Council of Canada (NRCC), spherical defects of ~3 to 6 nm diameter were observed by TEM in epilayers grown at 350° C. Positron annihilation measurements at UWO showed that these defects were microvoids (Simpson *et al.*, 1990). Such a finding is of interest both in terms of its relevance to MBE growth and the breakdown of epitaxy, and as an opportunity to study the process of positron trapping and annihilation in voids.

Layer growth

Silicon epilayers were grown in a VG Semicon V80 MBE system at a deposition rate of 0.5 nm s^{-1} on (100) n-type (phosphorus doped) Czochralski Si substrates rotated at 30 rpm. The substrate surface prior to growth was cleaned *in-situ* by heating to >850° C under a 0.01 nm s^{-1} Si flux to remove a UV-grown oxide (Jackman *et al.*, 1989).

Four samples are discussed here, denoted 586, 587, 588 and 589. In the case of samples 586, 587 and 588, a thin n+ layer was formed (15 minutes growth time) by low energy (1.0 keV for samples 586 and 587; 0.5 keV for sample 588) implantation of As (6×10^{18} As cm^{-3}) during the growth (Denhoff *et al.*, 1988). The concentration was then lowered to 2×10^{17} As cm^{-3} and a

thicker layer grown (150 minutes growth time). Then a thin p+ capping layer (4×10^{18} B cm^{-3}) was formed (10 minutes growth time) by co-evaporation of B_2O_3 with the Si, which incorporates both boron and oxygen at this growth temperature (Jackman *et al.*, 1988, 1989). Other than this layer, the oxygen concentration was the same as the substrate. Sample 586 was grown at a substrate temperature of 700° C, while 587 and 588 were grown at 350° C. Sample 589 was completely undoped, but was otherwise grown under the same nominal conditions as 587 and 588. To summarize, 587 and 588 were identical except for the energy of the implanted As, 586 was similarly doped but grown at a higher temperature, and 589 was grown at the same temperature as 587 and 588, but was undoped. These growth conditions are also shown in table 5-1.

Table 5-1: Sample growth conditions.

sample	doping	growth temperature (° C)	epilayer thickness (μm)
586	1 keV As	700	5.7
587	1 keV As	350	5.7
588	0.5 keV As	350	6.3
589	undoped	350	5.8

TEM results

Samples were studied using a Philips 430EM transmission electron microscope (TEM) in cross-sectional (figure 5-1) and plan view (figure 5-2)

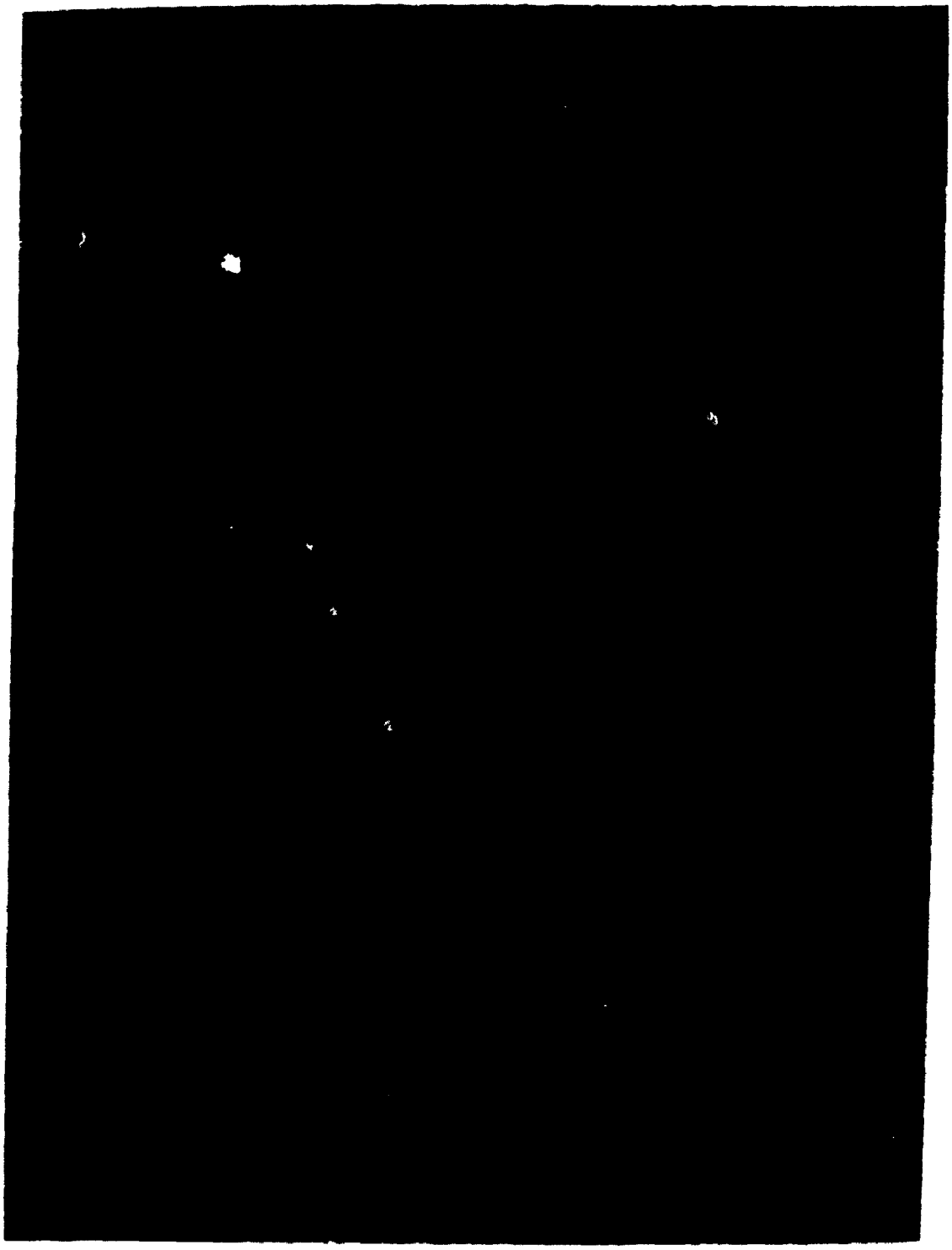

Figure 5-1: Cross-sectional TEM micrograph showing strings of ~6 nm voids in a silicon epilayer. The magnification is 3.2×10^5.

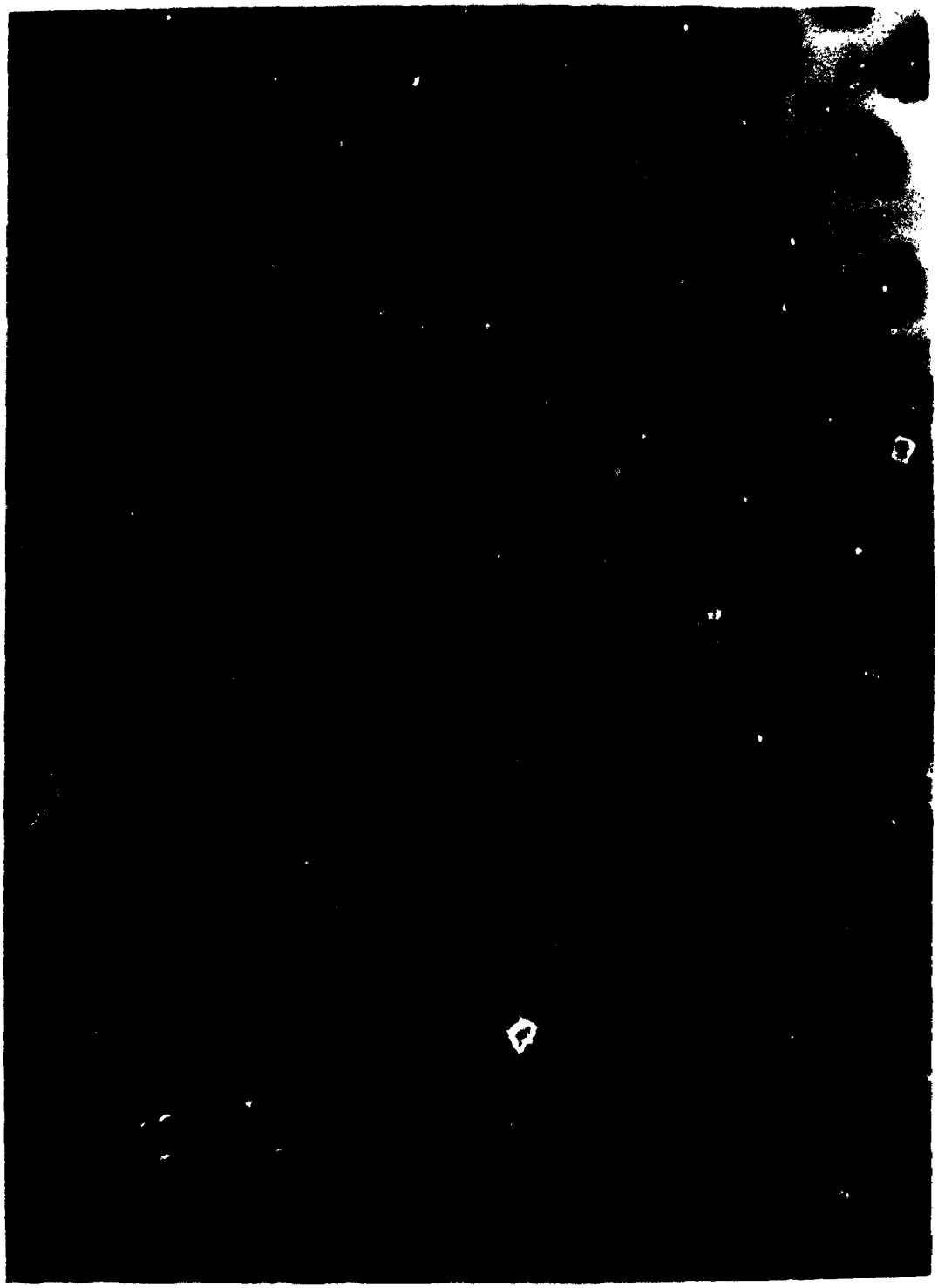

Figure 5-2: Plan view TEM micrograph, showing the regular spacing of void strings terminating at the surface of a silicon epilayer. The magnification is 3.2×10^5.

geometries. The TEM work was performed by D.D. Perovic and J.P. McCaffrey. Thin foils were prepared in the standard way using argon atom milling. Figure 5-1 shows strings of spherical defects which begin ~0.6 μm beyond the substrate-epilayer interface, and extend to the growth surface, where they terminate in {111} faceted cusps (Perovic *et al.*, 1991). The spherical defects are spaced along the strings with remarkable regularity, and plan view images (figure 5-2) show that the spacing of the strings is also regular.

It was not possible to determine the nature of the spherical defects with certainty by interpretation of electron micrographs alone. A parallel study using positron annihilation was used to unambiguously determine that the defects were in fact voids, and not amorphous regions as had alternatively been suggested.

From micrographs such as figure 5-1 the void diameter and the spacing of the voids along the strings can be determined. From plan-view micrographs, such as that shown in figure 5-2, the areal density of the void strings can be obtained, which allows the calculation of the void density. These results are summarized in table 5-2. It will be noted that samples 587 and 588 contain similar densities of voids (the same within experimental uncertainties), while 589 exhibits a lower void density, and 586 contains no voids at all.

It is apparent from the existence of voids in samples 587 and 588 (doped low temperature growth), and to a lesser extent in sample 589 (undoped low temperature growth), but not in sample 586 (doped high temperature growth) that the main controlling factor for void formation is growth temperature. The {111} faceting of the (100) growth surface precedes

void formation. Cylindrical voids are left in the wake of the surface cusps as growth continues, and these cylinders subsequently break up to form a series of spherical voids. Joining the voids are straight [100] tracks, along which it may be possible for impurities to diffuse. Since {111} is the minimum energy surface of silicon, it may be that the formation of {111} faceted cusps during low temperature growth is energetically favourable. It has been found (Perovic *et al.*, 1991) that where a faceted growth front develops, epitaxial layer thickness can exceed that predicted by Jorke *et al.* (1989a and b) and observed by Eaglesham *et al.* (1990).

Table 5-2: Void distributions in the samples, as determined using electron microscopy. Void depth refers to the depth below the surface at which void formation initiates. String density is the number of void strings per unit area, and void spacing is the average distance between voids along the strings. Vacancies per void is the equivalent volume of the voids in terms of lattice sites in the crystal, while the defect density is obtained by multiplying the void density by the number of vacancies per void.

sample	void depth (μm)	string density (μm^{-2})	void spacing (nm)	void density (cm^{-3})	void diameter (nm)	vac. per void	defect density ($atom^{-1}$)
587	5.2	303	22.2	1.36×10^{16}	6.5	7200	2.0×10^{-3}
588	5.3	304	22.3	1.36×10^{16}	6.0	5650	1.5×10^{-3}
589	5.4	26	23.0	1.13×10^{16}	7.3	10200	2.3×10^{-4}

Positron annihilation results

Doppler broadening measurements of samples 587 and 588 resulted in the narrowest lineshapes ever reported for sub-surface annihilations in silicon, consistent *only* with the identification of the spherical defects as voids.

Figure 5-3 shows the W parameter vs. positron beam energy for samples 586, 587, and 589. Data for sample 588 are not shown since they are very similar to data for sample 587. Solid lines show fits to the data, details of which are given in table 5-3. The data were fit assuming a constant defect density over the region determined by TEM to contain voids, and the defect concentration was varied until a good fit to the data was obtained. Since the positron trapping rate for the voids was not known, the monovacancy trapping rate $\nu = 3\times10^{14}$ s^{-1} (Dannefaer, 1987) was used; since it is only the product νC of concentration (per atom) times trapping rate which enters the analysis, errors in one parameter translate directly to errors in the other. Because of uncertainty in the trapping rate, the defect concentrations determined are somewhat arbitrary, but the trapped fractions obtained will still be meaningful. For order-of-magnitude calculations, we can assume that the trapping rate for the voids will be approximately equal to the number of vacant lattice sites per void times the monovacancy trapping rate given above. The validity of this approximation can be tested by comparing the defect density (in units of vacant lattice sites per atom) determined from the TEM results with that determined from the positron measurements. This comparison can be made by examination of tables 5-2 and 5-3: the defect concentrations determined by positron measurements are a factor of ten below those from TEM. Qualitatively this is reasonable since the probability of trapping into a particular vacant

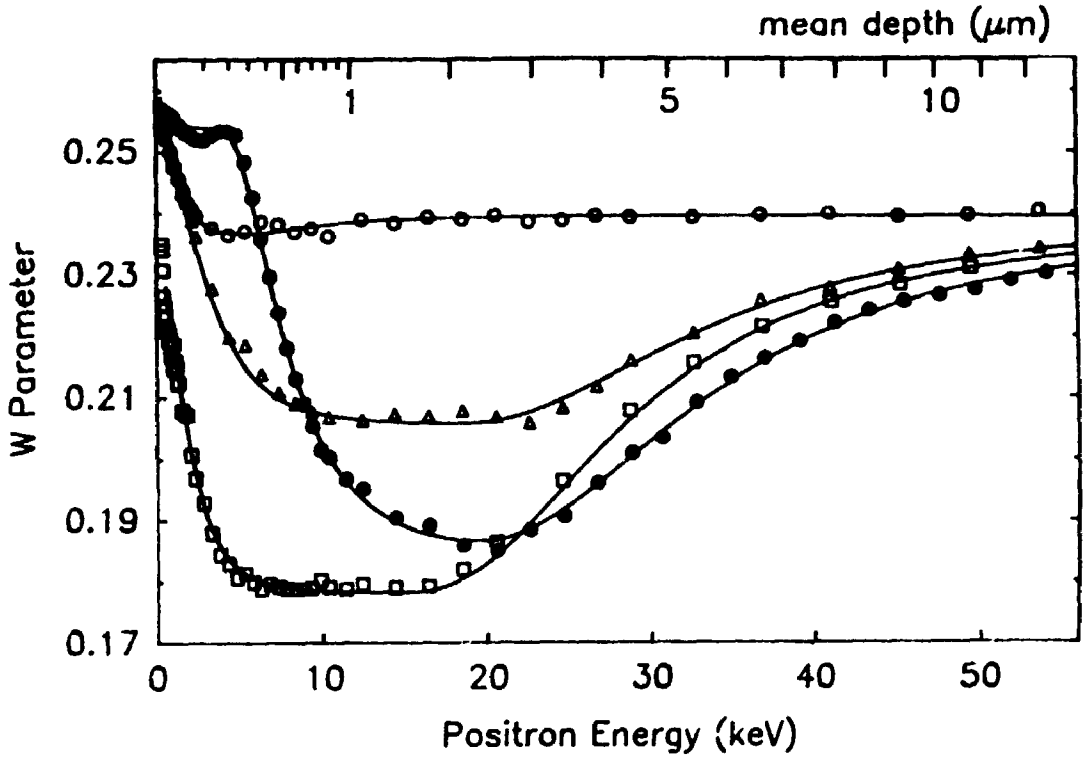

Figure 5-3: W parameter vs. positron energy, for samples 586 ○, and 587 before ● and after □ etching, and 589 △.

Table 5-3: Positron fitting parameters. In the "region" column, zero refers to the growth surface. The "free" lineshape parameter W_f was 0.24. The experimental trapped fraction was determined using equation 3-6 with the defect concentrations C (per atom) given in the third column (and a trapping rate $\nu = 3\times10^{14}\ s^{-1}$). The theoretical trapped fraction was determined using equation 5-4 and the void sizes and densities determined by TEM.

sample		region (μm)	C	W_d/W_f	trapped fraction (expt'l)	trapped fraction (theory)
586	as grown	0 - 0.45	1×10^{-3}	0.985		
587	as grown	0 - 0.45	1×10^{-3}	1.065		
		0.45 - 5.3	2×10^{-4}	0.752	0.93	0.96
	etched	0 - 4.13	2×10^{-4}	0.728	0.93	0.96
	aged	0 - 4.13	2×10^{-4}	0.699	0.93	0.96
588	as grown	0 - 0.45	1×10^{-3}	1.089		
		0.45 - 5.3	2×10^{-4}	0.794	0.93	0.96
	aged	0 - 0.45	1×10^{-3}	1.106		
		0.45 - 5.3	2×10^{-4}	0.728	0.93	0.96
	etched	0 - 4.5	2×10^{-4}	0.721	0.93	0.96
589	as grown	0 - 5.4	2×10^{-5}	0.855	0.57	0.70
	aged	0 - 5.4	2×10^{-5}	0.751	0.57	0.70

site is decreased by trapping into neighbouring vacant sites, which depletes the local positron density. Thus the fraction of positrons trapped should be less for a collection of vacancies assembled into voids than for a similar density of vacancies randomly distributed throughout the solid. The trapping model is discussed in greater detail below.

In initial attempts at fitting positron data for these samples poor agreement was found between the electron microscopy and positron annihilation results regarding the depth below the surface to which the voids extend. Since the expression used for the positron range (equation 3-1) was determined from work at energies below 10 keV, and the positron energies of interest here are significantly higher, it was suggested that the positron range in silicon at energies above 10 keV is greater than that given by equation 3-1. The data were well fit by assuming the mean positron range to be given by the expression $z = 400/\rho\ E^{1.65}$, i.e. replacing the parameter n=1.6 with n=1.65. This expression for the range was then used for all of the analysis discussed in this chapter. It should be noted that this is still within the stated range of error on the parameter n (=1.6±0.1). At a positron energy of 30 keV the mean range is increased from 4.0 to 4.7 μm, a change much greater than the uncertainty in the layer thicknesses measured by TEM.

The data from samples 587 and 588 exhibit a flat region near the surface (~0 to 5 keV positron energy) with W~0.255. This is due to the heavily doped B_2O_3 capping layer. The defect parameters obtained for this layer, W_d ~ 1.05 - 1.10, are consistent with those reported by Chilton *et al.* (1990) for oxygen precipitates in epilayers doped with B_2O_3. As a check of the positron results, this layer was removed by chemical etching, and the

samples were remeasured. The etchant used was a 1:10:4 mixture of hydrofluoric, nitric and acetic acids, which etches n-type silicon at a rate of ~90 $nm \cdot s^{-1}$. The etch rate varies with doping. By masking a part of the sample from the etchant, and removing the mask after etching, the amount of material removed can be determined by profilometer measurements of the resulting step edge. 1.2 μm of silicon was removed from sample 587, and 0.5 μm from sample 588. Positron beam measurements after etching were in excellent agreement (within a few hundred Å) with profilometer data regarding the amount of material removed (and remaining layer thickness) for sample 587. Agreement for sample 588 was not as good. It was possible to fit the data for all samples before and after etching using a consistent value (within uncertainties) for the parameter W_d/W_f (~0.75) in the region containing voids.

Positron data for sample 589 were consistent with the TEM observation that voids were present but in smaller quantity than in samples 587 and 588: the measured W parameter in the region containing voids (W/W_f ~ 0.88) is intermediate between the bulk value and that found for 587 and 588.

Data from sample 586 (no voids, high temperature growth) were fit by assuming the epilayer to be defect-free except for the final 0.45 μm in which the B_2O_3 doping occurred. The W_d parameter obtained for this region differed from that found for the B_2O_3 layer in samples 587 and 588. The reason for this is the higher growth temperature: at 700° C very little oxygen is incorporated in the layer, and precipitates are not formed (Jackman *et al.*, 1989).

To confirm the (somewhat controversial) finding that the samples contained voids, sample 587 was annealed at 700° C for 30 seconds, which

should be sufficient to regrow an amorphous region. Some faceting of the void surfaces was observed by TEM, but subsequent room-temperature positron measurements showed no change. Sample 587 was also measured during *in-situ* heating at 300° C; this too resulted in no change in the annihilation spectra.

Recently positron lifetime measurements were performed on sample 587 using a pulsed, variable-energy positron beam (Jackman *et al.*, 1991). These data appear to indicate that the fraction of positrons trapped by voids (at positron energies in the range ~5 to 20 keV) is only ~20%, significantly less than had been assumed (~93%) in fitting the Doppler-broadening data. In the As-doped epilayers a lifetime of 185 psec was measured. This is significantly shorter than the lifetime of ~215 psec measured in the substrate material. It is also shorter than the usual 220 psec lifetime reported for bulk silicon (Dannefaer, 1987). A longer lifetime component (~500 psec) was also observed, and was attributed to annihilation in voids, but the intensity (~20%) was much less than was expected from analysis of the Doppler-broadening data. At this point we therefore consider the pulsed-beam studies to be unreliable, although we do not know why. Further measurements are underway to find the origin of the 185 psec component, an understanding of which may help to resolve the discrepancy between the two techniques.

It can easily be proven that the void trapped fraction must be greater than 20%, as follows: the minimum experimental W parameter obtained was W_{exp} = 0.172, while the bulk parameter W_f was 0.239. At sufficiently high positron energies (above ~10 keV) the surface fraction is negligible, so the measured W parameter is just a weighted average of the defect parameter W_d

and the "free" or bulk parameter W_f:

$$W_{exp} = F \cdot W_d + (1-F) \cdot W_f \qquad (5\text{-}1)$$

Rearranging,

$$F = \frac{W_f - W_{exp}}{W_f - W_d} \qquad (5\text{-}2)$$

The smallest possible value for F is found by assuming the smallest possible value for W_d. In the limit of $W_d = 0$, and the values given above for W_{exp} and W_f, the minimum value for the trapped fraction is F = 28%. The true value of W_d is somewhere between the limits of $W_d = 0$ (F = 28%) and $W_d = 0.172$ (F = 100%), thus it is apparent that the lifetime analysis, suggesting a trapped fraction of 20%, cannot be correct. We expect that the true value of W_d is in fact close to the measured $W_{exp} = 0.172$, supporting our interpretation of near-saturation trapping. Further evidence for this is provided below.

Diffusion-limited trapping

The model used to fit data from samples 587 and 588 (i.e. near-saturation trapping in voids) is also supported by a prediction of the trapped fraction as calculated using the void densities and sizes determined by TEM, and a theory presented by Nieminen *et al.* (1979) for diffusion-limited trapping of positrons into voids.

If a positron trap is small compared with the positron wavelength (~60 Å at room temperature) then the trapping is rate-limited, i.e. the

fraction of positrons trapped by defects is determined by a specific trapping rate ν characteristic of the trap itself and independent of the distribution of such traps through the solid. For a homogeneous distribution of traps the fraction F of positrons trapped by defects is given by equation 3-6.

In the case of open volume defects with sizes comparable to the positron wavelength, the trapping process is no longer adequately described by the rate-limited trapping model. This is the case for the ~60 to 70 Å voids in this study. Since the positron density in the solid can be depleted in the vicinity of a strong trap, decreasing the net trapping probability, the trapping is diffusion-limited. In the case of extreme diffusion-limited trapping into a density N (cm^{-3}) of voids of radius r (cm), and intervoid Wigner-Seitz radius

$$R = \left[\frac{3}{4\pi N}\right]^{1/3}, \qquad (5\text{-}3)$$

the fraction F of positrons trapped by voids is given by (Nieminen *et al.*, 1979):

$$F = \frac{4\pi N' D_+ r}{4\pi N' D_+ r + \lambda_f}, \qquad (5\text{-}4)$$

where

$$N' = \frac{3}{4\pi(R^3 - r^3)} \qquad (5\text{-}5)$$

and D_+ ($cm^2 \cdot s^{-1}$) is the positron diffusion coefficient.

Fractions of positrons trapped by voids calculated using equation 5-4 above (with void diameters and densities from table 5-2) are given in table 5-3. The greatest source of uncertainty in these values is that associated with the positron diffusion coefficient D_+. It will be noted that agreement with the trapped fractions calculated from fitting Doppler broadening data is fair, ultimately supporting the hypothesis that there is near-to-saturation trapping of positrons by voids, and therefore that the W parameter for annihilations in the voids is $\sim W_d/W_f = 0.75$.

Physical interpretation of W parameters

The defect parameter $W_d/W_f \sim 0.75$ represents a much narrower lineshape than any previously measured for subsurface annihilations in silicon. What mechanism can account for such narrow lineshapes? In a large open volume defect it is possible for the positron to form positronium (Ps), i.e. a bound state with a single electron, in either the singlet state (lifetime $\sim 10^{-10}$ s, 25% probability) or the triplet state (lifetime $\sim 10^{-7}$ s, 75% probability) (Schultz and Lynn, 1988). The singlet state decays to two γ-rays of 511 keV with virtually no Doppler broadening, which could account for the narrow lineshapes observed. The triplet state decays to three γ-rays distributed in energy from ~0 up to 511 keV, thus causing an increase in γ-ray intensity at energies below the 511 keV peak region. No 3-γ annihilations were detected in this experiment, however this is not surprising in view of the long lifetime of the triplet state: Ps formed in the triplet state is likely to annihilate by pick-off (i.e. the positron annihilates with an electron other than that to which it is bound) before it decays. The transit time of Ps of thermal energy across a void of 6 nm

diameter is only $\sim 10^{-13}$ seconds, much less than the lifetime of either Ps state. It appears then that positronium may be forming, and annihilating mainly by pick-off, but with some fraction localized within the void producing the extreme narrowing of the γ-ray lineshape.

Another possible explanation for the narrow lineshapes is that the positron enters a bound state on the inner surface of the void (different from the external sample surface due to the surface oxide) and annihilates with a low-momentum electron there. Positron annihilation from bound states on clean surfaces has been previously observed (Schultz and Lynn, 1988, and references therein), *without* the observation of lineshapes as narrow as those in this study, so it appears that the former explanation (positronium formation) is more likely to be the correct one.

In a study of voids formed by neutron irradiation of vanadium, Hasegawa *et al.* (1988, 1989) used measurements of the angular correlation of annihilation radiation (ACAR) to examine annihilation lineshapes with much higher resolution than that available from Doppler broadening measurements. Narrow lineshapes were observed for all samples containing voids, and Ps formation was observed in some cases, as shown by the extremely narrow central component of some of the lineshapes in figure 5-4. The degree to which positronium was formed in the voids was correlated with the oxygen concentration in the samples. No 3-γ annihilations were detected in these experiments, consistent with the discussion presented above.

The angle θ (in radians) between photons in an angular correlation experiment is related to a single component p of the electron momentum: that in a direction perpendicular to both the detector slit and the direction of photon emission. Then

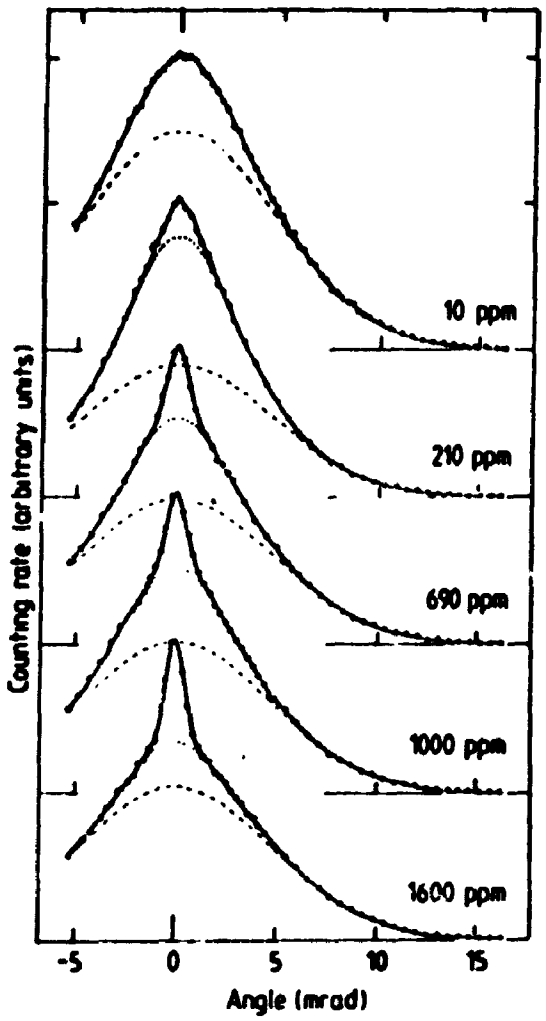

Figure 5-4: Angular correlation of annihilation radiation (ACAR) spectra from Hasegawa *et al.* (1989). The extremely narrow component attributed to positronium formation increases in intensity with increasing oxygen content.

$$\theta = \frac{p}{m_e c}, \qquad (5\text{-}6)$$

just the ratio of one component of electron momentum to the (approximate) momentum of the 511 keV photon (Hautojärvi and Vehanen, 1979). Thus angular correlation data can be interpreted rather directly in terms of electron momentum. To compare the data of Hasegawa and co-workers with our own, the equivalent Doppler broadened γ-ray energy spectra were calculated from their data, and then convolved with the resolution function of our detector (discussed below). This permits us to determine approximately the W parameters which would have been obtained had Hasegawa *et al.* performed a Doppler broadening measurement. Ratios of parameters W/W_f were obtained ranging from 0.75 to 0.90, in fair agreement with our own results. Although the densities and sizes of voids in Hasegawa's samples were similar to our own, it is not clear that the comparison can be carried any further since we have no way of knowing the positron diffusion coefficient in their samples, and this strongly affects the the fraction of positrons trapped by voids, as inspection of equation 5-4 will show.

Lineshape simulations

Although the Doppler-broadening technique does not allow us to resolve a distinct narrow component in the γ-ray lineshape due to positronium, we can still attempt to obtain some physical insight into the meaning of the annihilation lineshapes observed in these experiments. A number of schemes exist for performing mathematical deconvolution of Doppler-broadening data, to remove the "smearing" effect of the detector resolution function (see

e.g. Dannefaer and Kerr, 1975; Britton *et al.*, 1988; Wormeester *et al.*, 1988; McKee 1989). Unfortunately such schemes have met with limited success when applied to real experimental data with its attendant statistical fluctuations. Rather than attempting to directly deconvolute our experimental data, an attempt has been made to simulate the data by taking simple models for the "true" (unconvolved) spectral distribution, and convolving them with the detector resolution function.

The detector resolution was determined experimentally using a ^{7}Be source, which emits a γ-ray of energy 478 keV. Initially the resulting data were smoothed to reduce statistical fluctuations, but it was found that the detector resolution function could be modelled with adequate accuracy using a Gaussian distribution, so in subsequent calculations a Gaussian resolution function was assumed, rather than using the smoothed experimental data. The width of the resolution function was σ = 0.54 keV, or 1.28 keV full-width-half-maximum (fwhm). The W parameter obtained from the resolution data was W = 0.04. This gives a lower limit for the value of W_d applied in equation 3-2 above.

Several models were tested for the "true", or unconvolved spectrum, and that which most closely simulated the shape of the experimental data was a Gaussian distribution. Gaussians were generated, then convolved with the detector resolution function described above, then compared with experimental spectra, and the width of the initial Gaussian was adjusted until a good match was obtained. The experimental spectra analyzed in this way had W parameters of 0.243 (bulk) and 0.181 (voids). The resulting widths were σ = 0.90 keV for the case of "free" annihilations in bulk silicon, and σ = 0.71 keV for void-trapped annihilations. These Doppler

e.g. Dannefaer and Kerr, 1975; Britton *et al.*, 1988; Wormeester *et al.*, 1988; McKee 1989). Unfortunately such schemes have met with limited success when applied to real experimental data with its attendant statistical fluctuations. Rather than attempting to directly deconvolute our experimental data, an attempt has been made to simulate the data by taking simple models for the "true" (unconvolved) spectral distribution, and convolving them with the detector resolution function.

The detector resolution was determined experimentally using a ^{7}Be source, which emits a γ-ray of energy 478 keV. Initially the resulting data were smoothed to reduce statistical fluctuations, but it was found that the detector resolution function could be modelled with adequate accuracy using a Gaussian distribution, so in subsequent calculations a Gaussian resolution function was assumed, rather than using the smoothed experimental data. The width of the resolution function was σ = 0.54 keV, or 1.28 keV full-width-half-maximum (fwhm). The W parameter obtained from the resolution data was W = 0.04. This gives a lower limit for the value of W_d applied in equation 3-2 above.

Several models were tested for the "true", or unconvolved spectrum, and that which most closely simulated the shape of the experimental data was a Gaussian distribution. Gaussians were generated, then convolved with the detector resolution function described above, then compared with experimental spectra, and the width of the initial Gaussian was adjusted until a good match was obtained. The experimental spectra analyzed in this way had W parameters of 0.243 (bulk) and 0.181 (voids). The resulting widths were σ = 0.90 keV for the case of "free" annihilations in bulk silicon, and σ = 0.71 keV for void-trapped annihilations. These Doppler

shifts are equivalent to electron energies (assuming the annihilating positron to be at rest) of 3.17 and 1.98 eV respectively. No account is taken in these calculations of the geometric convolution required to incorporate the effect of the (random) angle between the electron momentum and the photon emission. The detailed shape of the electron momentum distribution cannot be determined, however we obtain some idea of the order of magnitude of the change in electron momentum required to produce the narrow lineshapes observed. Experimental and simulated spectra are illustrated in figure 5-5. Unfortunately it was not possible to determine through such simple calculations whether the experimental lineshapes were produced by a single, narrow distribution (such as might be caused by positron trapping in a surface state on the void interior) or by a superposition of a relatively broad lineshape with an extremely narrow component due to positronium formation.

Changes with time

Approximately one year after the initial measurements were made, samples 587, 588 and 589 were remeasured, and the results were found to be slightly different from those previously obtained, as shown in figure 5-6. It was assumed that the number of voids in the samples would not change during storage at room temperature, so the change in the data was due to a change in the lineshape parameter W_d due to annihilation in voids, rather than a change in the fraction of positrons trapped by voids. This could be due to a change in the condition of the interior surface of the voids, possibly due to humidity and absorption of water in the voids. The bulk parameter W_f was unchanged, so the change was not due to a drift in the

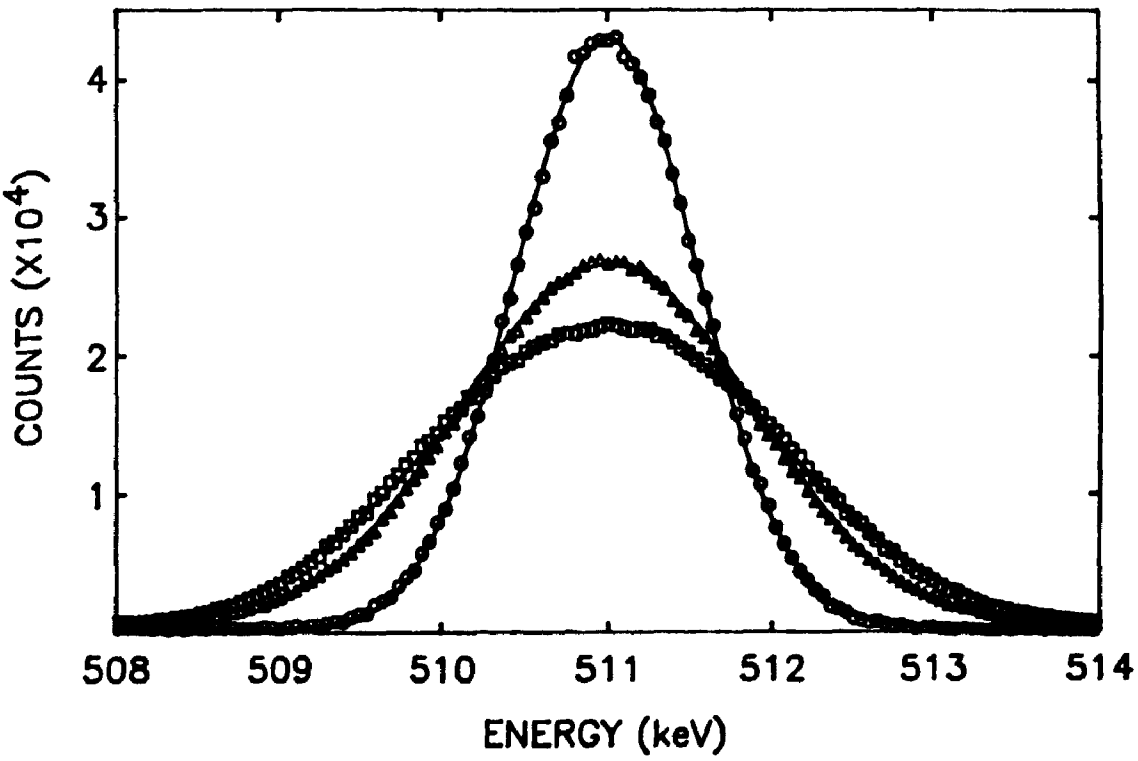

Figure 5-5: Experimental γ-ray energy spectra are compared with simulations (solid lines), for the detector resolution function ○, annihilation in bulk silicon □, and annihilation in voids △. All spectra contain 1.25×10^6 counts.

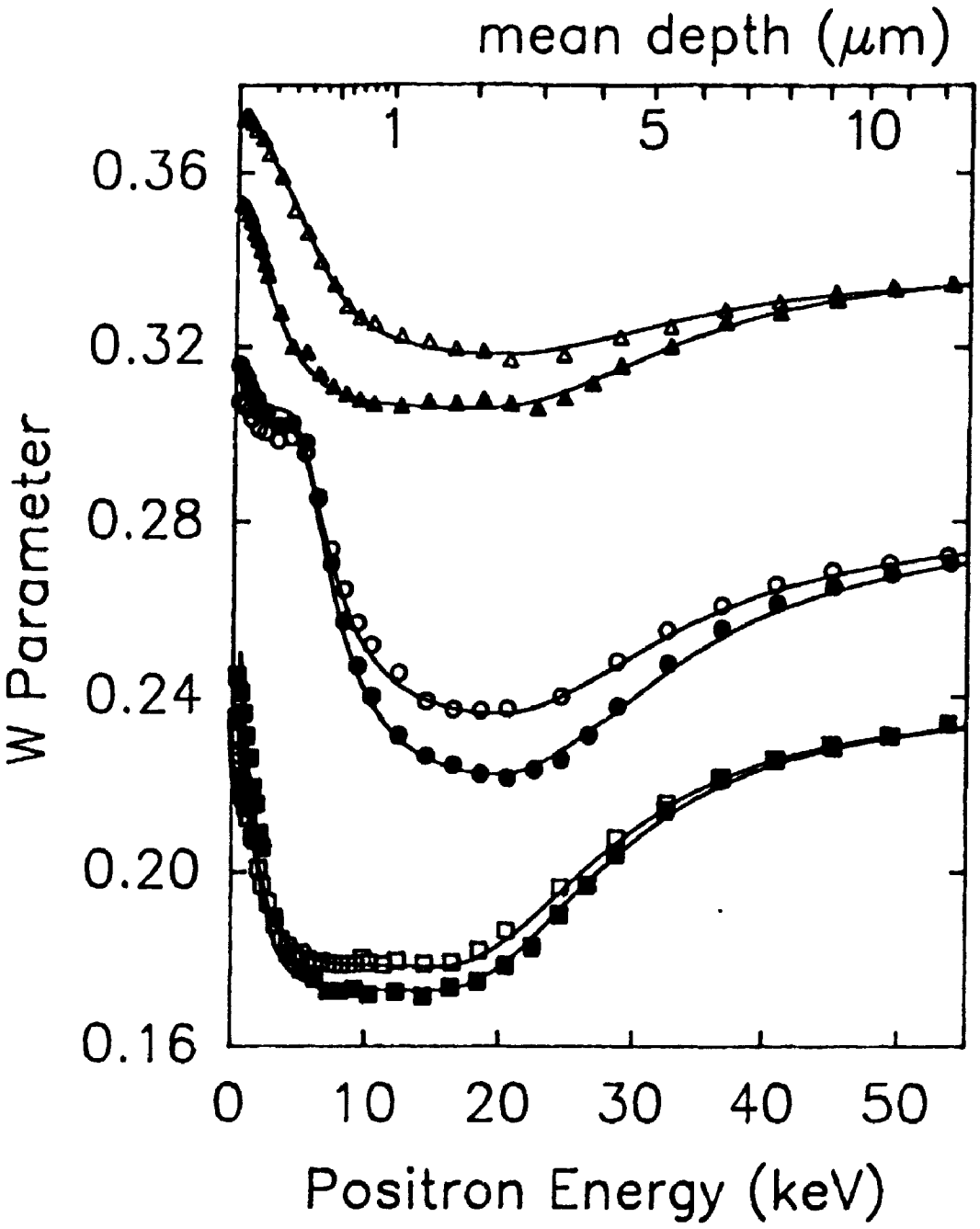

Figure 5-6: The change in lineshapes after storing the samples for ~1 year. Sample 587 (etched) before □ and after ■, 588 before ○ and after ●, 589 before △ and after ▲. Data have been scaled for clarity.

spectrometer. To further investigate this phenomenon, sample 587 was measured, and then heated at 250° C in vacuum for two weeks, and then remeasured. No change was observed, indicating that the cause of changes over time was not water content of the samples. Sample 587 was then subjected to a hydrogen plasma at a pressure of 2 Torr for 2 hours at 150° C and remeasured, with the intention that hydrogen (which is highly mobile in silicon even at room temperature (Seager and Anderson, 1988; Buda *et al.* 1989)) might accumulate on the void interior surfaces and change the γ-ray lineshape. No change was observed. It is postulated that the change over time of the γ-ray lineshapes was due to an increase in oxygen content. As can be seen in figure 5-1, the voids are joined by "strings" perpendicular to the sample surface, along which oxygen may be able to migrate. That oxygen content could have a pronounced effect on the observed γ-ray lineshapes was shown by the study of Hasegawa *et al.* (1988, 1989) discussed above. Further tests of controlled oxidation have not as yet been attempted.

Another possible explanation for the changes with time is the long-term recovery of competing defects, which would result in increased positron diffusion lengths and therefore a greater fraction trapped by voids. The absence of any change in the data after annealing at 700° C for 30 seconds need not rule out this possibility, but certainly does not support it.

Summary

We have observed regular arrays of voids in low-temperature grown Si epilayers. The controlling variable for void formation appears to be temperature. The voids constitute effective positron traps, trapping ~95%

of diffusing positrons. Extremely narrow annihilation lineshapes are observed, and these are attributed to Ps formation in the voids.

Chapter 6

Conclusions

It has been demonstrated that variable-energy positrons can provide a useful probe for defects in silicon layers. It is also clear however, that the resulting data must be interpreted with some caution.

In ion implanted silicon, we have observed distinct differences in silicon samples irradiated with He vs. Si ions. Although both contain large concentrations of divacancies as determined by infrared absorption measurements, positron annihilation spectra from Si-irradiated Si show no evidence of an annealing stage at the divacancy annealing temperature. This we attribute to vacancies clustering into aggregates larger than the divacancy, still forming efficient positron traps, but no longer producing an optical absorption band at 1.8 μm wavelength. A similar conclusion was reached for Si-irradiated InP (appendix 1), where evidence of vacancy clustering upon annealing was observed. By contrast, He-irradiated Si does show an annealing stage at the divacancy annealing temperature of 560K. The difference in behaviour is attributed to a difference in the rates of recombination and agglomeration of vacancies for the two cases. This could be due to the differing density of damage along the ion track in the solid, although it is not yet clear why varying the ion fluence does not then also produce a similar effect.

A further difference between the results for Si and He irradiations was evident in the defect depth distributions implied by the positron data. For the silicon irradiations, the positron data led to vacancy profiles

consistent with the shapes predicted by TRIM simulations. For the high-fluence He irradiations this was not the case, and the difference is attributed to the formation of a helium impurity-type defect at the end-of-range of the implanted ions.

In silicon layers grown by molecular beam epitaxy, we have identified voids which had been observed, but not identified, by electron microscopy. Regular arrays of voids form at growth temperatures in a narrow range around 350° C. These novel defects are efficient positron traps and result in the narrowest positron annihilation lineshapes ever observed for subsurface annihilations in silicon. The extremely narrow linewidths are attributed to the formation of positronium inside the voids.

The fundamental limitation of the Doppler broadening technique appears to be that it fails to provide specific information on defect types: only a single "average" type of defect can be profiled at one time, and any variation in defect type (or relative abundance amongst several defect types) within a single region can propagate errors in the analysis. Several defect types can be modeled simultaneously provided that information is available from other techniques to reduce the number of adjustable parameters in the fitting procedure. An example of this is provided by the B_2O_3-doped capping layer on the samples discussed in chapter 5, which was measured simultaneously with the region of the sample containing voids.

Usefulness of the technique hinges in part on acceptance of the results by others, particularly in the semiconductor industry. A factor which may delay this acceptance is the apparently arbitrary nature of the lineshape parameters W and S. This is largely a matter of calibration, however: other

techniques such as infrared absorption can similarly only provide an absolute measurement after calibration with samples of known characteristics. Further work is required to establish a more quantitative relationship between defects and their associated annihilation lineshapes. Ultimately, an extensive catalogue of defect parameters W_d or S_d, along with the positron trapping rates of defects, is required. To this end, further systematic studies are required, possibly combining positron lifetime measurements with Doppler broadening. Lifetime measurements have the advantage that defect-specific signals are obtained, i.e. two different kinds of defects which co-exist can produce separable signals, since the positron lifetime varies with the electronic environment. Unfortunately the technology required to make lifetime measurements with variable-energy positron beams, rather than with high-energy radioactive sources, is not very well developed. With further technical development a combination of the two techniques will likely be a fruitful area for study. Meanwhile, systematic studies of silicon wafers containing various doping species and concentrations may help to resolve some of the questions relating to the sensitivity of the positron technique to various defect complexes, such as vacancy-impurity combinations. The high sensitivity of the technique, particularly to vacancy-type defects, its sensitivity to structural properties of defects (and not just their electronic levels), its non-destructive nature, and the ability to profile buried layers, should ensure continuing interest.

References

In this list of references, ICPA denotes the International Conferences on Positron Annihilation. Proceedings of these conferences are identified by year (ICPA88 etc.) and full information on them is given below under ICPA. Similarly, SLOPOS90 refers to the proceedings of the 1990 International Workshop on Slow Positron Beams, and full information is given under SLOPOS.

Aers, G.C., in SLOPOS90, p. 162.

Baker, J.A., N.B. Chilton, K.O. Jensen, A.B. Walker and P.G. Coleman, J. Phys: Condens. Matter **3**, 4109, (1991); Appl. Phys. Letters (in press).

Bean, J.C., and E. Kasper, editors of *Silicon Molecular Beam Epitaxy Vol 1 and 2*, , C.R.C. Press, Boca Raton (1988).

Biersack, J.P., and L.G. Haggmark, Nucl. Inst. Meth. **174**, 257 (1980).

Britton, D.T., P. Bentvelsen, J. De Vries and A. van Veen, Nucl. Inst. and Meth. **A273**, 343 (1988).

Buda, F., G.L. Chiarotti, R. Car and M. Parrinello, Phys. Rev. Lett. **63**, 294 (1989).

Cheng L.J., and J. Lori, Phys. Rev. **171**, 856 (1968).

Chilton, N.B., J.A. Baker and P.G. Coleman, in SLOPOS90, p. 129.

Corbett, J.W., J.P. Karins and T.Y Tan, Nucl. Inst. Meth. **182/183**, 457 (1981a).

Corbett, Kleinhenz and Wilsey, in *Defects in Semiconductors*, edited by J. Narayan and T.Y. Tan, Elsevier North Holland, New York, (1981b), p. 1-19.

Dannefaer, S., and D.P. Kerr, Nucl. Inst. Meth. **131**, 119 (1975).

Dannefaer, S., G.W. Dean, D.P. Kerr, and B.G. Hogg, Phys. Rev. B **14**, 2709 (1976).

Dannafaer, S., Phys. Stat. Solidi, (a) **102**, 481 (1987).

Davies, J.A., in *Ion Implantation and Beam Processing*, edited by J.S. Williams and J.M. Poate, Academic Press, (1984) p. 81.

DeBenedetti, S., C.E. Cowan and W.R. Konneker, Phys. Rev. **76**, 440 (1949).

Denhoff, M.W., D.C. Houghton, T.E. Jackman, M.L. Swanson and N. Parekh, J. App. Phys. **64**, 3938 (1988).

Eaglesham, D.J., H.-J. Gossman and M. Cerullo, Phys. Rev. Lett. **65**, 1227 (1990).

Feldman, L.C., J.W. Mayer, and S.T. Picraux, *Materials Analysis by Ion Channeling*, Academic Press, New York (1982).

Hasegawa, M., S. Berko and E. Kuramoto, in ICPA88, p. 77.

Hasegawa, M., O. Yoshinari, H. Matsui and S. Yamaguchi, J. Phys. Condens. Matter 1, SA77, (1989).

Hautojärvi, P., and A. Vehanen, in *Positrons in Solids*, edited by P. Hautojärvi, Springer-Verlag, New York, (1979), p. 1-23.

Hautojärvi, P., P. Huttunen, J. Mäkinen, E. Punkka and A. Vehanen, Mat. Res. Soc. Symp. Proc Vol. **104**, Materials Research Society, 105 (1988).

Holland, O.W., S.J. Pennycook and G.L. Albert, Appl. Phys. Lett. **55**, (24), 2503 (1989).

ICPA82, *Positron Annihilation*, Proceedings of the 6th International Conference on Positron Annihilation, Arlington, Texas, edited by P.G. Coleman, S.C. Sharma, and L.M. Diana, North-Holland, Amsterdam, (1982).

ICPA88, *Positron Annihilation*, Proceedings of the 8th International Conference on Positron Annihilation, Gent, Belguim, edited by L. Dorikens-Vanpraet, M. Dorikens and D. Segers, World Scientific Publishing, Singapore, (1989).

ICPA91, *Positron Annihilation*, Proceedings of the 9th International Conference on Positron Annihilation, Szombathely, Hungary, in press (1991).

Jackman, T.E., D.C. Houghton, M.W. Denhoff, Song Kechang, J.McCaffrey, J.A. Jackman and C.G. Tupper, App. Phys. Lett. **53**, 877 (1988).

Jackman, T.E., D.C. Houghton, J.A. Jackman, A. Rockett, M.W. Denhoff, Song Kechang and J. McCaffrey, J. App. Phys. **66**, 1984 (1989).

Jackman, T.E., G.C. Aers, J.P. McCaffrey, D. Britton, P. Willutzki, P.J. Schultz, P.J. Simpson and P. Mascher, in ICPA91.

Jorke, H., H.-J. Herzog and H. Kibbel, Phys. Rev. B **40**, 2005 (1989a).

Jorke, H., H. Kibbel F. Schäffler and H.-J. Herzog, Thin Solid Films **183**, 307 (1989b).

Keinonen, J., M. Hautala, E. Rauhala, V. Kartiunen, A. Kuronen, J. Raisn, J. Lahtinen, A. Vehanen, E. Punkka and P. Hautojärvi, Phys. Rev. B **37**, 8269 (1988).

Lee, Y.H., and J.W. Corbett, Phys. Rev. B **9**, 4351 (1974).

Leffler, S.R., P.J. Simpson, P.J. Schultz and I.K. MacKenzie, in SLOPOS90, p. 231.

Lightowlers, E.C., in *Growth and Characterization of Semiconductors*, edited by R.A. Stradling and P.C. Klipstein, Adam Hilger, New York, (1990), p. 135-163.

Linnros, J., R.G. Elliman and W.L. Brown. J. Mater. Res. **3**, 1208 (1988).

Lynn, K.G., Phys. Rev. Lett. **43**, 391 (1979).

MacKenzie, I.K., T.L. Khoo, A.B. McDonald and B.T.A. McKee, Phys. Rev. Lett. **19**, 946 (1967).

Mäkinen, J., E. Punkka, A. Vehanen, P. Hautojärvi, J. Keinonen, M. Hautala and E. Rauhala, J. Appl. Phys. **67** (2), 990 (1990).

Mantl, S., and W. Triftshäuser, Phys. Rev. B **17**, 1645 (1978).

Mascher, P., S. Dannefaer and D. Kerr, Phys. Rev. B **40**, 11764 (1989a).

Mascher, P., S. Dannefaer, and D. Kerr, Materials Science Forum, **38-41**, 1157 (1989b).

Mayer, J.W., L. Eriksson, S.T. Picraux and J.A. Davies, Can. J. Phys. **46**, 663 (1968).

McKee, B.T.A., Can. J. Phys. **67**, 821 (1989).

Mills, A.P., Jr., Phys. Rev. Lett. **41**, 1828 (1978).

Mills, A.P., Jr., and C.A. Murray, Appl. Phys. **21**, 323 (1980).

Mills, A.P., Jr., and R. Wilson, Phys. Rev. A **26**, 490 (1982).

Newman, R.C., in *Growth and Characterization of Semiconductors*, edited by R.A. Stradling and P.C. Klipstein, Adam Hilger, New York, (1990), p. 105-134.

Nieminen, R.M., J. Laakkonen, P. Hautojärvi and A. Vehanen, Phys. Rev. B **19**, 1397, (1979).

Perovic, D.D., G.C. Weatherly, P.J. Simpson, P.J. Schultz, T.E. Jackman, G.C. Aers, J.-P. Noël and D.C. Houghton, Phys. Rev. B **43**, 14257 (1991).

Saarinen, K., P. Hautojärvi, J. Keinonen, E. Rauhala, J. Räisänen and C. Corbel, Phys. Rev. **B43**, 4249 (1991).

Schultz, P.J., Nucl. Inst. Meth. **B30**, 94 (1988).

Schultz, P.J. and K.G. Lynn, Rev. Mod. Phys. **60**, 701 (1988).

Schultz, P.J., E. Tandberg, K.G. Lynn, B. Neilsen, T.E. Jackman, M.W. Denhoff and G.C. Aers, Phys. Rev. Lett. **61**, 187 (1988).

Schultz, P.J., C. Jagadish, M.C. Ridgeway, R.G. Elliman and J.S. Williams, Phys. Rev. B **44**, 9118 (1991).

Seager, C.H., and R.A. Anderson, Appl. Phys. Lett. **53**, 1181 (1988).

Simpson, P.J., P.J. Schultz, I.V. Mitchell, T.E. Jackman and G.C. Aers, in *Impurities, Defects and Diffusion in Semiconductors: Bulk and Layered Structures*, edited by D.J. Wolford, J. Bernholc and E.E. Haller, MRS Press, Pittsburgh, (1989), p. 931.

Simpson, P.J., P.J. Schultz, T.E. Jackman, G.C. Aers, J.-P. Noël, D.C. Houghton, D.D. Perovic and G.C. Weatherly, in SLOPOS90, p. 125.

Simpson, P.J., M. Vos, I.V. Mitchell, C. Wu and P.J. Schultz, Phys. Rev. B, accepted for publication, (1991).

Stein, H.J., F.L. Vook, and J.A. Borders, Appl. Phys. Lett. **14** 328 (1969).

Stein, H.J., F.L. Vook, D.K. Brice, J.A. Borders and S.T. Picraux, Radiation Effects **6**, 19 (1970).

Stein, H.J., and W. Beezold, Appl. Phys. Lett. **17**, 442 (1970).

Sze, S.M., *Semiconductor Devices, Physics and Technology*, John Wiley and Sons, New York, (1985).

Tandberg, E., P.J. Schultz, G.C. Aers and T.E. Jackman, Can. J. Phys. **67** (4), 275 (1989).

Triftshäuser, W., and G. Kögel, Phys. Rev. Lett. **48**, 1741 (1982); ICPA82 p. 142; J. Nucl. Mater. **111&112**, 687 (1982).

Uedono, A., S. Tanigawa, J. Suguira and M. Ogasawara, in ICPA88, p. 690.

Uedono, A., L. Wei, Y. Tabuki, H. Kondo, S. Tanigawa, J. Sugiura and M. Ogasawara, in ICPA91.

Valkealahti, S., and R.M. Nieminen, Appl. Phys. A, **35**, 51 (1984).

van Veen, A., H. Schut, J. de Vries, R.A. Hakvoort and M.R. IJpma, in SLOPOS90, p. 171.

Vetter, Th., and A. Winnaker, J. Mater. Res. **6**, 1055 (1991).

Watkins, G.D., in *Radiation Damage in Semiconductors*, Dunod, Paris, (1965) p. 97.

Watkins, G.D., and J.W. Corbett, Phys. Rev. **138** A543 (1965).

Wertheim, G.K., A. Hausmann and W. Sander, *The Electronic Structure of Point Defects*, North-Holland, Amsterdam, (1971).

Wormeester, A., A.G.B.M. Sasse, and A. van Silfhout, Comp. Phys. Comm. **52**, 19 (1988).

Appendix 1

The following paper, entitled *Evidence for Vacancy Clustering in Silicon-implanted Indium Phosphide*, by P.J. Simpson and P.J. Schultz, has been submitted for publication to Physical Review B, Brief Communications.

EVIDENCE FOR VACANCY CLUSTERING IN SILICON-IMPLANTED INDIUM PHOSPHIDE

P.J. Simpson and P.J. Schultz

Department of Physics
The University of Western Ontario, London, Ontario, Canada N6A 3K7

ABSTRACT

Damage induced in InP wafers by ion implantation has been investigated using Doppler broadening of annihilation radiation from variable-energy positrons (VEP) and compared with previously reported Rutherford backscattering/channeling (RBS).[1] Si^+ ions were implanted at energies from 0.6 to 3.0 MeV and fluences from 10^{11} to 10^{14} ions cm^{-2}. VEP trapping increased with ion fluence, but the depth distribution of positron traps is not the same as the damage either predicted using Monte Carlo simulation or measured by RBS. Annealing at room temperature was monitored for ~100 days, during which both VEP and RBS showed recovery of the crystal toward the pre-implanted condition. RBS measurements of samples annealed at elevated temperatures showed that full restoration of lattice order occured at 375K, but VEP data for isochronal annealing up to 720K showed only a moderate reduction in the vacancy-type defect concentration with a significantly narrower lineshape, consistent with vacancy clustering.[2]

Profiling of near–surface defects using variable energy positrons (VEP) has been applied extensively to Si and GaAs. For both of these materials there is some understanding of the nature of the positron–trapping defects and their trapping rates, more so for the simpler case of (elemental) Si. There have been, however, few published reports of defect profiling in InP,[3,4] despite considerable interest in this material for optoelectronic applications and, in particular, in the use of ion implantation to produce shallow dopant profiles.[5]

One of the most important features of VEP studies of defects is a high sensitivity to dilute concentrations of vacancy–type structural defects ($C \sim 10^{-6}$ per lattice site). Virtually *all* of the more traditional defect–sensitive spectroscopies, such as electron paramagnetic resonance (EPR), infrared (IR) absorption, Raman spectroscopy, photoluminescence (PL) or deep level transient spectroscopy (DLTS) are sensitive to defects *because* of their electronic structure. In addition, electrical conductivity and capacitance methods are the "industry standard" techniques for overall quality determinations of bulk films and junctions, although both test *only* for those defects which exist in a depleted zone. VEP profiling provides a non–destructive, in–situ probe of structural defects in the top few microns of material, and thus offers a promising complement to the above techniques.

In the present study VEP was used to investigate the annealing of ion induced damage in highly doped InP. Both n–type (doped with $[S] \sim 4 \times 10^{18}$ cm^{-3}) and p–type ($[Zn] \sim 1 \times 10^{18}$ cm^{-3}) InP (100) wafers were implanted at room temperature with Si ions at energies from 0.6 to 3.0 MeV, at a flux of 0.01 μA cm^{-2}. The VEP experiments were done using the University of Western Ontario Positron Beam Facility,[6] and data were parameterized using the W–parameter, defined as the number of counts in the wings of the 511 keV peak (507.3 to 509.7 and 512.3 to 514.7 keV) divided by the total counts in the peak (506.2 to 515.8 keV).[7] W–parameter versus incident energy data are fit

with a model defect profile using the program POSTRAP.[8] There has been no report of a direct experimental determination of the positron stopping profile in InP, so we have assumed the usual[7] mean range $\bar{z}=(A/\rho)E^{1.6}$ (Å) where E (keV) is the positron beam energy, ρ the material density (=4.79 g cm^{-3} for InP) and A=400. Rutherford backscattering/channeling (RBS) analyses done for some of the samples studied here have been published elsewhere.[1] In addition, survey PL measurements confirmed that the doping level was sufficiently high as to mask any sensitivity of PL to ion–induced damage.[9]

Figure 1 shows data for the as–received S–doped wafer (o). Total defect concentrations, listed in Table 1, show that there are significant defect levels in all unimplanted wafers studied so far, consistent with other studies.[4] We find that the concentration for the unimplanted InP(Zn) is about an order of magnitude higher than for the InP(S). It has been suggested in other cases of low defect concentrations ($<<1\times10^{-5}$ cm^{-2}) that the same results could be modelled using a positron mobility term due to sufficiently strong electric fields near the surface,[7,8] but in the present case the material is too heavily doped to sustain sufficiently large fields.

Also shown in Fig. 1 are VEP results for the S–doped InP implanted with 600 keV Si ions to fluences from 3.6×10^{11} to 1.0×10^{13} cm^{-2}. For these samples, RBS showed implantation damage extending from the surface to a depth of ~0.7μm,[1] in agreement with the range of the implanted ions predicted by the computer simulation TRIM.[10] The minimum W parameter decreases with increasing ion fluence, indicating a progressive narrowing of the Doppler–broadened annihilation line due to an increasing concentration of vacancy–type defects, as expected. The ratio of defect to "bulk" InP parameter was consistently W_d/W_f=0.91 for all data except the thermally annealed sample, #24, as noted in Table 1. It was found, however, that the range of significant concentrations of ion–induced positron traps was below ~0.5μm (with a weak tail

extending to 1.5–2.5 μm), which is much less than the range of ion–induced damage.

To further explore the disagreement in the apparent depth of the damaged regions measured by RBS and by positrons for 600 keV Si irradiation, InP(S) wafers were also implanted with Si ions at energies of 1, 2 and 3 MeV, and fluences from 5×10^{11} to 3×10^{13} cm^{-2}. Figure 2 shows representative data which highlight the anomalous range of positron traps, and Fig. 3 shows the TRIM calculation of vacancy production at these energies, together with a representative defect profile used to fit the VEP data. Virtually all data, irrespective of incident ion energy, were fit with the same depth distribution of defects that is shown in Fig. 3, with varying defect concentrations as reflected in the total defect density, listed in Table 1.

In the past, we have found for the case of self–ion irradiation of Si good agreement between the range of damage measured with VEP and that derived by RBS.[11] This is, however, not always the case. In particular, for cases where the implanted species *differs* from the substrate material[11-14] we note that the damage profiles obtained from VEP are *not* usually in agreement with the predictions of TRIM. In addition, we have preliminary data which suggest that the trapping distribution may be a strong function of substrate temperature and ion flux, *even* for self–ion irradiation of Si. All of this evidence suggests that the discrepancy is not due to a failure of the positron defect profiling model, but instead is related to some fundamental aspect of the damage production process.

One possibility for the profile–anomaly is suggested by a study of high levels of As incorporated in silicon overlayers grown on Si(100) by molecular beam epitaxy (MBE).[15] A defect was found that was an efficient trap for positrons, but for which the electronic environment (and thus the W–parameter) was indistinguishable from that for the undefected bulk lattice. It was suggested that the defect was an interstitial As cluster, and this was supported by other theoretical and experimental

evidence for a stable vacancy–tetra–As configuration. It may turn out that the relatively high impurity concentrations near the end–of–range for (dissimilar) implanted ions leads to similar positron traps with "bulk–like" characteristics.

A second possibility relates to the different mechanism of stopping in the near–surface region of the solid as compared with the region near the end–of–range of the incident ions.[16] Near the surface, energy transfer is dominated by electronic excitations, whereas deeper in the solid inelastic nuclear collisions are more important. This is why vacancy production is in fact *enhanced* towards the end–of–range. It may turn out that this process results in a profile of defect charge states, which would lead to different positron trapping rates in near–surface vacancies than in those closer to the end–of–range. It is not possible to confirm either of these possibilities with the data presently available, although both suggest an interesting series of systematic measurements in ion–irradiated semiconductors.

Annealing of the implantation damage at room temperature was monitored for ~100 days. RBS measurements on an InP(Zn) wafer implanted with 2×10^{13} cm^{-2} 600 keV Si ions showed that ~65% of the initial damage recovered in 3 weeks, with similar results for all Si ion fluences $\lesssim 4\times10^{13}$ cm^{-2} in both InP(Zn) and InP(S) wafers.[1] VEP measurements on identical samples also indicated a reduction in residual damage with time at room temperature, although the maximum reduction was only ~25% as shown by the change from sample #24A (•) to #24D(□) in Figure 4. Several of the implanted samples were also annealed at elevated temperatures. RBS analysis of InP(Zn) samples implanted with 3×10^{13} cm^{-2} 600 keV Si ions and subjected to isochronal anneals showed that an anneal at 375K for 30 minutes was sufficient to remove ~90% of the disorder.[1] In contrast with this, annealing a similar sample at 375K for 30 minutes had no effect on the positron annihilation spectra. Subsequent annealing to higher temperatures resulted in a decrease in the total defect

concentration measured by VEP, but with a significant reduction in the W parameter (W_d/W_f=0.88), as shown in Figure 4 for an anneal to 600K. Annealing to 720K (not shown) caused a further reduction in W to a minimum of W_d~0.215 (W_d/W_f=0.84); it is not expected that temperatures in this range would lead to significant loss of phosphorus from the near–surface region of the sample.[17] The strong effect on the lineshape parameter was observed in both p– and n–type wafers, and is consistent with the formation of vacancy clusters, or microvoids.[2]

The fact that thermal annealing led to a reduction in lattice disorder as determined by RBS, while VEP demonstrated defect growth, may be explained by the activation of negatively–charged substitutional Si atoms and/or antisite defects (undetectable by RBS). However, it is unlikely that these would produce such a strong reduction in the W parameter value. A more probable interpretation is that during annealing, mobile vacancies agglomerate into vacancy clusters, stable at elevated temperatures. Such clusters would be less numerous than the smaller defects present prior to annealing, but may have a more extreme effect on the annihilation lineshape due to their larger size.[2] This suggestion would be consistent with the RBS observation of reduced disorder since RBS is most sensitive to displaced atoms, exhibiting only limited sensitivity to vacancy–type defects. The reason this phenomenon does not appear to occur during annealing at room temperature is perhaps due to limited vacancy diffusion, although it may also be indicating that the large defect structures require thermal activation to form. In the case of silicon there are numerous examples of defects which *only* form at elevated temperatures.[18,19]

A complex array of defect types can be formed in a binary semiconductor, making it difficult to understand ion irradiation damage in InP. In addition, the quality and reproducibility of commercially available wafers is not as high as it is for Si. The commercial material can be inhomogenous, both in depth (as demonstrated in Figs. 1

& 4), and across the wafer.[20] The positron range in InP is not well established, nor have the lineshape parameters and trapping rates of any specific defect types been reliably determined. We have, however, demonstrated the ability of positrons to provide unique information not available from other techniques such as RBS or photoluminescence. These results, and others beginning to appear now, support the need for additional fundamental work which will establish defect profiling with variable energy positrons as a viable technique for characterization of InP.

The authors acknowledge useful discussions with U.G. Akano, who also performed all of the InP implantations, and with T.E. Jackman, I.V. Mitchell, and M. Thewalt. Research conducted at the University of Western Ontario Positron Beam Facility is supported by grants from the Natural Sciences and Engineering Research Council of Canada.

References

1. U.G. Akano, I.V. Mitchell and F.R. Shepherd, Appl. Phys. Lett., to be published.
2. D.D. Perovic, G.C. Weatherly, P.J. Simpson, P.J. Schultz, T.E. Jackman, G.C. Aers, J.–P. Noel, and D.C. Houghton, Phys. Rev. B 43, 14257 (1991).
3. Y. Iwase, A. Uedono, S. Tanigawa and H. Araki, in Positron Annihilation, edited by P.C. Jain, R.M. Singru and K.P. Gopinathan, World Scientific Publishing Co., 753 (1985).
4. A. Uedono and S. Tanigawa, Japn. J. Appl. Phys. 29, 909 (1990).
5. D.K. Sadana, Nuc. Inst. Meth. B7/8, 375 (1985).
6. P.J. Schultz, Nuc. Inst. Meth. B30, 94 (1988).
7. P.J. Schultz, and K.G. Lynn, Rev. Mod. Phys. 60, 701 (1988).
8. G.C. Aers, p.162 in Positron Beams for Solids and Surfaces, ed. P.J. Schultz, G.R. Massoumi and P.J. Simpson (AIP Press, New York, 1990).
9. Photoluminescence was done at Simon Fraser University with the assistance of M. Nissan and M. Thewalt, to whom we are grateful.
10. J.P. Biersack, L.G. Haggmark, Nuc. Inst. Meth. 174, 257 (1980).
11. P.J. Simpson, M. Vos, I.V. Mitchell, C. Wu and P.J. Schultz, Phys. Rev. B (MS #BD4759) in press (1991).
12. P. Hautojärvi, P. Huttunen, J. Makinen, E. Punkka and A. Vehanen, Mat. Res. Soc. Symp. Proc Vol. 104, Materials Research Society, 105 (1988).
13. J. Keinonen, M Hautala, E. Rauhala, V. Karttunen, A. Kuronen, J. Raisn, J. Lahtinen, A. Vehanen, E. Punkka and P. Hautojärvi, Phys. Rev. B 37, 8269 (1988).
14. A. Uedono, S. Tanigawa, J. Suguira and M. Ogasawara, in Positron Annihilation, edited by L. Dorikens–Vanpraet, M. Dorikens and D. Segers, World Scientific

Publishing, p. 690 (1989).

15. T.E. Jackman, G.C. Aers, M.W. Denhoff, and P.J. Schultz, Appl. Phys. A, Rapid Commun. 49, 335 (1989).

16. J.F. Gibbons, IEEE Proceedings 60, 1062 (1972).

17. W.C. Dautremont–Smith, J. Lopata, S.J. Pearton, L.A. Koszi, M. Stavola and V. Swaminathan, J. Appl. Phys. 66, 1993 (1989).

18. J.W. Corbett, J.P. Karins and T.Y.Tan, Nuc. Inst. Meth. 182/183, 457 (1981).

19. P.J. Schultz, T.D. Thompson, and R.G. Elliman, Appl. Phys. Lett. (MS #L–0317), in press.

20. Th. Vetter and A. Winnaker, J. Mater. Res. 6, 1055 (1991).

Table 1: Sample characteristics are listed, together with total defect concentrations as determined using the analysis program POSTRAP4. Defect profiles were in all cases similar in depth to that shown in Fig. 3, and the defect parameter was W_d/W_f = 0.91 for all data except #24A (for which W_d/W_f = 0.90) and the thermally annealed sample #24H (for which W_d/W_f = 0.88).

InP Sample (Dopant)	Figure & Symbol	Si^+ ion Fluence (cm^{-2})	& Energy (MeV)	Total Defects (cm^{-2})
#3(S)	1(○)	unimplanted		3.8e13
#32(S)	1(●)	3.6×10^{11}	0.6	2.9e14
#30(S)	1(□)	3.5×10^{12}	0.6	4.0e14
#31(S)	1(△)	1.0×10^{11}	0.6	5.4e14
#24A(Zn)	2(○)/4(●)	3.0×10^{13}	0.6	2.1e15
#47(S)	2(●)	3.0×10^{13}	1.0	1.6e15
#42(S)	2(□)	3.0×10^{13}	2.0	8.0e14
#41(S)	2(△)	3.0×10^{13}	3.0	6.4e14
#5(Zn)	4(○)	unimplanted		1.7e14
#24D(Zn)	4(□)	3.0×10^{13}	0.6	1.6e15
#24H(Zn)	4(△)	3.0×10^{13}	0.6	8.3e14

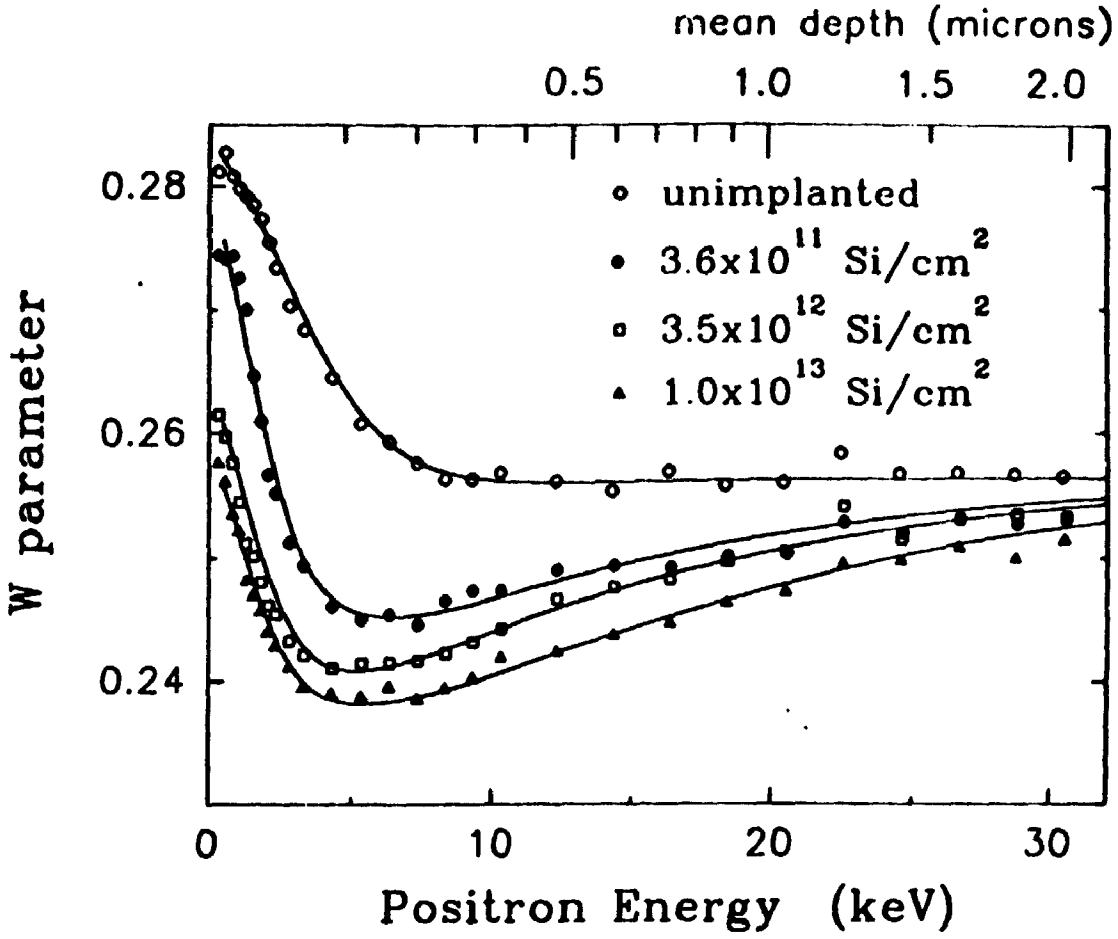

Figure 1: W–parameter vs incident positron energy for S–doped InP(100) implanted with various fluences of 0.6 MeV Si ions. The decrease in W with increasing fluence is due to the increase in positron trapping in vacancy–type defects, and the solid curves are fits to the data of models produced using POSTRAP4.[8]

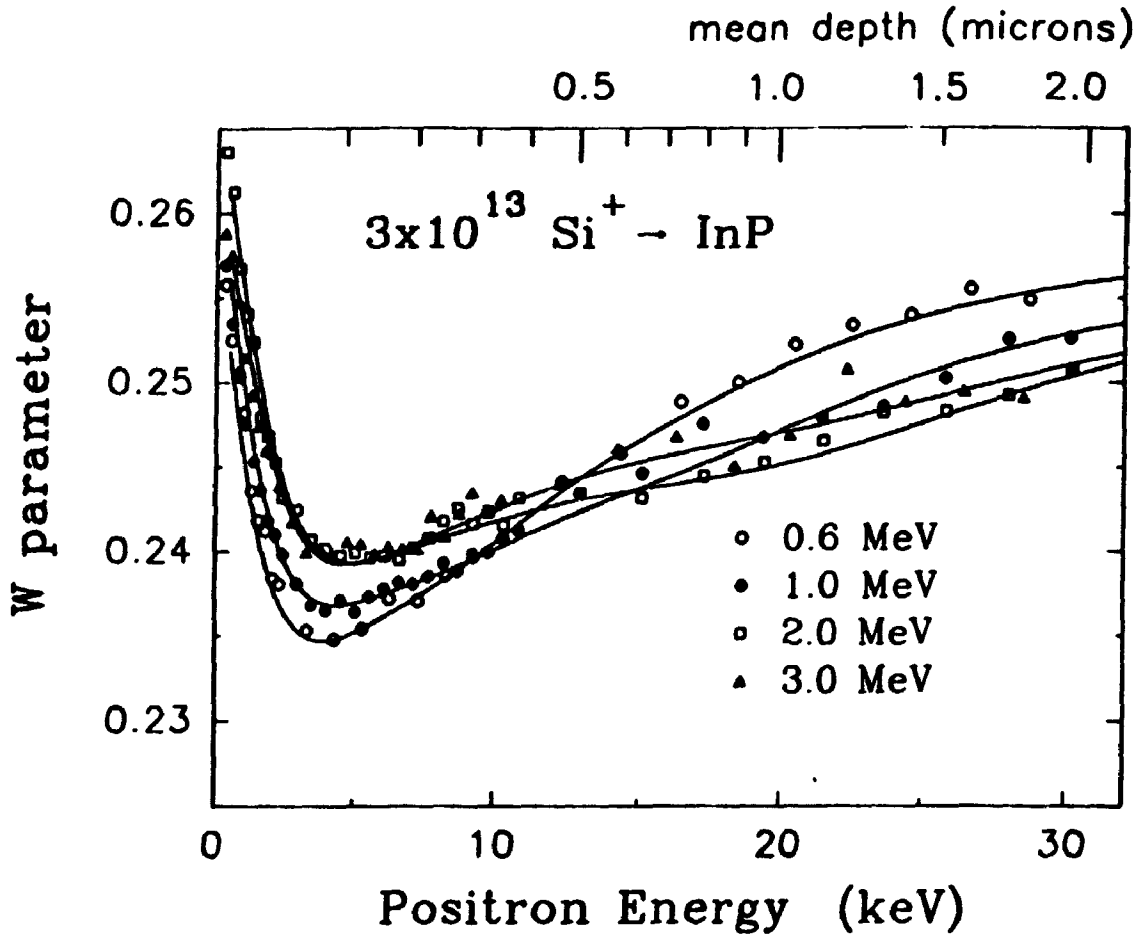

Figure 2: W–parameter vs incident positron energy for Zn– (∘) and S–doped InP(100) implanted with 3×10^{13} Si ions at the energies shown. Implantation and defect parameters are summarized in Table 1.

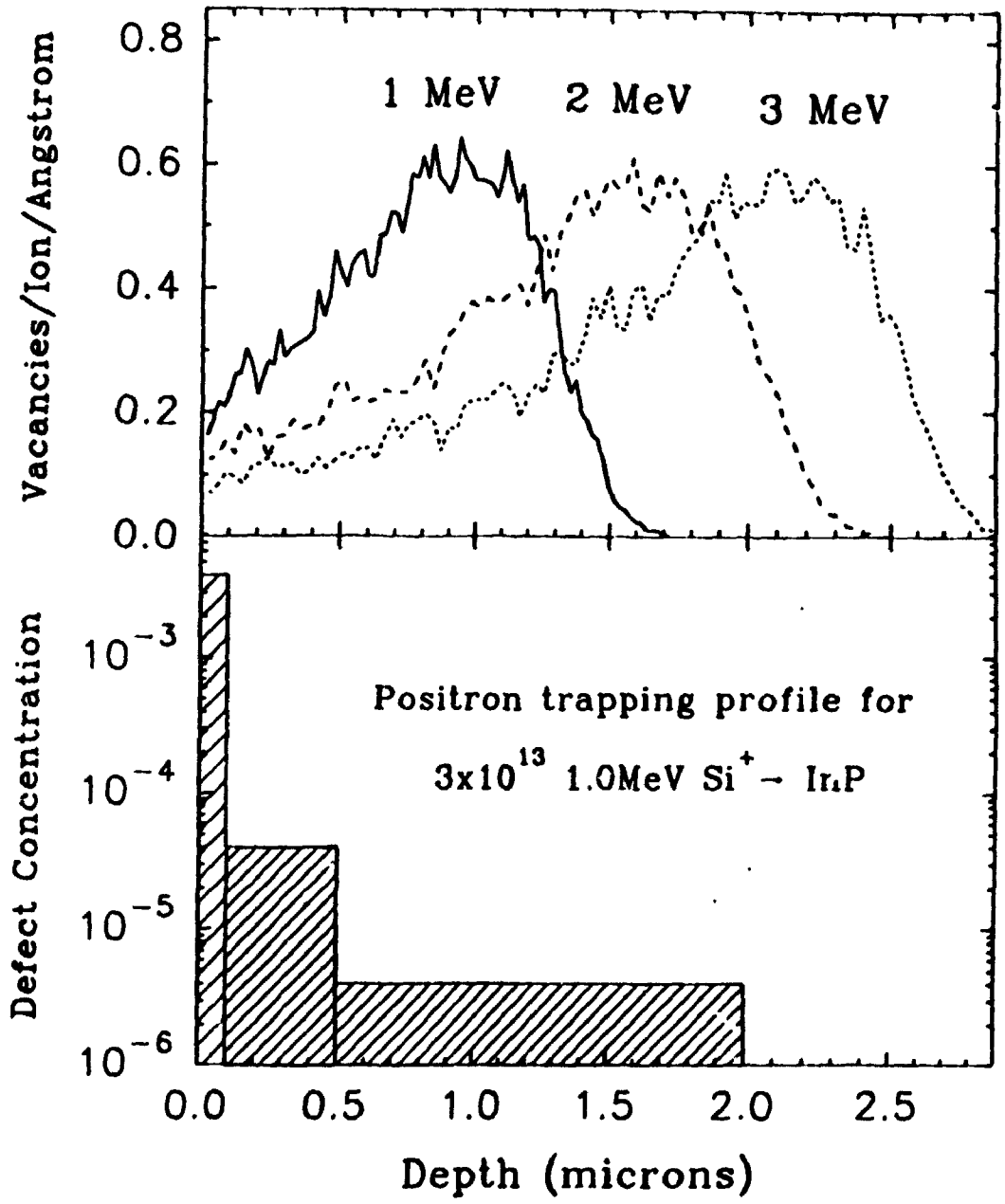

Figure 3: Monte–Carlo "TRIM" calculation[10] of the number of vacancies per incident ion per Å of depth in the InP, calculated for 1, 2, and 3 MeV Si ions. Also shown is the defect profile used to fit the data for 1.0 MeV Si ions, shown in Fig. 2 (•).

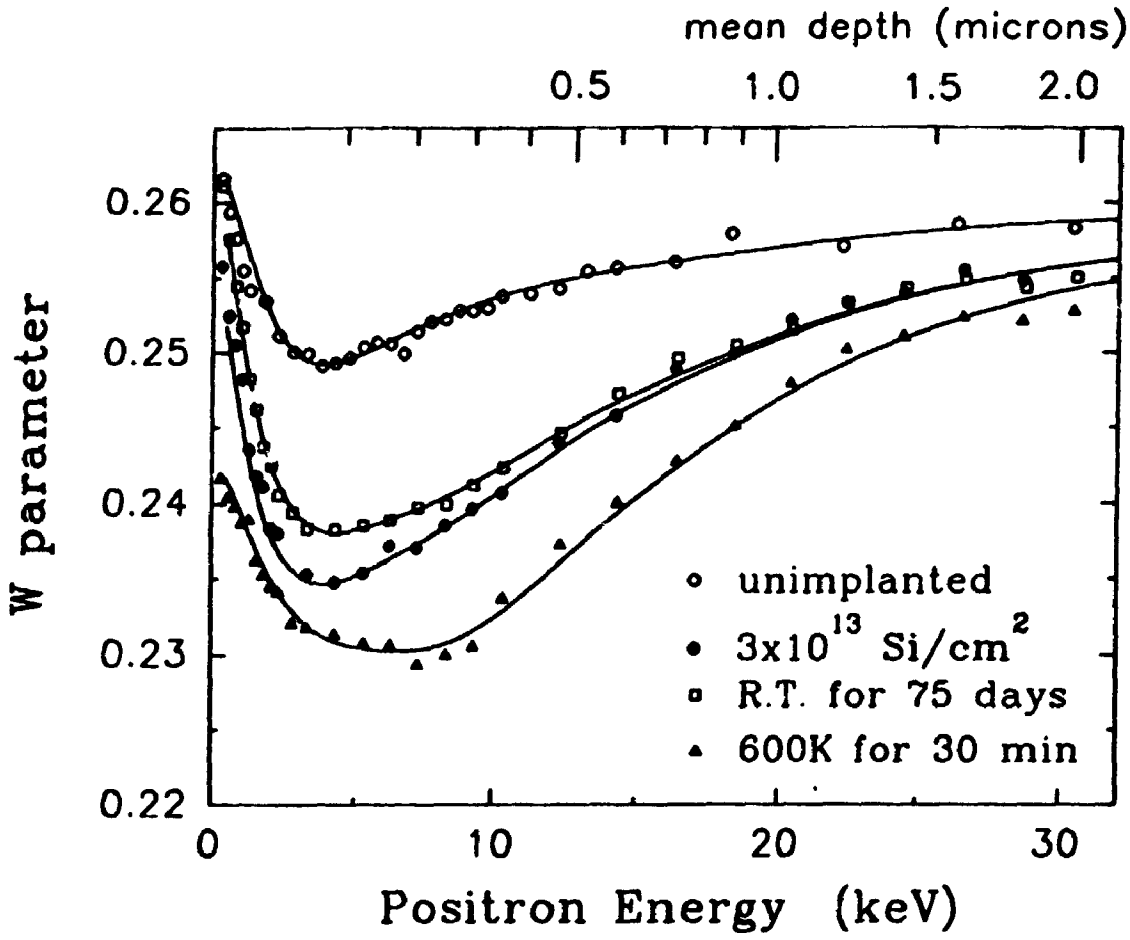

Figure 4: W–parameter vs incident positron energy for Zn–doped InP(100) before (∘) and after (•) implantation, illustrating annealing both at room temperature (□) and for 30 minutes at 600 K (▲). The decrease in lineshape parameter following thermal annealing is attributed to the formation of vacancy clusters, or microvoids.

Appendix 2

The following paper, entitled *Annealing of Si-implanted GaAs Studied Using Variable-energy Positrons*, by P.J. Simpson, P.J. Schultz, S.-Tong Lee, Samuel Chen and G. Braunstein, has been submitted for publication to the Journal of Applied Physics.

Annealing of Si-implanted GaAs studied using variable-energy positrons

P.J. Simpson and P.J. Schultz
Department of Physics, the University of Western Ontario
London, Ontario, N6A 3K7, Canada

S.-Tong Lee, Samuel Chen, and G. Braunstein
Corporate Research Laboratories, Eastman Kodak Company
Rochester, NY 14650-2132, U.S.A.

ABSTRACT:

Modification of GaAs by Si^+ ion implantation is an important process for selective doping of the material. Defects caused by the implantation process often lead to incomplete electrical activation, and annealing procedures are used to recover the crystal quality. We present here results of variable-energy positron (VEP) and cross-sectional transmission electron microscopy (XTEM) studies of a series of GaAs samples implanted with moderate to high fluences of 3×10^{13}, 3×10^{14}, and 1×10^{15} Si^+ ions cm^{-2}. Samples were irradiated at room temperature, and studied both before and after thermal annealing for one hour at 850° C. In all cases XTEM results show a high density of small extrinsic dislocations after implantation, and VEP shows high concentrations of point (vacancy-type) defects. Annealing leads to a decrease in the point defect concentration in the lowest fluence sample, but both XTEM and VEP confirm the formation of macroscopic (*i.e.* >20 Å diameter) voids following annealing. These data are discussed in the context of microscopic models for defect formation and migration.

INTRODUCTION:

Annihilation of variable–energy positrons (VEP) has been used for several years to profile point defects in semiconductors.[1,2] The technique is non–destructive, provides depth resolved information, and can measure point defect concentrations as low as ~1 per 10^6 lattice sites. Comparative and qualitative interpretation of results is straightforward. Quantitative analysis is more difficult, but progress is being made in this area, which is more advanced for the simpler case of Si than for GaAs.

Ion implantation is becoming an increasingly useful step in the fabrication of GaAs–based devices to create either a doped region as an active layer or a highly resistive region for electrical isolation.[3] In both cases, the defects caused by the implantation and subsequent annealing play an important role in determining the ultimate characteristics of the implanted layers. It is thus not surprising that extensive research efforts have been devoted to understanding the properties of implantation–induced defects and their annealing behavior. Silicon is an important n–type dopant for GaAs based materials, and ion implantation followed by annealing is the common method of choice for its introduction. It is widely recognized that electrical activation of silicon implanted in GaAs is a highly complex phenomenon. At low implant fluences ($<1\times10^{13}$ cm^{-2}) close to 100% activation can be achieved, but activation rapidly decreases at higher fluences and can be as low as a few percent at fluences $>1\times10^{14}$ cm^{-2}. Silicon normally occupies the gallium lattice site and behaves as an n–type dopant. At high concentrations, a significant fraction of silicon occupies arsenic sites and behaves as a p–type dopant. This amphoteric behavior of silicon leads to self–compensation and thus low electrical activation. Damage–induced defects, which are invariably formed in the implantation process, can also play an influential role in the subsequent thermal activation. Whereas the self–compensating nature of silicon is well understood, the effect of the defects on dopant activation in

GaAs is complicated and is not. This situation is in part due to the difficulty in identifying and characterizing these defects.

The sensitivity of VEP has recently been exploited for measurements of the depth profile of vacancy–type defects in silicon–implanted GaAs.[4-6] These studies have provided insights into the creation and annealing of implantation–induced defects and their influence on Si activation.[6] Recently, it has been observed by XTEM that vacancy clustering to form macroscopic voids can occur following thermal annealing of Si–irradiated GaAs.[7-9] The observed degradation of electrical activation may be attributed to either of two possible mechanisms. The first is that Si atoms may segregate at the void surface where they become electrically inactive. The second is that surface states in the form of deep acceptors can exist at the void surface, which would deplete nearby carriers.

In the present paper we have used VEP and XTEM to measure defects formed by implantation damage, as well as to study the effects of post–irradiation annealing on the damaged materials. The previous XTEM observation of voids in GaAs is supported by the VEP observations, and results are correlated for both techniques.

EXPERIMENTAL:

Undoped, semi–insulating, liquid–encapsulated Czochralski (100) GaAs wafers were implanted with 220 keV Si^+ ions to fluences of 3×10^{13}, 3×10^{14}, and 1×10^{15} cm^{-2}. Implantation was performed at room temperature, with a current density of ~0.3 $\mu A\ cm^{-2}$ to minimize beam heating. Part of each as–implanted wafer was retained for characterization, and part was encapsulated with Si_3N_4 and furnace annealed at 850° C for one hour in flowing H_2/Ar. The Si_3N_4 cap was then removed.

All samples were cross–sectioned and studied by XTEM. Two types of defects were visible in the XTEM images of the annealed, implanted samples: dislocation

loops and voids. It has been shown[9] that voids form very rapidly during annealing at 850°C, becoming visible after an anneal time of only 5 seconds.

The University of Western Ontario Positron Beam Facility is described elsewhere.[10] Monoenergetic positrons (in the energy range 0.3–60 keV) are implanted into the sample where they rapidly lose energy, thermalizing in ~10 picoseconds. The mean depth $\bar{z}$ (Å) of implantation into the sample is related to the incident beam energy E(keV) by

$$\bar{z} = (A/\rho)\, E^n , \qquad [1]$$

where ρ is the density of the solid (g cm^{-3}), and n and A are constants deduced empirically to be n=1.6±0.1 and A=400±100 (for aluminum).[11] In this study we have use the values n=1.65, following Simpson et al.[12], and A=500, since recent evidence suggests that A should be larger for heavier elements.[13]

The depth at which the positrons annihilate is determined both by the implantation profile and the diffusion that occurs after the positron has thermalized. The diffusion coefficient[14] for positrons in GaAs at room temperature is ~1.9 cm^{2}s^{-1}. Thermal positrons diffuse through GaAs for ~230 picoseconds before annihilating,[15] and during this time may be trapped by a defect in the crystal lattice, with a probability determined by the product of the defect trapping rate ν (s^{-1}) and defect concentration C (per atom). Annihilation may occur from one of several possible states: freely diffusing, trapped at the surface of the solid, or trapped in a variety of defect states. To simplify the modelling procedure we generally assume only one predominant defect type in any one sample.[16,17] Annihilation of the essentially momentum–free positron leads to a Doppler shift in the energy of the γ–radiation emitted which is caused by the momentum distribution of the electrons. Thus, the width of the 511 keV line is

sensitive to the local electronic environment in the solid, and this differs for freely diffusing and different trapped positron states.

The γ–ray spectra are measured using a conventional spectrometer system, consisting of a 65% efficient intrinsic Ge detector, with the ADC stabilized (at 477.6 and 511 keV) for gain and zero shifts. Data are analyzed using the W parameter, which is defined as the number of counts in the wings of the 511 keV peak (507.3–509.7 and 512.3–514.7 keV) divided by the total counts in the peak (506.2–515.8 keV). The W parameter vs incident positron energy (E) data are modelled using the program POSTRAP4,[17] which analytically solves the diffusion equation for positrons in a semiconductor, including the effect of defects and electric fields. POSTRAP4 uses an input model of defects and electric fields in the sample to calculate the fractions of positrons which annihilate in defects, $F_d(E)$, while freely diffusing in the bulk crystal, $F_f(E)$, and while localized at the sample surface, $F_s(E)$. The experimental lineshape parameter W(E) is fitted using the equation:

$$W(E) = W_s F_s(E) + W_f F_f(E) + W_d F_d(E) , \qquad [2]$$

where W_s, W_f and W_d are the characteristic lineshape parameters for the different states. The parameter W_s is obtained directly from the data for low energy implantation, in which nearly all positrons diffuse to and become trapped at the sample surface. W_s depends on the condition of the surface, and usually varies slightly from sample to sample. W_f is obtained from high incident energy positrons, which annihilate in the defect–free bulk crystal beyond the depth of the ion–induced damage.

An iterative procedure of modelling and fitting is used to deduce the correct defect–profile, and the fitted result of W_d provides some guidance as to the nature of the predominant defect type. Alternately, a value for W_d can be assumed (appropriate

data of reference 6 is such that a 2× reduction in point–defect concentration would not be clearly evident, and without the full numerical modelling procedure that we have applied to the present data[17] their interpretation[6] can only be qualitative.

A second significant difference is in the way that the GaAs samples were encapsulated. It is well established that the silox cap used by Lee et al. injects Ga vacancies at the material surface during annealing as a result of outdiffusion of Ga interstitials through the silox.[25] Using the published diffusivity of Ga vacancies[25] under their annealing conditions,[5,6] we estimate the diffusion length of Ga vacancies to be >600 Å, which is comparable to the depths profiled. Consequently, the vacancy concentration in GaAs profiled by Lee et al. is at best represented by the combined result of vacancy annealing by rapid thermal processing and vacancy generation via Ga outdiffusion through the silox cap. The silicon nitride cap we have used in the present study is nominally inert for GaAs annealing, and we therefore do not expect any vacancy injection to be influencing the VEP data we have presented.

CONCLUSIONS:

In conclusion, we have presented a study of the defects introduced during 220 keV Si^+ ion irradiation of GaAs for total fluences ranging from 3×10^{13} to 1×10^{15} cm^{-2}. VEP data show that vacancy–type point defects extend from the surface to ~0.28 μm for all samples, in a concentration which increases with ion fluence. The depth profile of the defects is in reasonable agreement with Monte Carlo simulations. XTEM micrographs of the same samples show some evidence for dislocation loops in the same region.

All samples were furnace annealed for 1 h at 850°C. VEP results show that the defect concentration was reduced ~2× in the lowest fluence sample (3×10^{13} cm^{-2}), and that large voids were formed in the two higher–fluence samples. The latter observation was supported by the XTEM results, and is consistent with previous

This suggests that vacancy–interstitial recombination is even more important in the present case than for previous similar studies of irradiated silicon, where the recombination fraction was ~85%.[23,24] A defect lineshape parameter $W_d/W_f=0.90$ is in this case assumed, as is the value for the trapping rate (per lattice site) $\nu=1\times10^{15}$ s^{-1} of positrons into open volume defects in GaAs.[14] Errors in either of these parameters would change the absolute defect concentrations measured, but relative comparisons are more reliable.

Figure 3 shows XTEM micrographs for the samples following post–implantation annealing, with the void distributions deduced from these summarized in Table 2. After annealing at 850°C for one hour, voids are observed in the implanted region of the high fluence samples. No voids are observed in the sample implanted to 3×10^{13} ions cm^{-2}. The XTEM micrographs show that voids extend at least from ~400 Å to a depth of ~2600 Å in the sample irradiated with 3×10^{14} ions cm^{-2}. Between the surface and 400 Å it is difficult to resolve any of the characteristic "spherical" defects, which could mean that there are no voids or that they are below the ~10–20 Å resolvable limit. In the sample implanted with 1×10^{15} ions cm^{-2} voids appear to lie in a narrower band extending from a depth of ~1400 Å to ~2700 Å. While the void sizes are statistically similar in the two samples, the number density of voids determined from the micrographs is slightly higher (2.73×10^{16} cm^{-3} vs 2.34×10^{16} cm^{-3}) in the lower fluence sample.

Positron data for the annealed samples were fit with models that were similar to the XTEM–deduced void distributions (Table 1 and Fig. 2 vs Table 2). The data resulted in extremely low W_d parameters ($W_d/W_f=0.835$) characteristic of material containing voids.[12,19] For the highest fluence sample the low parameter is less apparent in Fig. 1 because the distribution of voids is relatively narrow, but in the iterative fitting procedure we assumed that the defect parameters for samples #2A and

#3A were the same, and this resulted in defect profiles that agree well with TEM observations.

It is significant that the void distribution required to fit the VEP data for sample #2A extended from the surface to the 0.26 μm depth, rather than from 0.04 μm as observed by XTEM. This is convincing evidence that voids do in fact extend through the near–surface region, but it is possible that they are smaller than ~15 Å as suggested above.

DISCUSSION:

Many of the general characteristics of defect generation and annealing in ion–implanted GaAs and related materials are well studied and understood. However, the observation of voids in implanted and annealed GaAs is a relatively new phenomenon.[7-9] For the ease of the following discussion, a brief description of the processes leading to void formation is given. In implanted GaAs defects are primarily discrete point or line defects, *i.e.*, interstitials and vacancies, and dislocations. Upon subsequent annealing, aside from point defect recombination, the majority of fast–moving interstitials diffuse either to the surface or deeper into the bulk, where they are annihilated or trapped at dislocations, respectively. The lack of efficient interstitial–vacancy recombination means that the damage–induced supersaturation of vacancies persists beyond the initial phase of annealing. In highly implanted samples (#2 & #3), the degree of supersaturation is sufficient that vacancy condensation to form voids is possible.[7-9] The threshold fluence at which voids are formed and detected is dependent on ion mass, flux, and energy, as well as substrate temperature during implantation. For 220 keV Si implantation at room temperature, the threshold fluence is around 3×10^{13} Si cm^{-2}. However, at higher fluences amorphization occurs, and it has been observed that voids are not formed in the amorphous region.[8] This is

possibly due to the fact that there are relatively few clearly defined vacancies in amorphous material.

The observation of voids by XTEM shown in Fig. 3 and in previous studies[7-9] supports the above discussion. The only defects observed by XTEM in the implanted but unannealed samples are dislocations (point defects cannot be resolved). The observation of a void–free region adjacent to the surface (particularly in the high–fluence 1×10^{15} cm^{-2} sample) is possibly due to the existence of amorphous or heavily damaged material, as suggested in the above discussion, or possibly due to the depletion of vacancies at the surface. However, one would expect vacancy–depletion to be similar for all samples (*i.e.* it would depend primarily on ion flux and target temperature), which is not what we observe.

Besides the annihilation of positrons from surface or freely–diffusing bulk states, two kinds of defects are revealed by the analyses of the VEP data (Table 1). The first, with $W_d/W_f=0.90$, is found in the unimplanted and *all* implanted but unannealed GaAs, and in the annealed material implanted to the lowest fluence (#1A). This defect is attributed to discrete vacancies or small vacancy–complexes (possibly linear chains). As expected the concentration of this kind of defect increases with increasing fluence. The second defect type resolved has $W_d/W_f=0.835$, and it occurs in the two higher fluence samples following annealing (#2A & #3A). As discussed above, this unusually low value is associated with trapping in voids, and supports the conclusion based on XTEM results that the spherical defects are voids and not amorphous material. It is likely that sufficient experience with defects of this type will ultimately allow a determination of the void "type" (*i.e.*, gas–filled or evacuated bubble), but to date this is not possible.

The above discussion supports the following picture of defect behavior. Upon annealing of sample #1U a reduction of implantation induced defects occurs, although

the nature of the defect (as determined by the lineshape parameter) remains the same, *i.e.*, vacancy point defects. In contrast, the defect concentration in #2U and #3U remains high after annealing, but the defects change from vacancy–type point defects to voids. In addition, after annealing the defect concentration in the sample receiving the medium fluence (#2A) is a factor of ten larger than that in the sample receiving the highest fluence (#3A), while XTEM shows only a 15% higher void concentration. The reason for this large difference is probably associated with the mean void diameter being larger in sample #2A than in #3A. The typical void diameter is estimated (Table 2) to be 50±30 Å (slightly larger than in the previous study, reference 9), which is in excellent agreement with the *atomic* defect concentration deduced from the VEP data for *either* sample. Within this limit, if we allow a variation of 20 Å *or less* in void radius, together with a 15% overall reduction suggested by the XTEM data, can easily account for the order of magnitude difference in the density of vacant sites in the GaAs lattice. This underscores the highly sensitive capabilities of the VEP technique for *relative* defect densities and changes.

Recently Lee et al.[5,6] have used VEP to study the annealing of Si implanted GaAs and found that annealing had no noticeable effect on the VEP profiles. This observation led them to conclude that implantation–induced vacancy–type defects were not annealed out, and to suggest that Si electrical activation was due to interstitial Si exchanging with substitutional Ga, rather than direct recombination of the Si with Ga vacancies. Our VEP results, however, show that annealing did cause a reduction (by about a factor of 2×) in the vacancy–type defect concentration in GaAs implanted to the same fluence of 3×10^{13} Si cm^{-2}. The discrepancy is perplexing, as it is not expected that the different incident ion energies (130 keV vs 220 keV) and annealing processes (rapid thermal processing vs furnace annealing) should be significant. The difference may in part be due to statistics, since the scatter in the

data of reference 6 is such that a 2× reduction in point–defect concentration would not be clearly evident, and without the full numerical modelling procedure that we have applied to the present data[17] their interpretation[6] can only be qualitative.

A second significant difference is in the way that the GaAs samples were encapsulated. It is well established that the silox cap used by Lee et al. injects Ga vacancies at the material surface during annealing as a result of outdiffusion of Ga interstitials through the silox.[25] Using the published diffusivity of Ga vacancies[25] under their annealing conditions,[5,6] we estimate the diffusion length of Ga vacancies to be >600 Å, which is comparable to the depths profiled. Consequently, the vacancy concentration in GaAs profiled by Lee et al. is at best represented by the combined result of vacancy annealing by rapid thermal processing and vacancy generation via Ga outdiffusion through the silox cap. The silicon nitride cap we have used in the present study is nominally inert for GaAs annealing, and we therefore do not expect any vacancy injection to be influencing the VEP data we have presented.

CONCLUSIONS:

In conclusion, we have presented a study of the defects introduced during 220 keV Si^+ ion irradiation of GaAs for total fluences ranging from 3×10^{13} to 1×10^{15} cm^{-2}. VEP data show that vacancy–type point defects extend from the surface to ~0.28 μm for all samples, in a concentration which increases with ion fluence. The depth profile of the defects is in reasonable agreement with Monte Carlo simulations. XTEM micrographs of the same samples show some evidence for dislocation loops in the same region.

All samples were furnace annealed for 1 h at 850°C. VEP results show that the defect concentration was reduced ~2× in the lowest fluence sample (3×10^{13} cm^{-2}), and that large voids were formed in the two higher–fluence samples. The latter observation was supported by the XTEM results, and is consistent with previous

studies done under similar conditions.[7-9]

The Positron Beam Facility at UWO and research conducted there is supported by the National Sciences and Engineering Research Council of Canada.

REFERENCES:

[1] P.J. Schultz and K.G. Lynn, Rev. Mod. Phys. 60, 701 (1988).

[2] Positron Beams for Solids and Surfaces, *Proceedings of the 4th International Workshop*, edited by: P.J. Schultz, G.R. Massoumi and P.J. Simpson (AIP Press, New York, 1990).

[3] S.J. Pearton, Mat. Sci. Rep. 4, 313 (1990).

[4] J.–L. Lee, J.S. Kim, H.M. Part, D.S. Ma, S. Tanigawa, and A. Uedono, Appl. Phys. Lett. 53, 1302 (1988).

[5] J.–L. Lee, K.–H. Shim, J.S. Kim, H.M. Part, D.S. Ma, S. Tanigawa, and A. Uedono, J. Appl. Phys. 65, 396 (1989).

[6] J.--L. Lee, A. Uedono, S. Tanigawa, and J.Y. Lee, J. Appl. Phys. 67, 6153 (1990).

[7] S. Chen, S.–T. Lee, G. Braunstein, and T.Y. Tan, Appl. Phys. Lett. 55, 1194 (1989).

[8] S. Chen, S.–T. Lee, G. Braunstein, K.Y. Ko, and T.Y. Tan, J. Appl. Phys. 70, 656 (1991).

[9] S. Chen, S.–T. Lee, G. Braunstein, K.–Y. Ko, L.R. Zheng, and T.Y. Tan, Jap. J. Appl. Phys. 29, L1950 (1990).

[10] P.J. Schultz, Nucl. Instrum. Meth. B 30, 94 (1988).

[11] S. Valkealahti and R.M. Nieminen, Appl. Phys. A 35, 51 (1984).

[12] P.J. Simpson, P.J. Schultz, T.E. Jackman, G.C. Aers, J.–P. Nöel, D.C. Houghton, D.D. Perovic, and G.C. Weatherly, pp.125–128 in ref. 2 (1990).

[13] P.G. Coleman, private communication.

[14] K. Saarinen, P. Hautojärvi, J. Keinonen, E. Rauhala, J. Räisänen, and C. Corbel, Phys. Rev. B 43, 4249 (1991).

[15] S. Dannefaer, B. Hogg., and D. Kerr, Phys. Rev. B 30, 3355 (1984).

[16] E. Tandberg, P.J. Schultz, G.C. Aers and T.E. Jackman, Can. J. Phys. 67, 275 (1989).

[17] G.C. Aers, pp. 162–170 in ref. 2 (1990).

[18] P.J. Schultz and C.L. Snead, Jr, Metall. Trans. 21A, 1121 (1990).

[19] D.D. Perovic, G.C. Weatherly, P.J. Simpson, P.J. Schultz, T.E. Jackman, G.C. Aers, J.–P. Nöel, and D.C. Houghton, Phys. Rev. B 43, 14257 (1991).

[20] T.E. Jackman, G.C. Aers, M.W. Denhoff, and P.J. Schultz, Appl. Phys. A, Rapid Commun. 49, 335–339 (1989).

[21] P.J. Schultz, E. Tandberg, K.G. Lynn, B. Nielsen, T.E. Jackman, and M.W. Denhoff, Phys. Rev. Lett. 61, 187 (1988).

[22] "TRIM90" is based on the paper by J.P. Biersack and L.G. Haggmark, Nucl. Instrum. Meth. 174, 257 (1980).

[23] I.V. Mitchell, P.J. Simpson, P.J. Schultz, M. Vos, U. Akano, and C. Wu, pp.121–124 in ref. 2 (1990)

[24] P.J. Simpson, M. Vos, I.V. Mitchell, C. Wu, P.J. Schultz, and H.J. Stein, accepted for publication in Phys. Rev. B (1991).

[25] K.B. Kahen, D.L. Paterson, G. Rajeswaran, and D.J. Lawrence, Appl. Phys. Lett. 55, 651 (1989).

TABLE 1: Model parameters for POSTRAP4 are listed for the fit of the positron data shown in Fig. 1.

GaAs Sample	Si^+ ion Fluence (cm^{-2})	Defect Region (μm)	Concentration (per atom)	W_d/W_f	Field (surface +ve)
Unimplanted		0–1.0	1.2e–6	0.90	–
UNANNEALED:					
#1U	3×10^{13}	0–0.28	1.0e–5	0.90	–
		0.28–1.80	2.0e–6	"	–
#2U	3×10^{14}	0–0.28	1.5e–5	0.90	–
		0.28–1.50	1.8e–6	"	–
#3U	1×10^{15}	0–0.20	3.0e–4	0.90	–
		0.20–1.50	2.0e–6	"	–
ANNEALED:					
#1A	3×10^{13}	0–0.30	5.5e–6	0.90	300 Å, 0.15 V
#2A	3×10^{14}	0–0.26	4.0e–4	0.835	–
#3A	1×10^{15}	0.14–0.27	2.8e–5	0.835	200 Å, 0.11 V

TABLE 2: Void distributions determined from XTEM micrographs shown in Fig. 3.

GaAs Sample	Si^+ ion Fluence (cm^{-2})	Void Band Distribution (μm)	Band Centre (μm)	Void Density (cm^{-3})	Void Size (Å)
#1A	3×10^{13}	–	–	–	–
#2A	3×10^{14}	0.04–0.26	0.127	2.73e16	20–80
#3A	1×10^{15}	0.14–0.27	0.206	2.34e16	20–80

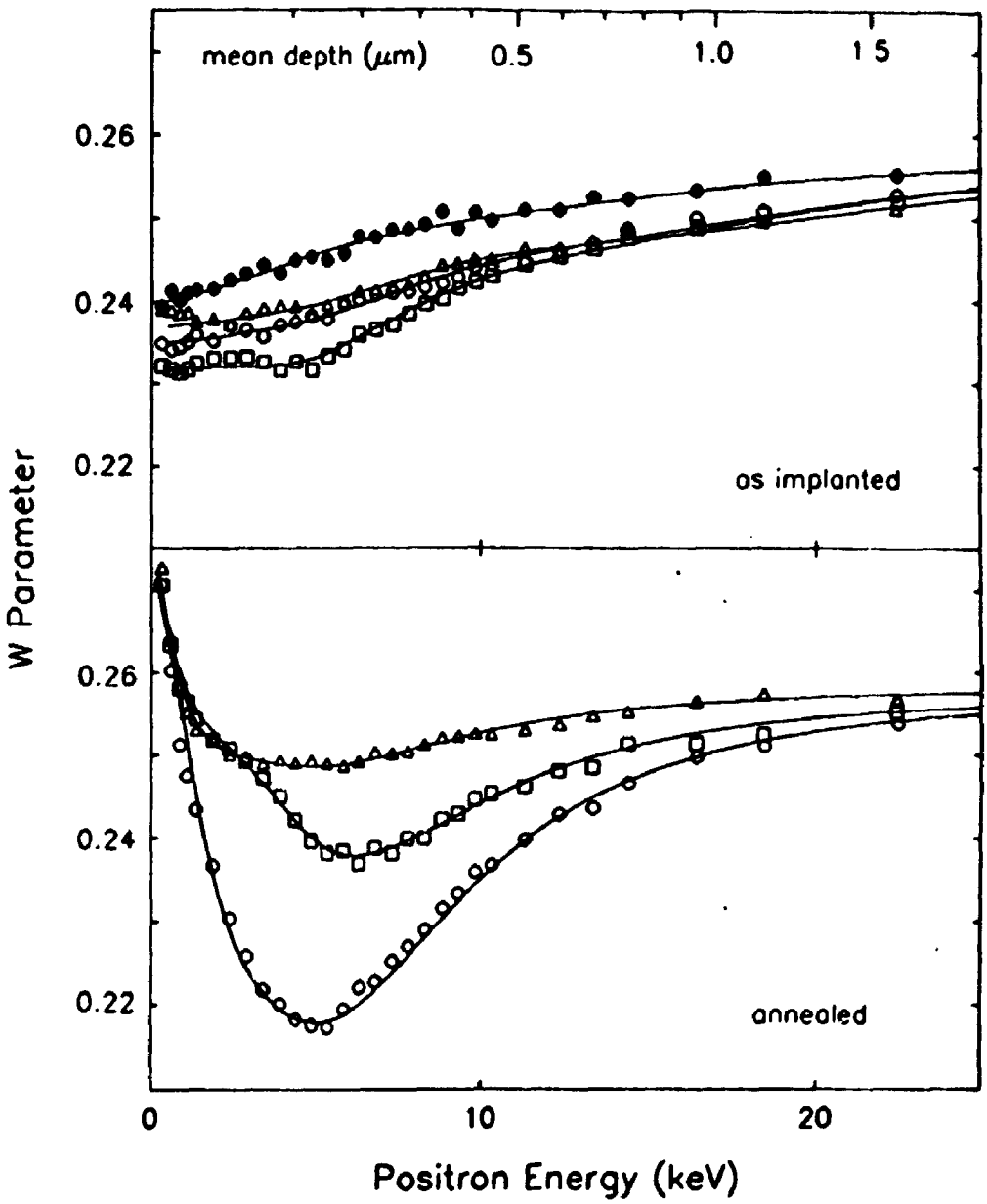

Figure 1: Defect profiling in Si–ion irradiated GaAs with variable–energy positrons (VEP). W parameter data versus incident positron energy are shown for an unimplanted GaAs wafer (•), as well as for the 3 samples before and after annealing (#1, Δ=3×10^{13} cm^{-2}; #2, ○=3×10^{14} cm^{-2}; #3, □=1×10^{15} cm^{-2}). All solid lines are fits to the data based on the models summarized in Table 1. The presence of voids following annealing is most evident in the intermediate fluence sample (#2A) by the unusually low value of the lineshape parameter.

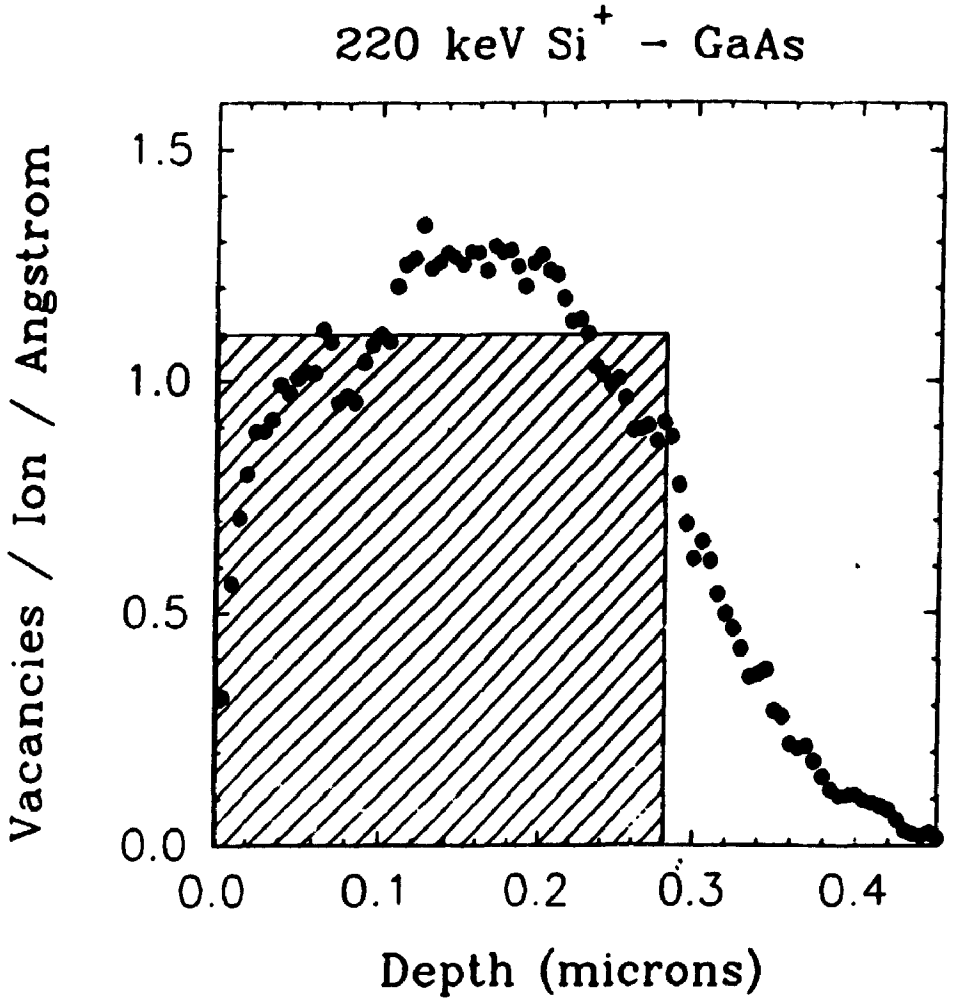

Figure 2: Monte–Carlo calculation[22] of the number of vacancies per incident ion per Å of depth in the GaAs, calculated for 220 keV Si ions. Also shown is a normalized representation of the defect–profile used to model the as–irradiated samples #1U and #2U. The concentration of point–defects used to model the VEP data (Table 1) was several orders of magnitude smaller than that predicted by the TRIM90 code, indicating that vacancy–interstitial recombination is even more significant than previously found for Si–ion irradiation of silicon.[23,24]

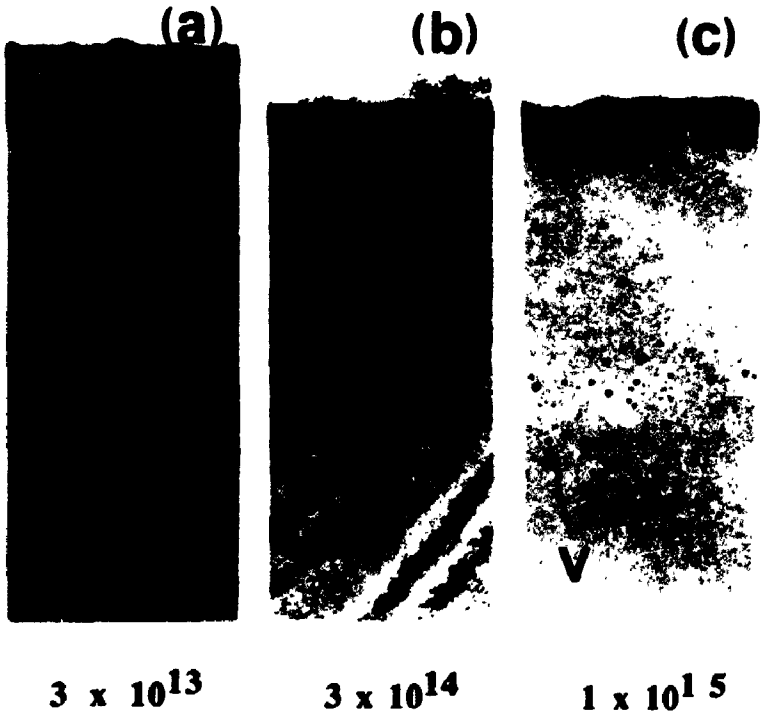

Figure 3: Cross–sectional transmission electron microscopy (XTEM) micrographs are shown for samples #1–#3 irradiated with (a) 3×10^{13} cm^{-2}, (b) 3×10^{14} cm^{-2}, and (c) 1×10^{15} cm^{-2} silicon ions, respectively, and annealed at 850°C for 1 h. The voids are evident in (b) and (c), and the parameters deduced from XTEM data are listed in Table 2.